國 立 交 通 大 學

材 料 科 學 與 工 程 研 究 所

博 士 論 文

溶液法半導性氧化鋅薄膜製備及其薄膜電晶體特性研究

The Fabrication and Characteristics of ZnO Semiconducting Thin Film and Thin Film Transistors by Solution Method

研 究 生 ： 鄭華琦

指導教授 ： 陳家富 博士

呂志鵬 博士

中 華 民 國 九 十 七 年 十一月

溶液法半導性氧化鋅薄膜製備及其薄膜電晶體研究

The Fabrication and Characteristics of ZnO Semiconducting Thin Film and Thin Film Transistors by Solution Method

研 究 生 ： 鄭華琦　　Student ： Hua-Chi Cheng

指導教授 ： 陳家富 博士　　Advisor：Dr. Chia-Fu Chen

呂志鵬 博士　　Dr. JihPerng Leu

國 立 交 通 大 學

材 料 科 學 與 工 程 學 系

博 士 論 文

A Thesis

Submitted to Department of Material Science and Engineering

College of Engineering, National Chiao Tung University

In partial Fulfillment of the Requirements

for the Degree of Doctor of Philosophy

in Material Science and Engineering

November 2008

Hsinchu, Taiwan, Republic of China

中 華 民 國 九 十 七 年 十 一月

溶液法半導性氧化鋅薄膜製備及其薄膜電晶體研究

學生：鄭華琦　　　　　　　　　　指導教授：陳家富 博士

呂志鵬 博士

國立交通大學材料科學與工程研究所 博士班

摘要

氧化鋅屬於 n 型透明之寬能隙(wide energy band gap, 3.2 eV)半導體，近來廣泛應用於光電元件及平面顯示器領域。本論文利用溶液法(solution method)成長氧化鋅(zinc oxide；ZnO)半導性薄膜，並對其薄膜電晶體(thin film transistor；TFT)之物理及電性做一系列研究；採用的溶液法包含化學浴鍍著法(chemical bath deposition；CBD)與溶膠-凝膠(sol-gel)法。此外利用陽離子調和(cat ion- mediation)之化學溶液鍍浴方法探討氧化鋅薄膜結晶取向與透光性質，更運用摻雜的原理探討溶液中鎂離子(magnesium ion；Mg^{2+})對氧化鋅結晶成長的影響，藉由鎂離子在溶液中之干擾作用改變氧化鋅結晶之優選方向(prefer orientation)，並獲得 90 %良好透光性氧化鋅薄膜，將能隙(energy band gap)由 3.38 eV 降低至 3.23 eV。最後利用不同溫度退火的溶膠-凝膠氧化鋅薄膜作為溶液浴鍍著氧化鋅之種子層，研究溶膠-凝膠結晶種子對溶液浴鍍著氧化鋅之結晶取向的影響，並且以其作為主動層的全透明薄膜電晶體(transperent thin film transistors；TTFT)元件之電性研究。

在氧化鋅薄膜特性上，主要探討合成之純氧化鋅的結晶性(crystallization)、光學性質 (optical property)、晶粒大小以及載子濃度(carrier concentration)等物理

性質，以及研究氧化鋅薄膜之形貌，結構，晶相與組成的關係。

在薄膜電晶體應用研究中，探討低溫成長之氧化鋅薄膜在沒有退火(annealing)的情況下製作之元件基本電性，其次以溶膠–凝膠法製備不同鎂離子摻雜之氧化鋅薄膜電晶體，分別探討多元氧化物薄膜與其電晶體之物性與電性，研究發現氧化鋅藉由鎂的摻雜可以提高膜厚均勻性與透光度，並且使其薄膜電晶體有較高之電流開關比。

最後利用溶膠-凝膠法與化學溶液浴鍍著法混合成長氧化鋅薄膜，以自體結晶成核的方式，解決離子摻雜效應對電晶體的影響，並提高載子遷移率，增加元件開關速度，同時使用銦錫氧化物(ITO)為閘極、源極、和汲極材料，製作全透明薄膜電晶體元件。針對電性上解決常開效應，並且提高元件開啟時的電流，此元件為常關型(normally off)，或稱增強型(enhancement mode)薄膜電晶體，經元件結構與薄膜成長方法改善後，可獲得較佳之薄膜電晶體元件(電子遷移率為 0.647 $cm^2 V^{-1} s^{-1}$；元件之開關比大於 10^7)。

The Fabrication and Characteristics of ZnO Semiconducting Thin Film and Thin Film Transistors by Solution Method

Student：Hua-Chi Cheng　　　　Advisor：Dr. Chia-Fu Chen

Dr. Jih-Perng Leu

Institute of Material Science and Engineering

National Chiao Tung University

Abstract

Zinc oxide is an n-type transparent semiconductor with wide band gap of 3.2 eV, which has been extensively applied to photoelectric components and flat panel displays. This thesis was aimed at ZnO thin film preparing by solution method, the properties of the grown ZnO films, and the physical and electrical characteristics of the thin film transistors. The solution methods were including chemical bath deposition (CBD) and sol-gel deposition. In addition, this investigation explored the influence of cation-mediation on the orientation and transmittance of ZnO crystals in chemical bath deposition. Moreover, the doping effect of ZnO crystalline which grown in Mg ion (Mg^{2+}) contained solution was investigated. In particular, the prefer orientation of the ZnO crystalline was changed by the Mg ion mediating in chemical solution. The ZnO crystalline film exhibited good optical transmittance of over 90%. Additionally, the direct band gap value was 3.22eV, which is less than 3.38eV obtained using a non-mediation solution bath. Finally, the ZnO sol-gel films were

annealed at different temperatures, which were used as seed layers and nuclei sites for further ZnO films fabrication by chemical bath deposition. Base on the investigation, the influence of sol-gel seed layers on crystallinity and orientation of ZnO by chemical bath deposition were discussed. Also, the electrical characteristics of transparent thin film transistors obtained using this active layer were demonstrated.

In the ZnO films study, the physical properties of the ZnO film by solution methods, including the growth mechanism on crystallization, the optical property, the crystal size, and carrier concentration of the ZnO thin film were investigated. In the ZnO thin film transistors (TFTs) study, the electrical characteristics of ZnO thin film transistors by using low temperature solution process without annealing were demonstrated. In addition, the electrical characteristics of ZnO TFTs with Mg doped and without Mg doped by sol-gel method were demonstrated respectively. The A significant improvement of surface roughness with Mg doping could be noticed. In addition, this result was in good agreement with the discussions of higher current on and current off ratio.

Finally, the ZnO film were grown by sol-gel and chemical solution bath combination method, to resolve the doping effect on thin film transistors by using the self-crystal as the growing sites for further deposition. Since indium tin oxide was used as the conducting electrodes (source, drain, and gate) for transparent thin film transistors. Current-voltage properties measured through the gate infer that the ZnO channel was *n*-type enhancement mode device due to a positive gate voltage were required to induce a conducting channel, and the current increases with increasing positive gate bias. The optimum device had field-effect mobility of 0.67 cm^2 /V s and an on-off ratio more than 10^7.

誌　　謝

感謝國立交通大學所有教導過我的老師，尤其是我的指導教授－陳家富老師。工作多年後，再度接受更高的學術訓練，陳老師當初授予我跨領域學習的機會，謝謝他在研究上的指導與鼓勵，更重要的是對學生的照顧愛護與觀念上的導正。

感謝學弟妹在實驗上提供意見及討論以及庶務上事務的幫忙。以及曾在工作上的好同事目前任職於逢甲大學的蔡健益博士，不僅提供不少的建議及指教，並在研究上給予協助。謝謝工研院與 TTLA 的長官及同仁的支援；此外，感謝任職於台積電的好朋友們加油鼓勵，得以使研究遇到瓶頸時獲得突破。

感謝我的家人，這些年來的精神支持，讓我能同時兼顧家庭、工作、與學業，完成取得博士學位的心願。

最後，僅以此論文獻給在天上最敬愛的父親，雖然這項喜悅來不及讓您親身感受，但是，我做到了!

數年來，有著無數人的幫助，要謝的人太多了，一切恩惠銘記在心。

Contents

Page

Abstract (Chinese) -- I

Abstract (English) -- Ⅲ

Acknowledge (Chinese) -- V

Contents -- VI

List of Figures -- X

List of Tables -- XⅢ

Chapter 1 Introduction -- 1

1.1 Background -- 1

1.2 Motivations -- 2

1.3 Organization of this Thesis -- 4

Chapter 2 A brief literature review and technical background ------ 6

2.1 Application of Thin Film Transistor on Liquid Crystal Display (TFT-LCD) -- 6

2.2 Overview of thin film transistor -- 10

2.3 Transparent metal oxide semiconductors ----------------------------- 14

2.4 Zinc oxide -- 15

2.5 Device structure of Thin Film Transistor ----------------------------- 19

2.6 Basic operation of TFT device -- 20

Chapter 3 Experimental method and measurement techniques ----- 23

3.1 Experimental Details -- 23

3.1.1 The sol-gel method -- 23

3.1.2 Synthesis of the precursors --- 24

3.1.3 Chemical bath deposition (CBD) ------------------------------------ 25

3.1.4 The fabrication of thin film transistor devices ------------------------ 26

3.2 Characterization for materials and devices --------------------------- 26

3.2.1 Scanning electron microscopy (SEM) -------------------------------- 26

3.2.2 Transmission electron microscopy (TEM) --------------------------- 26

3.2.3 X-ray diffraction spectroscopy -------------------------------------- 27

3.2.4 UV absorption -- 27

3.2.5 Thermal gravimetric analysis --------------------------------------- 27

3.2.6 Hall effect measurement --- 28

3.2.7 Atomic force microscope (AFM) ------------------------------------ 30

3.2.8 X-ray photoelectron spectroscopy ----------------------------------- 31

3.3 Electrical properties measurement for TFT devices ------------------- 31

Chapter 4 Results and Discussions ------------------------------------- 32

4.1 Thin film transistors with active layers of zinc oxide (ZnO) fabricated by low-temperature chemical bath method ------------- 32

4.1.1 Descriptions -- 32

4.1.2 Conceptions --- 32

4.1.3 Specifics methods --- 33

4.1.3.1 Film deposition procedure -- 33

4.1.3.2 Characterization techniques -- 35

4.1.4 Achievements and explanations -------------------------------------- 35

4.1.5 Summary --- 39

4.2 Cation-Mediated Effects on Zinc Oxide Films Formed by Chemical Bath Deposition -- 40

4.2.1 Descriptions -- 40

4.2.2 Conceptions --- 40

4.2.3 Specifics methods --- 41

4.2.3.1 Deposition of films -- 41

4.2.3.2 Characterization --- 42

4.2.4 Achievements and explanations -- 42

4.2.5 Summary -- 49

4.3 Performance of sol-gel deposited $Zn_{1-x}Mg_xO$ films used as active channel layer for thin-film transistors ------------------------------ 50

4.3.1 Descriptions -- 50

4.3.2 Conceptions --- 50

4.3.3 Specifics methods --- 52

4.3.4 Achievements and explanations ------------------------------------- 53

4.3.5 Summary -- 61

4.4 High-quality oriented ZnO films by sol-gel and chemical bath deposition combination method ----------------------------------- 62

4.4.1 Descriptions -- 62

4.4.2 Conceptions --- 62

4.4.3 Specifics methods --- 63

4.4.4 Achievements and explanations -- 64

4.4.5 Summary -- 71

4.5 Transparent ZnO thin-film transistor fabricated by sol-gel and chemical bath deposition combination method --------------------- 72

4.5.1 Descriptions -- 72

4.5.2 Conceptions --- 72

4.5.3 Specifics methods --- 73

4.5.4 Achievements and explanations -- 75

4.5.5 Summary -- 79

Chapter 5 Conclusions and Suggestions -------------------------------- 80

5.1 Conclusions -- 80

5.2 Suggestions -- 81

Reference -- 83

Publication list -- 103

List of Figures

Fig. 2.1 (a) the cross-sectional view of the whole panel, and (b) the storage capacitor-on-gate of one sub-pixel design ------------------------------------ 9

Fig. 2.2 Schematic cross-sectional views of TFTs: (a) adapted from Lilienfeld [32] at U.S. Patent 1930; (b) Weimer [33] at 1962 IRE; and (c) Spear and LeComber [37] at 1979 IEEE --------------------------------------- 10

Fig. 2.3 The hexagonal (wurtzite) crystal structure of ZnO --------------------------- 16

Fig. 2.4 Four basic TFT structures: (a) co-planar top gate, (b) co-planar bottom gate, (c) staggered top gate, and (d) staggered bottom gate ------------------ 19

Fig. 2.5 (a) The basic structure of a TFT and the corresponding energy band diagrams as viewed through the gate for several conditions, including (b) equilibrium, (c) $V_{GS} < 0$ and (d) $V_{GS} > 0$ -------------------------------------- 21

Fig. 3.1 The flow chart of the precursor preparation and ZnO films processing by spin coating --- 25

Fig. 3.2 Schematic of the Hall effect in a long, thin bar of semiconductor with four ohm contacts. The direction of the magnetic field *B* is along the z-axis and the sample has a finite thickness *d* --- 29

Fig. 4.1 Schematic (a) cross-sectional and (b) top view of the ZnO-based thin-film transistor --- 34

Fig. 4.2 X-ray diffraction spectrum of the ZnO thin film on SiO_2 surface prepared by the CBD -- 36

Fig. 4.3 SEM images of ZnO film deposited at 60℃ from 0.1 mol/L zinc nitrate and 0.03 mol/L --- 37

Fig. 4.4 Electrical characteristics of the ZnO-TFT which the active channel layer ZnO was fabricated by CBD method (a) I_d-V_d curve, (b) I_d-V_g curve ------ 38

Fig. 4.5 XRD pattern of ZnO films: (a) growth without cation mediation in the solution bath and (b) growth with cation mediation in the solution bath --- 43

Fig. 4.6 SEM images of ZnO film: (a) cross-sectional morphology and (c) plane-view morphology of film deposited in bath without cation mediation solution; (b) cross-sectional morphology, and (d) plane-view morphology of film deposited in cation-mediated-solution bath ------------- 44

Fig. 4.7 EDS of ZnO film deposited in cation-mediated solution bath ---------------- 45

Fig. 4.8 Lattice constants of ZnO in both a and c-axes --------------------------------- 46

Fig. 4.9 Optical transmittance spectra of ZnO films deposited in (a) bath without cation-mediated solution and (b) cation-mediated-solution bath ------------ 47

Fig. 4.10 Square of the absorption coefficient as a function of photon energy for ZnO growth in (a) bath without cation-mediated solution and (b) cation-mediated- solution bath -- 49

Fig. 4.11 TGA-DSC curves of the dried of $Zn_{1-x}Mg_xO$ sols with x=0, 0.2 or 0.3 ----- 54

Fig. 4.12 X-ray diffraction patterns of $Zn_{1-x}Mg_xO$ thin films ($0 \leqq x \leqq 0.36$) , which were annealed at 500 ^oC for 1 hr --- 55

Fig. 4.13 SEM micrographs of cross-sections of $Zn_{1-x}Mg_xO$ thin films: (a) x=0; (b) x =0.2; (c) x=0.3 and (d) x=0.36 -- 56

Fig. 4.14 SPM images of the surface of $Zn_{1-x}Mg_xO$ thin films: (a) x =0; (b) x= .2; (c) x=0.3 and (d) x=0.3 --- 58

Fig. 4.15 The transmittance spectra of $Zn_{1-x}Mg_xO$ thin films with x=0, 0.2, 0.3 or 0.36 -- 59

Fig. 4.16 (a) Output characteristics (I_D-V_D curve) and (b) transfer characteristics (I_D-V_G curve) of TFT using $Zn_{0.8}Mg_{0.2}O$ thin film as the active channel layer -- 60

Fig. 4.17 Typical TGA/DSC curves measured in air at a heating rate of 5℃/min for ZnO sol-gel --- 65

Fig. 4.18 X-ray diffraction pattern of ZnO films, seed layers post-baked at (a) 150℃, (b) 250℃, and (c) 550℃; combination ZnO films of CBD ZnO films grown on post-baked seed layers at (d) 150℃, (e) 250℃, and (f) 550℃ --- 66

Fig. 4.19 (a) TEM image and the (b) SEAD patterns of the ZnO film on glass substrate --- 67

Fig. 4.20 SEM images of ZnO film; seed layers post-baked at (a) 150℃, (b) 250℃, and (c) 550℃; combination ZnO films of CBD ZnO films grown on post-baked seed layers at (d) 150℃, (e) 250℃, and (f) 550℃ --------------- 68

Fig. 4.21 XPS pattern of ZnO films which the CBD ZnO film grown on post-baked seed layers at 250℃ -- 69

Fig. 4.22 The Hall-effect mobility of the ZnO films grow by sol-gel and CBD combination method --- 70
Fig. 4.23 Top-gate structure of ZnO- TFT in which (a) is cross-sectional schematic and (b) is top view schematic --- 74
Fig. 4.24 SEM images of (a) ZnO films on Corning 1737 glass substrate by 45° tilt angle, the insert is a cross section view of scale up from the local of ZnO film with a 400 nm scale. (b) local cross section view of ZnO-TFT on Corning 1737 glass substrate --- 76
Fig. 4.25 Optical transmission spectra for the Top-gate structure of ZnO-TFT (except substrate) through the ITO film (gate), SiNx (gate insulator), and (ZnO film) channel region, and the thicknesses are 100nm, 300nm, and 200nm respectively. The insert shows a 5 × 5 cm^2 substrate with 75 devices of ZnO-TFT on Corning 1737 glass substrate ----------------------- 77
Fig. 4.26 (a) Drain current-drain voltage (I_D-V_D) curves at gate voltage (V_G) between 0 and 40V for a ZnO-TFT with channel width to length ratio (W/L) of 50. (b) Transfer characteristics, I_D versus V_G at V_{DS} =20V for the same ZnO-TFT. It is also indicated the square root of drain current versus the gate voltage from which is determined the threshold voltage --- 79

List of Tables

Table 2.1 TFT/AMLCD Design Factor -- 8

Table 2.2 Processing methods employed and electrical performance characteristics for several fully transparent ZnO TFTs. -- 13

Table 2.3 Thin film electrical and optical properties of n-type transparent conductors -- 15

Table 2.4 Physical properties of wurtzite ZnO -- 18

Table 4.1 Chemical composition of the solutions used for ZnO film deposition ------ 42

Chapter 1

Introduction

2/2 **Background**!

Recently, researchers have paid increasing attention to new materials for accomplishing specific demands. In the electronic applications, good transparency, high performance, simple fabrication, low cost, and no environmental concerns are nowadays a crucial requirement in materials for the next generation application. The only possibility to perform transparent device is by using oxide materials. These oxide materials are very interesting materials because they combine simultaneously high/low conductivity with high visual transparency and have been widely used in a variety of applications.!

In the past, devices based on Si base had presented some limitations, such as light sensitivity, light degradation, and must be processed in expensive equipments. Therefore, investigate on the new material developing is necessary and important.

Oxide-based materials, a branch of material research, supplying a great platform for applications in optical electronic field, represents rapidly expanding research area due to their potential applications in electronics [1], optoelectronics [2], catalysts [3], sensors [4] and so on. Recently, the ZnO-based material was paid much attention, since it was multifunction and used in additives, medicines and optical devices[5-9]. Moreover, crystalline ZnO-based thin films have attracted considerable interest as a transparent conductive oxide and as a semiconductor in both the visible spectrum and part of the UV range. Crystalline ZnO materials exhibit electro-optical properties, high electro-chemical stability, large band gap, abundance in nature and absence of

toxicity which make them very popular for use in solar cells [10], photo detectors [11], light-emitting devices [12], gas sensor elements [13] and surface acoustic wave guides [14], which could lead to improving progress in solid state devices development.

Crystalline ZnO, in particular, provide a growing number of applications which apparently depend on its growth constitution. In practical applications, the shape, size and arrangement of crystallites limit suitability of films to specific functions. Therefore, microstructure and crystallinity should be improved further, and both simple and low cost methods for preparing high-quality ZnO should be studied. Based on the backdrop the above, it is possible to accelerate the progress of materials development in advance electronic elements.

Many methods for ZnO preparing, including chemical and physical, such as sputtering [15], pulsed laser deposition [16], chemical vapor deposition (CVD) [17], molecular beam epitaxy [18] and sol-gel process [19]. Several methods for growing ZnO films at low temperature that use solution methods have been reported [20-25]. Among these, solution method is of particular interest because of its simplicity, low cost and the large area of its coatings. However, the solution method is based on the controlled precipitation of the material to be prepared, so as to form a film upon the substrate surface. Also, the morphologies depend on the control of precipitation during film growth. Numerous articles have addressed control of the growth mechanism to adjust the formation of the crystal [26-28]. More stable and consistency microstructures must be improved for further applications.

1.2 Motivations

ZnO has many superior properties for application; especially in transparency

and wide band gap. ZnO-based TFTs exhibit higher transparency in visible wavelength and relative low process temperature compare with the silicon-based TFTs, thus has received much attention recently. Several methods are applied to prepare ZnO films, both physical and chemical deposition technologies, which include magnetron sputtering [29-43], pulsed laser deposition [44-48], chemical vapor deposition (CVD) [18], molecular beam epitaxy [19], and sol-gel process [49] etc.. The mobility of devices demonstrates among the researches ranging from 0.05 to 70 cm^2/Vs by those methods. However, most of the methods were not well suited for large area coating and low temperature processing; especially for those need vacuum facilities which result in high cost. For the issues, beside the deposition methods of ZnO films involving vacuum facilities mentioned, some studies [17, 50, 51] investigated another deposition method, chemical solution deposition (CSD), a method for films growth in atmosphere. For large area deposition, the CSD process may provide a more economic way to fabricate device components than vacuum techniques. Moreover, from the scientific point of view, polycrystalline ZnO based films are generally recognized in electronic application that high quality crystalline materials can be applied to semiconductor in active devices. It will stir a new field of research on the ZnO thin films deposition by solution method. Also, it will provide a new simple and direct patterning which approach to deliver high performance n-type ZnO TFTs.

From the industrial point of view, low temperature, simple, and low cost method are regarded as excellent technique for TFTs fabrication. Currently, increasing the aperture ratio of the TFT-LCD is only of the main topic that are able to save the power consumption resulted from poor backlight transmission through low aperture ratio

pixel structure. In addition, the excellent device characteristics of ZnO based TFTs can be fabricated directly on the glass substrates of displays, which makes the integration of LCD pixel with complicated driving circuits possible.

We believe these approaches of generating high-quality ZnO based TFTs will not only stir the fundamental research on new electronic application and characterizations on the polycrystalline semiconductor but also benefit the new industry in Taiwan to develop low-cost, highly reliable, transparent and flexible electronics.

However, most of the methods are not well suited for large area coating and low temperature processing. For the issues, chemical bath deposition (CBD) has been an attractive technology which is simple and low-cost for fabricating thin film. There are many previous articles discussing the ZnO films using electroless deposition in solution bath and indicating the feasibility of low temperature [15-19]. These make the films good compatibility with substrate materials.

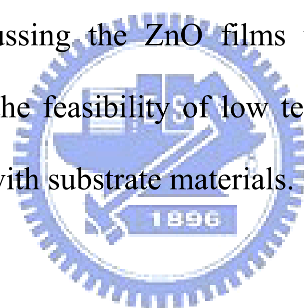

1.3 Organization of this Thesis

There are other four chapters in this thesis. A concise summary of these chapters is described as follows:

Chapter 2 A brief literature review and technical background: The aim of this chapter is to provide a basic understanding about ZnO and its thin film transistors application concept. A general overview of transparent conducting oxide semiconductors, followed by a detailed exploration of zinc oxide properties is presented. In addition, basic TFT operation, TFT structures, and ZnO-based TFTs are reviewed.

Chapter 3 Experimental methods and measurement techniques: In this chapter,

solution methods for ZnO films depositing are introduced. Also, thin-film processing techniques relevant to the fabrication of TFTs are briefly discussed. Finally, thin-film characterization techniques are discussed, including crystallinity, morphology, Hall and optical transmission measurements etc..

Chapter 4 Results and Discussions: There are five subjects in this chapter. Research objectives listed above are interpreted, and the more concerned literature review is also discussed in this chapter.

Chapter 5 Conclusions and Suggestions: The results of the present investigation are summarized. On the other hand, some proposed relevant works are provided for further study.

Chapter 2

A brief literature review and technical background

2.1 Application of Thin Film Transistor on Liquid Crystal Display (TFT-LCD)

The technologies and applications of AMLCDs are developing rapidly in recent decades. The products such as portable computer, projection light valve, and miniature display, owing to their characteristics including the brightness, viewing angle, low power consumption, and integrated circuit (IC) process compatibility. In the past, the cathode ray tubes (CRTs) played the leading role in display electronics. However, CRTs have been completely replaced by LCDs. AMLCDs have penetrated into the desktop monitor market and even take possession of the market of television. Desktop monitor engineering specifications emphasize high visual performance, such as higher resolution, higher pixel content, wider viewing angle, larger color gamut, higher brightness and a moderate price. Another large area display product, such as HDTV (high definition television), would underscore lower cost while accepting a lower cost while accepting a lower cost while accepting a lower resolution and lower pixel content display. However, in order to quickly occupy the TV market, several AMLCD makers increase the size of LCD panels rapidly.

Even the fabrication cost of passive-matrix is slightly lower than that of active-matrix arrays, it would be important to understand why an active matrix array design is necessary. A TFT is a MOSFET fabricated on an insulating substrate (preferably glass for low cost products) by employing all thin film components. It has all the advantages of a silicon-on-insulator (SOI) device; fabrication simplicity, strong latch-up, immunity and possible high packing density. When TFTs are used in

AMLCDs, the semiconductor film of TFT channel is composed of either amorphous Si (a-Si), various degrees of recrystalized a-Si (poly-Si), or II-VI group semiconductors such as CdSe and ZnO, and most recently, even organic materials, such as pentacene, are being considered. The computer simulations are commonly used to optimize the TFT active-matrix array design and analyze the electrical performance of the TFTs based on statistical extraction of the devices and fabrication process parameters. Since this approach is the most efficient way to predict the statistical mean and variance in display performance, it is more instructive to carry out a simple, physically based parameter analysis to identify functional dependencies, performance limits, and minimum requirements, and this analysis is applicable to any kind of TFT processing technologies. Table 2.1 [52-54] list the major TFT and AMLCDs design factors. The pixel size, the TFT geometry, and the desired fill factor will determine the amount of parasitic capacitance to the adjacent rows and columns, while the display size and pixel content will dictate the resistance of the row and column lines. The number of rows and the frame time dominate the charging time of the pixel capacitance, including the liquid crystal capacitance and charge retention time. The minimum TFT on-state current determines the number of gray levels to accurately charge up the pixel. The LC mode will dictate the pixel voltage, and the allowable gray bit error rate, along with specifications for flicker, will determine the TFT and pixel off-state current.

Table 2.1 TFT/AMLCD Design Factors and Examples

TFT AMLCD design factors	Examples
Display size	Diagonal (14", 15", 18", 20", 40", etc.)
Light modulator/ mode	(TNLC-NW, TNLC-NB, IPS, FELC, etc.
Illumination conditions	Contrast ratio (2:1, 300:1, etc.) Maximum brightness (100 cd/m2, 500 cd/m2, etc.) Ambient illumination (dark room, room light, sunlight readable, etc.)
Display format (number of lines)	Content (VGA, SVGA, XGA, SXGA, UXGA, QUXGA-W, etc.)
Frame time	Film, 1/24 sec; video, 1/30 sec; data 1/60 sec etc.
Number of gray levels	6-bits (262K colors), 8-bits (16.8M colors), etc.
TFT geometry	Bottom-gate staged BCE, I-stopper, top gate, etc.
Fill factor	30%, 60%, 75%, 100%

(a)

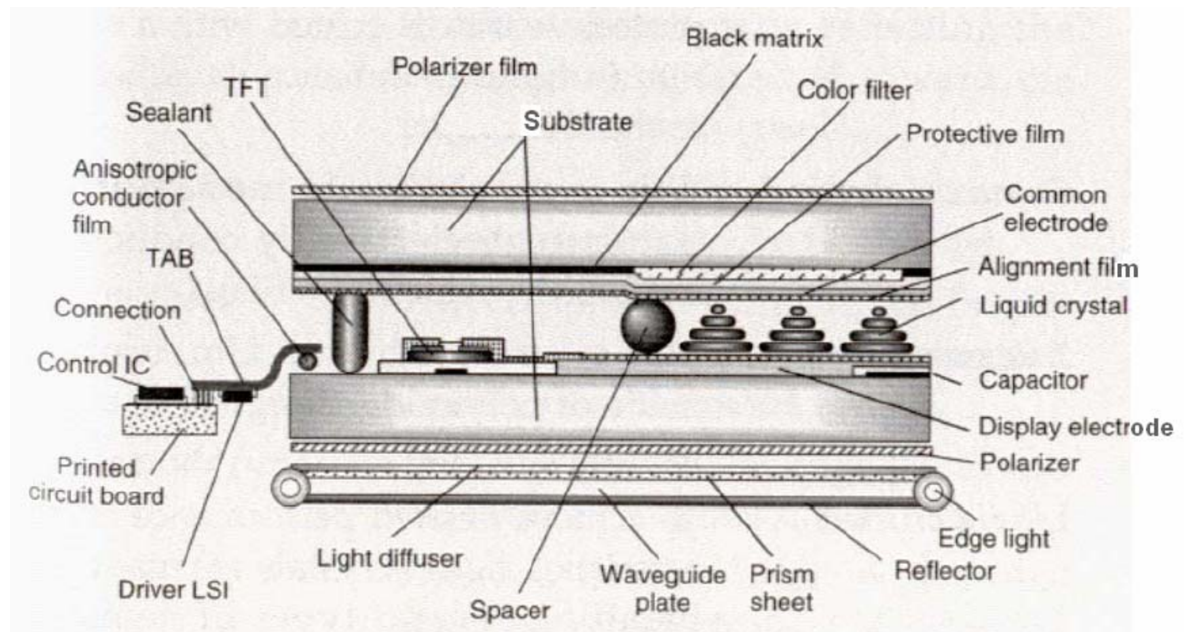

(b)

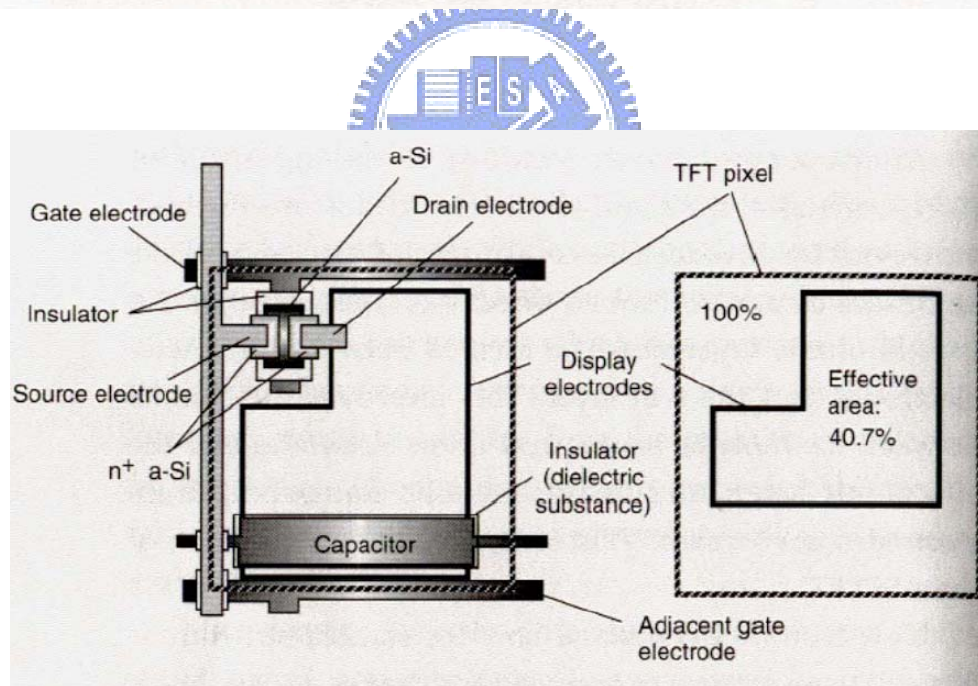

Fig. 2.1 (a) the cross-sectional view of the whole panel, and (b) the storage capacitor-on-gate of one sub-pixel design.

TFTs have been intensively researched for possible electronic and display applications. In the early 1960's TFT technology was in competition with single

crystal silicon MOSFET for the integrated circuit field. Due to the rapid progress of the latter and the difficulty in consistently producing good quality devices of the former, TFTs were not successful at that time. However, the application of TFTs to displays will not be given up. The first active matrix LCD (AMLCD) was realized in 1973. Fig. 2.1 shows (a) the cross-sectional view of the whole panel, and (b) the storage capacitor-on-gate of one sub-pixel design.

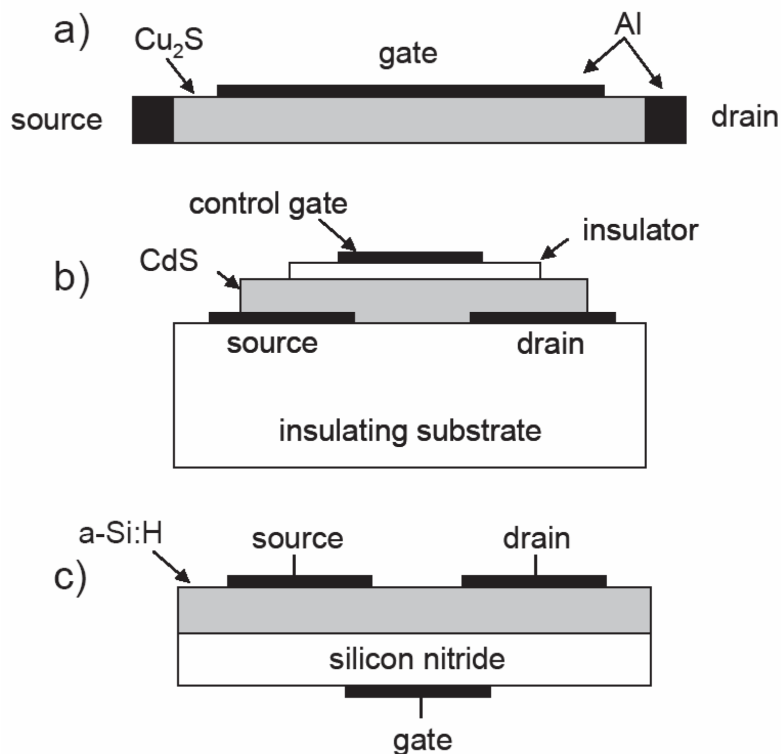

Fig. 2.2 Schematic cross-sectional views of TFTs: (a) adapted from Lilienfeld [55] at U.S. Patent 1930; (b) Weimer [56] at 1962 IRE; and (c) Spear and LeComber [57] at 1979 IEEE.

2.2 Overview of thin film transistor

Although the concept of a thin film field-effect transistor was presented as early

as 1925 and patented in 1930 [55] (see Fig. 2.2(a) where an adaptation of the cross section of the device is shown), the first TFT was demonstrated by P. K. Weimer of RCA Laboratory in 1961 [58]. The represented device is now called a staggered structure, which was composed of polycrystalline cadmium sulfide, similar to those developed for photo detectors, and monoxide as insulator films. The simplified structure is shown in Fig. 2.2(b).

In LCD application, the first CdSe TFT was used as a switching element by Brody et al. in 1973 [59]. Even though the many successful demonstrations of TFT LCDs, the industry did not enter in this market until the report on the feasibility of doping amorphous silicon (a-Si:H) by the glow discharge technique [57, 60]. LeComber, Spear and Ghaith reported the first a-Si:H TFT in 1979s [61], whose structure is indicated in Fig. 2.2 (c). The hydrogenated amorphous silicon could be doped with donors or acceptors to reduce n- or p-type conductivity, in contrast to pure amorphous silicon in previous investigation [62]. Furthermore, LeComber et al. demonstrated TFT which fitted criteria for driving liquid crystal display, as published by Brody [59]. The first polycrystalline silicon grown by chemical vapor deposition was employed to achieve good electrical properties, which was proposed by Depp et al. [63] in 1980s. In order to achieve good electrical performance, chemical vapor deposition was used for the polycrystalline silicon growth, the gate insulator SiO_2 grown at 1050 3 thermally, quartz was utilized as substrates for the poly-Si TFTs.

IBM [64] and Mitsubishi [65] groups used laser recrystalization approach to improve the mobility and threshold voltage of poly-Si TFTs by 1982, and an electron mobility of 400 cm^2/Vs was obtained. The purpose of mobility improving was ot integrate the driving circuits matched with providing pixel TFTs. In general, the a-Si

TFT technology is more popular, which could be used for commercial products such as AMLCDs in portable computers application. However, for high speed response application, poly-Si TFTs are superior to a-Si TFTs in mobility performance. For the reason, the pixel transistors and high speed circuits must be operated in coordination. Recently, TFTs have undergone extensive evolution, development, and refinement. The potential for new applications, lightweight, mechanically robust electronics for displays and other devices on flexible substrates have motivated considerable research on new materials [65–68] and improved processes [69,70] for fabricating thin film transistors. More recently, transparent electronics are nowadays a crucial technology of optoelectronic devices. Oxide semiconductors are very interesting materials because they combine simultaneously high/low conductivity with high visual transparency and have been widely used in a variety of applications (e.g. antistatic coatings, touch display panels, solar cells, flat panel displays, heaters, defrosters, optical coatings, among others) for more than a half-century. A new generation of oxide semiconductors are being studied and applied as the active material to TFT, in special zinc oxide (ZnO). Transparent oxide based semiconductor transistors have been proposed using as active channel non-doped ZnO, because of its low photosensitivity, no environmental concerns, and especially high mobility [50, 51, 71–76].

Table 2.2 summarizes the processing methods employed in fabrication of several transparent channel-layer TFTs and their electrical performance characteristics. All the channel mobility, current ratio, and threshold voltage can be compatible to amorphous Si TFTs.

Table 2.2 Processing methods employed and electrical performance characteristics for several fully transparent ZnO TFTs.

Technique	Temperature (3)	Channel mobility (cm^2/V s)	I_{on}/I_{off}	V_{th}(V)	I_{sat} (μA)
Ion beam [73]	600-800	0.3-2.5	10^6	10-20	70
Sol gel [76]	700	0.2	10^7	No mentioned	14
Pulsed laser	450	0.031-0.97	10^6	-1.0 to 2.5	80
Rf magnetron [76, 77]*	room temp	20-70	5×10^5	1.8	1000

*The devices present some instability and after several measurements they collapse.

One of the main advantages exhibited by these transistors rests on the influence of the electron channel mobility which leading to higher drive current and faster device operating speed. Oxide-based transistors have recently been proposed as active channel [29, 30, 51, 71-77]. Among them, wurtzite structured ZnO thin films have been studied as the active layer in the TFTs! because of its low cost, low photosensitivity, no environmental concerns, and especially high mobility. In fact, ZnO has the greatest potential to grow high quality crystalline zinc oxide at low temperature. This is particularly advantageous for electronic drivers, which need to be processed at temperature that is low enough to be compatible with plastic substrates. Nowadays, TFTs based on α-Si:H have presented some limitations, such as light

sensitivity, light degradation, and low mobility. On the contrary, TFTs based on ZnO are transparent in the visible region of the spectra and less light sensitive. Besides, because of their high transparency, high mobility, simple processing method, and low cost, ZnO is presently attracting much attention due to its possibilities for replacing amorphous Si that has been widely used as the channel layer in conventional TFTs [71-73].

2.3 Transparent metal oxide semiconductors

Transparent property is nowadays a new target for materials development in electronics application. The simultaneous existence of optical transparency and electrical conductivity require a wide band gap (≥3 eV) material which due to the large electro negativity of oxygen [84], doping is a general method for modulate the Fermi level close enough to the conduction (valence) band to induce mobile electrons (holes). For the relatively low mobility exhibited by this class of materials, typical transparent conductors used in passive applications are degenerately doped in order to maximize their conductivity.

Transparency oxide semiconductors are currently utilized in a number of applications, including thin-film solar cells and flat-panel displays. The first report of p-type conductivity in a transparent material ($CuAlO_2$) came in 1997 [81]. After that, a number of new p-type as well as n-type transparent conducting materials have been discovered. Table 2.3 lists known n-type semiconductors along with typical values of important thin film electrical and optical properties (optical bandgap, average transmission in the visible region, Hall mobility, carrier concentration, and conductivity) as available. In Table 2.3, Eg^{opt} denotes optical bandgap, T denotes

typical optical transmission in the visible region, μ_H denotes typical Hall mobility, n denotes typical carrier concentration, and ρ denotes typical resistivity.

Table 2.3 Thin film electrical and optical properties of n-type transparent conductors.

Material	E_g^{opt} (eV)	T (%)	μ_H (cm^2V^{-1} s)	n (cm^3)	ρ (Ω-cm)
$CuAl_2O$ [81, 82]	3.5	70-80	0.13	3×10^{19}	3.33
$CuGaO_2$ [83, 84]	3.6-4.3	70-85	0.23	1.7×10^{18}	100
$CuInO_2$ * [85]	3.9	50-80			3.57×10^{2}
CdO [86]	2.2-2.6	75	220	10^{19}-10^{21}	2×10^{-3}
Cd_2GeO_4 [87]	3.15			1.3×10^{18}	3.3×10^{-1}
Cd_2SnO_4 [86-89]	2.9-3.1	90	35-60	1-7×10^{20}	1.4-12×10^{-4}
In_2O_3 [90-92]	3.7	80-90	10-40	$\leq10^{21}$	$\geq10^{-4}$
$GaInO_3$ [93]	3.3	90	10	10^{20}	2.5×10^{-3}
SnO_2 [90, 91, 94]	3.6	80-90	5-30	$\leq10^{20}$	$\geq10^{-3}$
$Zn_2In_2O_5$ [88, 95]	2.9	80	12-20	2.4-5×10^{20}	1-4×10^{-3}
$ZnSnO_3$ [96, 97]	3.5	80	7-12	10^{20}	4-5×10^{-3}
Zn_2SnO_4 [83, 85, 88]	3.3-3.9	90	12-26	6-30×10^{18}	1.5×10^{-2}

*Bipolar conductive material [81, 94]

2.4 Zinc oxide

Zinc oxide, known as zincite in mineralogy, was first described in North America around 1810 as the red oxide of ZnO is one of zinc. It is silvery-gray colour in pure form. Zinc oxide can take the form of two different crystallographic structures namely

the zinc-blend structure and wurtzite structure (show as Fig. 2.3). The zinc-blend structure is composed of two interpenetrating face-centered cubic (fcc) sub-lattices, while the wurtzite structure consists of two interpenetrating hexagonal close packed (hcp) sub-lattices, which have the similar properties to GaN [100].

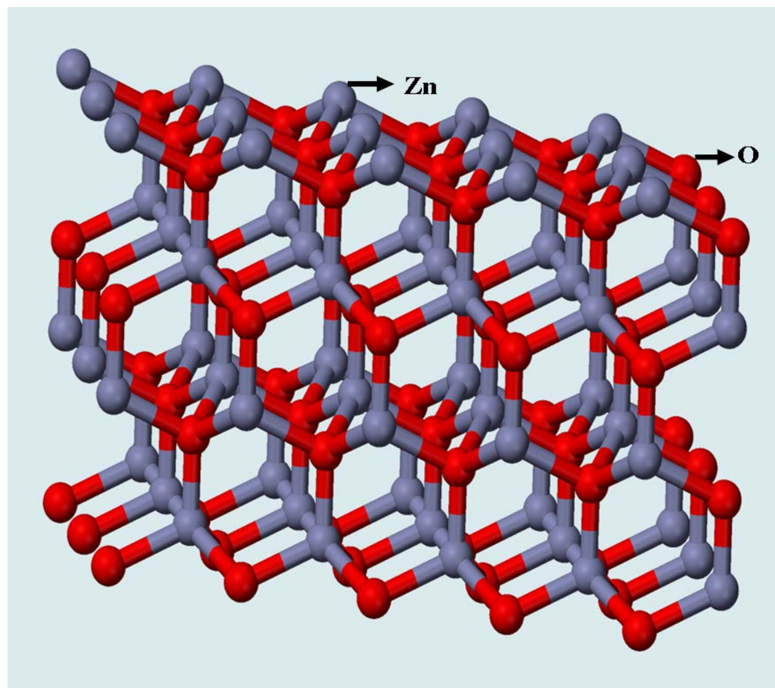

Fig. 2.3 The hexagonal (wurtzite) crystal structure of ZnO

ZnO is one of the group Ⅱ-Ⅵ materials, in the new century, gradually becomes the new focus in material research because it has a wide direct band gap (E_g= 3.3eV, while E_g= 3.4eV for GaN [100]) at room temperature (RT), a high exciton binding

energy (E_b=60meV, while E_b=28meV for GaN [101]) and a direct transition character, band states arising from point defects, interstitial zinc ions, oxygen vacancies or dislocations, which allow its use in a number of applications. It is one of the common transparent conducting materials [102]. Also, ZnO can function as a phosphor (cathodoluminescent [103], photoluminescent [104, 105], electroluminescent [106]); as a thin film chemical sensor [107]; and as a piezoelectric material [108]. The band gap energy of ZnO could be changed via substituting various cation ions into the lattice. For the electrical properties of ZnO-based device, controlling over the carrier concentration of ZnO is important. The carrier concentration of ZnO was not only affected by the intrinsic crystal defects (the interstitial zinc ions and oxygen vacancies) but also influenced by the extrinsic impurities, called dopants. The intrinsic defects and dopants determine the domination of the ZnO were electrons or holes. The basic physical properties of ZnO are summarized in Table 2.4 [109]. Since ZnO has melting temperature as high as 2248K. The strength of Zn-to-O bond is larger than that of Ga-to-N. Moreover, ZnO could resistive to high energy radiation [110-112], which is suitable for application in air. These excellent properties of ZnO make a good candidate material for optical devices, such as blue LED's, and semiconductor devices besides widely used GaN [113].

ZnO thin films have been deposited using a number of methods, including reactive sputtering (DC [114], RF [114], and ion beam [115]), activated reactive evaporation (ARE) [116], spray pyrolysis [117], sol-gel [118], laser ablation [119], pyrosol [77], metal-organic chemical vapor deposition (MOCVD) [74], and electrochemical reaction [75]. Among these, solution route is of particular interest because of its simplicity, low cost and the large area of its coatings.

Table 2.4 Physical properties of wurtzite ZnO.

Property	Value
Lattice parameters at 300K:	
$\boldsymbol{a_0}$	0.32495nm
$\boldsymbol{c_0}$	0.52069
$\boldsymbol{a_0/c_0}$	1.602(1.633 for ideal hexagonal structure)
u	0.345
Density	5.606 g/cm^3
Stable phase at 300K	Wurtzite
Melting point	1975 3
Thermal conductivity	0.6, 1-1.2
Linear expansion coefficient (/ 3)	a_0: 6.5×10^{-6} , c_0: 6.5×10^{-6}
Static dielectric constant	8.656
Refractive index	2.008, 2.029
Energy gap	3.4eV(direct band gap)
Intrinsic carrier concentration	< 10^6 cm^{-3}
Exciton binding energy	60meV
Electron effective mass	0.24
Electron Hall mobility at 300K for low n-type conductivity	200 cm^2/Vs
Hole effective mass	0.59
Hole Hall mobility at 300K for low p-type conductivity	5-50 cm^2/Vs

2.5 Device structure of Thin Film Transistor

The four basic TFT structures are showed in Fig. 2.4, which have co-planar top-gate, co-planar bottom gate, staggered top-gate, and staggered bottom-gate [123]. Electrodes placement distinguished the various structures, i.e. electrodes are placed on opposite sides of the interface (and hence the channel) for staggered structures, while electrodes are placed on the same side of the interface for the co-planar structure.

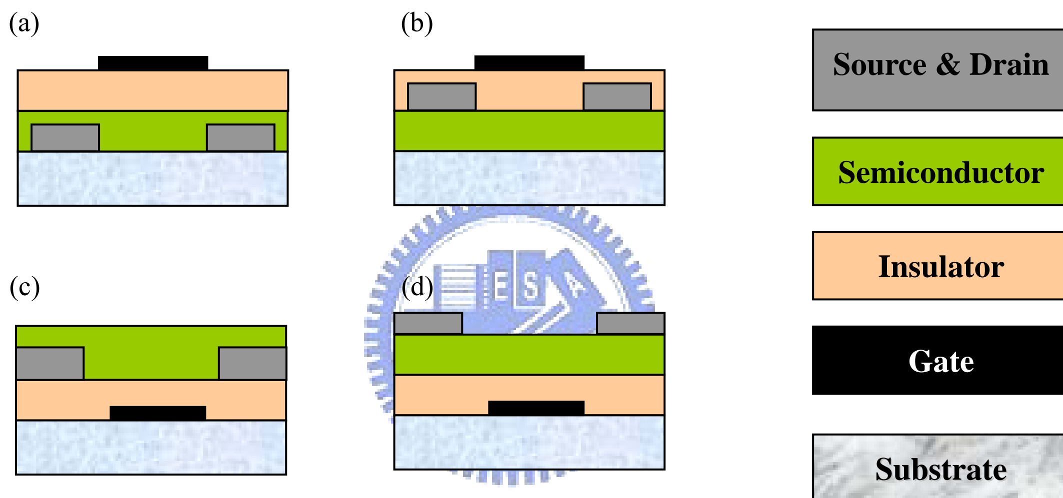

Fig. 2.4 Four basic TFT structures: (a) co-planar top gate, (b) co-planar bottom gate, (c) staggered top gate, and (d) staggered bottom gate.

Process integration is determined on the use of different structures. In the coplanar top-gate structure, the semiconductor is deposited first. Therefore, the maximum semiconductor processing temperature is limited only by the semiconductor and the substrate. The co-planar structure is difficult to realize in some technologies, damage from implantation cannot be remedied. This implies that the channel must be protected during implantation.

For both bottom-gate structures, the insulator is deposited first. The channel

layers would not be damaged by plasma-induced, such as RF sputtering or plasma-enhanced chemical vapor deposition (since insulator deposition typically requires the use of a higher power as compared to deposition of other layers).

2.6 Basic operation of TFT device

For the general principles just discussed, a TFT, the structure and energy band diagrams as showed in Fig. 2.5 Talking the semiconductor to be n-type, consider first the application of a positive bias. The equilibrium band diagram shown in Fig. 2.5(b) assumes an ideal situation, i.e. there is no charge in the semiconductor before the application of a gate bias.

Consider several biasing schemes showed in Fig. 2.3, $V_{GS} < 0$, $0 \leq V_{GS} \leq V_{th}$, and $V_{GS} = V_{th}$, where V_{GS} is the gate-source voltage and V_{th} is the threshold voltage. For the application of a small negative sloping of the energy bands in both the insulator and semiconductor, as displayed in Fig. 2.5(b). It is clear that the concentration of majority carrier electrons has been decreased and depleted, in the vicinity of the insulator-semiconductor interface. A similar conclusion results from charge considerations. Setting $V_{GS} < 0$ places a minus charge on the gate, which in turn repels electrons from the insulator-semiconductor interface and exposes the positively charged donor sites. This particular situation, where the electron concentrations at the insulator- semiconductor interface are less than the background doping concentration, is known for obvious reasons as depletion. On the other hand, application of a small positive gate bias ($0 \leq V_{GS} \cdot\leq V_{th}$) attracts electrons towards the interface, creating an accumulation layer (or channel) near the interface and a depletion region in the bulk. Biasing in this “subthreshold” regime causes downward

band bending in the insulator and the semiconductor (near the interface), as shown in Fig. 2.3(d). Increasing the gate bias modulates the conductivity of the surface layer and is reflected in an increased degree of band bending. The gate voltage at which there is an appreciable electron carrier density present at the interface establishes the threshold voltage (i.e. $V_{GS} = V_{th}$).

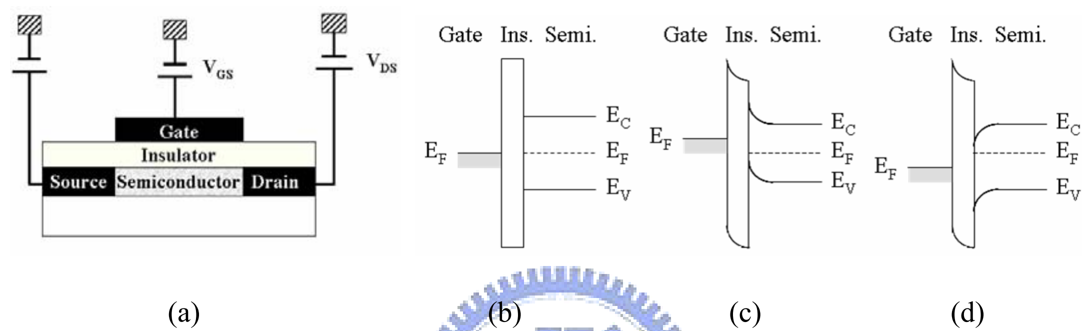

Fig. 2.5 (a) The basic structure of a TFT and the corresponding energy band diagrams as viewed through the gate for several conditions, including (b) equilibrium, (c) $V_{GS} < 0$ and (d) $V_{GS} > 0$.

The application of $V_{GS} > 0$ lower E_F in the gate relative to E_F in the semiconductor and causes a positive sloping of the energy bands in both the insulator and semiconductor. As show in the result energy band diagram, Fig. 2.3(d), the major conclusion to be driven is that the electron concentration inside the semiconductor increases as one approached the insulator-semiconductor interface. This particular situation, where the majority carrier concentration is greater near the insulator-semiconductor interface than in the bulb of the semiconductor, is known as accumulation.

Now that channel formation has been established, application of a positive voltage on the drain attracts electrons towards the drain and accounts for the drain

current, I_D. Initially, the channel is modeled as a resistor, i.e. linearly increasing drain current with drain-source voltage, V_{DS}. Continuing to increase the drain voltage obviously causes the channel to narrow more and more, especially near the drain, until eventually the top and bottom depletion regions touch in the near vicinity of the drain. The complete depletion of the channel, touching of the top and bottom depletion regions, is an important special condition and is referred to as "pinch-off". When the channel pinches off inside the device, the slop of the I_D-V_D characteristic becomes approximately zero, negating the effect of the surface accumulation layer, and the drain bias at the pinch-off point is given the designation V_{Dsat}. For drain biases in excess of V_{Dsat}, the I_D-V_D characteristic saturates, that is, remains approximately constant at the I_{Dsat} value.

Chapter 3

Experiments and measurement techniques

3.1 Experimental methods

3.1.1 The sol-gel method

Sol-Gel method is one of the promising processes to prepared high quality thin films at relative low temperatures compared to other depositions. The first step to form the gels in the sol-gel process is hydrolysis, a hydroxyl attached to the metal atoms as in the following reaction [124]:

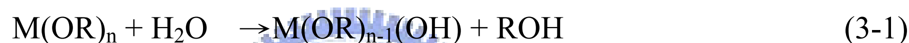

$$M(OR)_n + H_2O \rightarrow M(OR)_{n-1}(OH) + ROH \quad (3\text{-}1)$$

The R and ROH represented a ligand and an alcohol. The second step of sol-gel process is polymerization which was achieved by two partially hydrolyzed molecules linked together, such as

$$M(OR)_n + M(OR)_{n-1}(OH) \rightarrow M_2O(OR)_{2n-2} + H_2O \quad (3\text{-}2)$$

A long chain molecule could be obtained from the reaction of hydrolysis and polymerization mentioned above. Since the coating ability and preferential direction of thin preparation of thin films depend on the molecules, the reaction plays an important role in the preparation of thin films. In an organic system, the solute is usually the metal alkoxide, such as $M(OR)_n$ which M is represented metal and R represented alkyl group(CH_3, C_2H_5,…..etc.).

As a result of the sol-gel solution still maintains liquid phase before gelled, and is easy to film on different substrates. There are many coating methods, such as dip

coating, spray coating, and spin coating. The quality of the thin films depends on coating method and coating conditions.

Among the wet coating approaches, spin coating is an easier way to obtain uniform thin films. The quality of the thin films is influenced by the following procedures; the cleanliness of the substrates, the chemical properties of the solution (viscosity, stability, and volatile rate), the speed and time of spin, and the adhesion between the solution and substrates. The most significant disadvantage of spin coating is that if used for small or asymmetric substrates.

There are many advantages of the conventional sol-gel method. The cost and maintenance of the facilities of the sol-gel are much lower than that of vacuum techniques such as sputtering or chemical vapor deposition. In addition, the precursor solution prepared by sol-gel method could be purified by crystallization and distillation methods; thereby the high purity thin films could be obtained.

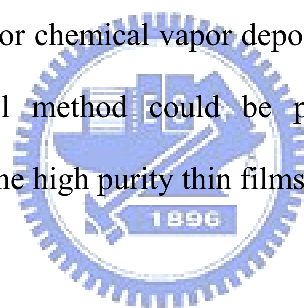

3.1.2 Synthesis of the precursors

Zinc acetate dehydrate ($Zn(CH_3COO)_2 \cdot 2H_2O$) is used as precursor or mixed with magnesium acetate tetra-hydrate ($Mg(CH_3COO)_2 \cdot 4H_2O$) were dissolved in 2-methoxyethanol, and then added monoethanolamine (MEA) to the solution. The concentration of metal ions in ZnO or $Zn_{1-x}Mg_xO$ sols were controlled between 0.375M and 0.75M, the mole ratio of Mg^{+2} can be varied from 0 to 0.36 (for x values); after 2 hr stirred for the mixed solution at 60 3 !a clear and homogenous sol was obtained. The $Zn_{1-x}Mg_xO$ thin film was filmed on the alkali-free glass (Corning 1737) using spin coating method, which was under different spin speed. These as-coated films were dried at 100-120 3 for 10 minutes, and then annealed at 150 to 550 3

respectively for 1 hr in air atmosphere. The flow chart of the precursor preparation and ZnO films processing is showed in Fig. 3.1.

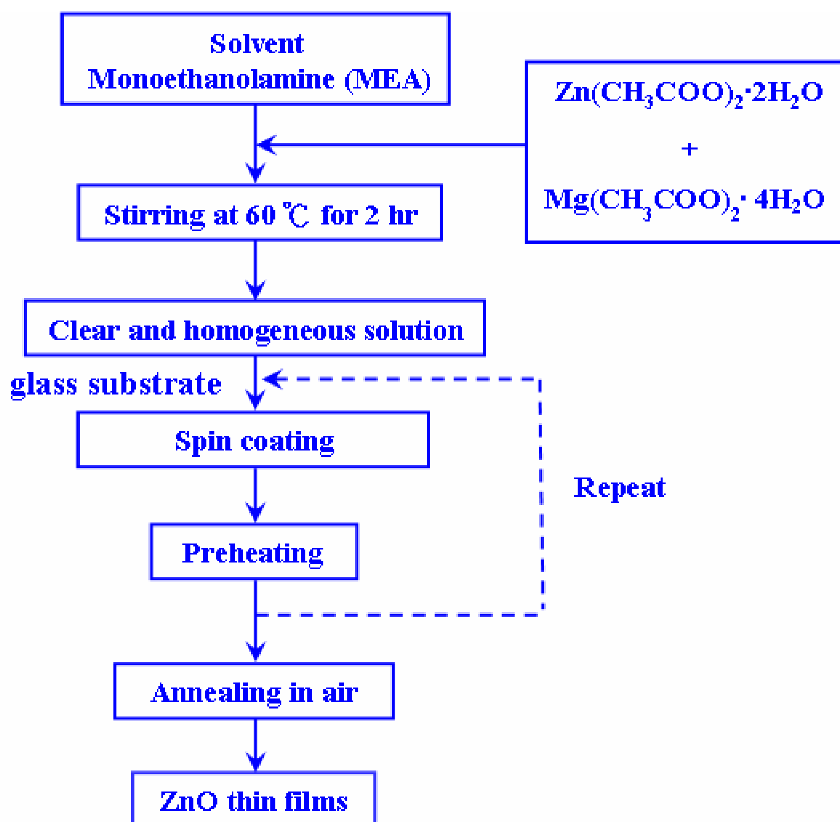

Fig. 3.1 The flow chart of the precursor preparation and ZnO films processing by spin coating.

3.1.3 Chemical bath deposition (CBD)

CBD was carried out in a beaker with a soak aqueous solution containing 0.1 mol/L zinc nitrate and 0.03 mol/L dimethylamineborane placed upon a heater-stirrer during the growth process at temperature range of 60 to 65℃. Prior to deposition, the glass substrate was activated by an industrially employed two-step Pd/Sn process using sensitizer ($SnCl_2$, 1 g/L; 32% HCl, 1 ml/L) and activator ($PdCl_2$, 0.1 g/L; 32%

HCl, 0.1 mol/L) [20, 21], then immersed the substrate in the soak solution for 30 min. The thickness of the ZnO film could be controlled by tuning the soak concentration or immersing time. Finally, the substrate was rinsed with DI water and dried with nitrogen gas then baked on hot-plate at 100 3 for 5 min.

3.1.4 The fabrication of thin film transistor devices

The typical thin film transistors were fabricated by following procedures. All of conductive layer (source, drain, or gate electrode) was deposited by sputtering on glass substrate. Silicon dioxide or silicon nitride was served as the gate insulator with a thickness of 300nm by plasma-enhanced chemical vapor deposition (PECVD). The channel width and length were defined by photolithography. Finally, the $Zn_{(1-x)}M_xO$ (M = Mg) thin film were deposited by solution methods with the same processes mentioned in section 3.1.1 and 3.1.2 the above.

3.2 Characterization for materials and devices

3.2.1 Scanning electron microscopy (SEM)

The scanning electron microscopy (SEM) was used the secondary electron mode to observe the morphology of ZnO materials and electronic device. The model of the SEM used here is Hitachi 4700.

3.2.2 Transmission electron microscopy (TEM)

One of the typical characters of nano-phase materials is the small object size. Although some structural features can be revealed by x-ray and neutron diffraction, direct imaging of nanomaterials is only possible using high resolution transmission

electron microscopy (HRTEM, FEI / Philip Tecnai F20). TEM is a unique technique because it can produce a real space image on the atom distribution in the nanocrystal surface. With a finely focused electron probe, the structural characteristic of a single nanomaterial can be fully understood. Normally, the chemical analysis system, the energy disperse X-ray spectrometer (EDX), was attached on TEM system.

3.2.3 X-ray diffraction spectroscopy

X-ray diffraction analysis of the ZnO specimens was carried out by using an X-ray diffractometry (XRD) (Philips PW3710 or MAC Science MAXP3) with conventional θ/2θ scans. The X-ray was generated by a Cu target (Cu Kα) operated at 50kV and 60mA, and the scanning speed was 0.02 deg/step, 1deg/min from 20° to 80°.

3.2.4 UV absorption

UV absorption was done in UV-VIS-NIR scanning spectrophotometer (SHIMADZU UV-3101PC) at wavelengths from 350 to 800 nm by employing both a tungsten-iodide (WI) lamp for the visible region and a deuterium (D2) lapmp for the ultraviolet region.

3.2.5 Thermal gravimetric analysis

Thermal weight loss was measures by thermal Gravimetric Analysis (TGA; Perkin-Elmer, thermal gravimetric analyzer 7), which is a simple analytical technique that measures the weight loss (or weight gain) of a material as a function of temperature. As materials are heated, they can loose weight from a simple process

such as drying, or from chemical reactions that liberate gasses. Some materials can gain weight by reacting with the atmosphere in the testing environment. Since weight loss and gain are disruptive processes to the sample material or batch, knowledge of the magnitude and temperature range of those reactions are necessary in order to design adequate thermal ramps and holds during those critical reaction periods.

A sample of the test material is placed into a platinum cup that is supported on, or suspended from an analytical balance located outside the furnace chamber. The balance is zeroed, and the sample cup is heated according to a predetermined thermal cycle. The balance sends the weight signal to the computer for storage, along with the sample temperature and the elapsed time. The TGA curve plots the TGA signal, converted to percent weight change on the Y-axis against the reference material temperature on the X-axis.

3.2.6 Hall effect measurement

The importance of the Hall-effect [125-127] is underscored by the need to determine accurately carrier density, electrical resistivity, and the mobility of carriers in semiconductors. The Hall-effect provides a relatively simple method for doing this. Because of its simplicity, low cost, and fast turnaround time, it is an indispensable characterization technique in the semiconductor industry and in research laboratories. It is listed as one of the most-commonly used characterization tools.

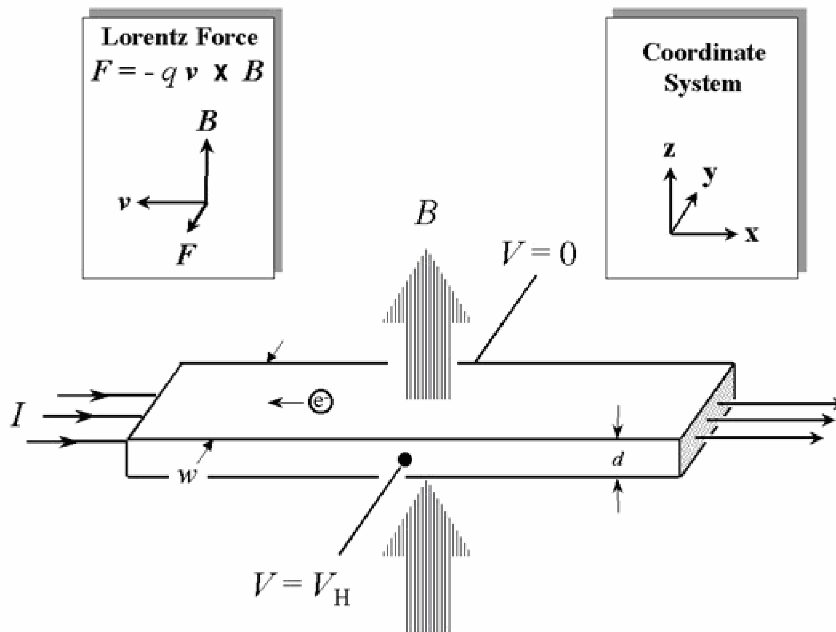

Fig. 3.2 Schematic of the Hall effect in a long, thin bar of semiconductor with four ohm contacts. The direction of the magnetic field *B* is along the z-axis and the sample has a finite thickness *d*.

The basic physical principle underlying the Hall-effect is the Lorentz force. When an electron moves along a direction perpendicular to an applied magnetic field, it experiences a force acting normal to both directions and moves in response to this force and the force affected by the internal electric field. For an n-type, bar-shaped semiconductors shown in Fig. 3.2, the carriers are predominately electrons of bulk density *n*. Assume that a constant current *I* flow along the x-axis from left to right in the presence of a z-directed magnetic field. Electrons subject to the Lorentz force initially drift away from the current line toward the negative y-axis, resulting in an excess surface electrical charge on the side of the sample. This charge results in the Hall voltage, a potential drop across the two sides of the sample. (Note that the force

on holes is toward the same side because of their opposite velocity and positive charge.) This transverse voltage is the Hall voltage V_H and its magnitude is equal to *IB/qnd*, where *I* is the current, *B* is the magnetic field, *d* is the sample thickness, and *q* (1.602 x 10^{-19} C) is the elementary charge. In some cases, it is convenient to use layer or sheet density ($n_S = nd$) instead of bulk density. One then obtains the equation

$$\boldsymbol{n_S = IB/q|V_H|} \tag{3.3}$$

Thus, by measuring the Hall voltage V_H and from the known values of *I*, *B*, and *q*, one can determine the sheet density n_s of charge carriers in semiconductors. If the measurement apparatus is set up as described later in Section III, the Hall voltage is negative for *n*-type semiconductors and positive for *p*-type semiconductors. The sheet resistance R_S of the semiconductor can be conveniently determined by use of the van der Pauw resistivity measurement technique. Since sheet resistance involves both sheet density and mobility, one can determine the Hall mobility from the equation

$$\boldsymbol{\mu = |V_H|/R_S IB = 1/(qn_S R_S)} \tag{3.4}$$

If the conducting layer thickness *d* is known, one can determine the bulk resistivity ($\rho = R_S d$) and the bulk density ($n = n_S/d$)

3.2.7 Atomic force microscope (AFM)

The atomic force microscope (AFM) is a very high-resolution type of scanning probe microscope, with demonstrated resolution of fractions of a nanometer, more than 1000 times better than the optical diffraction limit. The AFM was invented by Binnig, Quate and Gerber in 1986, and is one of the foremost tools for imaging,

measuring and manipulating matter at the nanoscale. The term 'microscope' in the name is actually a misnomer because it implies looking, while in fact the information is gathered by feeling out the surface with a mechanical feeler.

3.2.8 X-ray photoelectron spectroscopy

The XPS was taken to investigate the bonding energy between each element of thin film. By absorbing a photo, an atom gains an energy amount equal to hν. It then releases an electron to regain its original stable energy state. The released electron retains all the energy from the striking photon, which can escape from the atom and keep it moving. The incident photons usually carry an energy range from 1 to 2keV by XPS analysis.

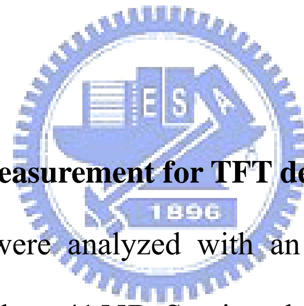

3.3 Electrical properties measurement for TFT devices

The transistor devices were analyzed with an Agilent 4155B semiconductor parameter analyzer. The Agilent 4155B Semiconductor Parameter Analyzer is an engineering instrument that allows the measurement of current-voltage characteristics of microelectronics devices and small circuits with up to eight terminals, also, the dc characterization of semiconductor devices and materials. It stimulates voltage and current sensitive devices, measures the resulting current and voltage response.

Chapter 4

Results and Discussions

4.1 Thin film transistors with active layers of zinc oxide (ZnO) fabricated by low-temperature chemical bath method

4.1.1 Descriptions

Thin film transistors (TFTs) with active channel layers of zinc oxide (ZnO) using a low-temperature chemical bath deposition have been studied. The ZnO films were fabricated on the defined-areas of bottom-gate type TFTs plate by immersing in a chemical bath containing zinc nitrate ($Zn(NO_3)_2.6H_2O$) and dimethylamineborane (DMAB) aqueous solution at 60℃. Silicon oxide (SiO_2) uses as the insulator. Produced TFTs plate is dried in the air at 100℃, specially, without any annealed. Capacitance-voltage (I-V) properties measured through the gate infer that the ZnO channel is n-type. Devices were achieved that I_{on}/I_{off} ratio was more than 10^5, for which the channel mobility on the order of 0.248 $cm^2\ V^{-1}\ s^{-1}$ has been determined.

4.1.2 Conceptions

Zinc oxide (ZnO), a transparent film is very popular used due to its unique optical and electronic properties in solar cells [123], photo detectors [11], light emitting devices [12], gas sensor elements [128], and surface acoustic wave guides [14]. Also, ZnO films exhibiting n-type semiconductive characteristic with wide band gap of 3.3 eV, excellent chemical and thermal stability, and can be well-oriented crystalline on various substrate, have recently been studied as the active channel

material in thin film transistors development [51, 71, 129]. Especially, the Hall effect mobility measured at room temperature for single crystals is on order of 200 $cm^2 V^{-1} s^{-1}$ [130].

Several methods are applied to prepare ZnO films, both physical and chemical deposition technologies which include sputtering [15], pulsed laser deposition [131], chemical vapor deposition (CVD) [17], molecular beam epitaxy [18], and sol-gel process [19] etc. However, most of the methods were not well suited for large area coating and low temperature processing. For the issues, chemical bath deposition (CBD) has been attracted technology which is simple and low-cost for fabricating thin film. There are many previous articles discussing the ZnO films using electroless deposition in solution bath and indicating the feasibility of low temperature [21, 23, 132-134]. These make the films good compatibility with substrate materials.

In the present article, we decided the patterning method of ZnO film, and performed the bottom-gate type TFT device with a patterned active channel ZnO film on that used CBD method. Also, the properties of films and characteristics of ZnO-TFT are studied.

4.1.3 Specifics methods

4.1.3.1 Film deposition procedure

The TFTs had a simple bottom-gate device configuration on a Corning 1737 glass substrate (Fig. 4.1 insert), where underlying ITO, 100 nm thick, was used as the gate electrode, selecting a silicon oxide (SiO_2) film for the gate dielectric which thickness was 300nm, and ITO film of 100-nm as the source and drain electrodes. Each source-drain pair that was defined of a channel width W=500 μm wide and

channel length L=10 μm. The active channel pattern was fabricated using standard lithography then processed ZnO film following by CBD technique and yield TFTs after photo resist stripped (Fig. 4.1(a), (b)).

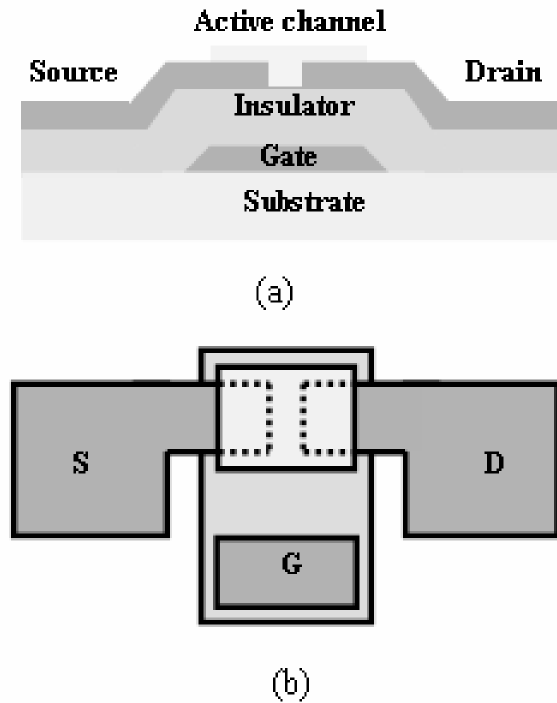

Fig. 4.1 Schematic (a) cross-sectional and (b) top view of the ZnO-based thin-film transistor.

CBD was carried out in a beaker with a soak aqueous solution containing 0.1 mol/L zinc nitrate and 0.03 mol/L dimethylamineborane placed upon a heater-stirrer during the growth process at temperatures 60℃. Prior to deposition, the glass substrate was activated by an industrially employed two-step Pd/Sn process using sensitizer ($SnCl_2$, 1 g/L; 32% HCl, 1 ml/L) and activator ($PdCl_2$, 0.1 g/L; 32% HCl, 0.1 mol/L) [135, 136], then immersed the substrate in the soak solution for 30 min. The thickness of the ZnO film could be controlled by tuning the soak concentration or

immersing time. Finally, the substrate was rinsed with DI water and dried with nitrogen gas then baked on hot-plate at 100℃ for 5 min.

4.1.3.2 Characterization techniques

The deposited crystal structure was identified by X-ray diffractometry (XRD) (Mac Science M18XHF-SRA) using a conventional 2θ scans over a range from 15° to 80° operated at 50KV and 200mA, the morphology was characterized by scanning electron microscopy (SEM; LEO 1530). The transistors were analyzed with an Agilent 4155B semiconductor parameter analyzer. The samples were measured in the dark.

!

4.1.4 Achievements and explanations

The crystallographic structure of the films has been studied by X-ray diffraction. Fig. 4.2 shows the XRD spectrum of ZnO films which were deposited on the SiO_2 surface of a TFT device by soaking in the aqueous solution with 0.1mol/L zinc nitrate and 0.03mol/L DMAB. The diffraction peaks (100), (002), and (101) indicate that, the produced ZnO crystals are wurtzite structure, and the morphologies consist of hexagonal column. In addition, mainly peak (002) indicates preferential c-orientation of the crystals [137], in other words that grains are mainly grown with c-axis vertical to the substrate. The regular direction growth can be explained as follows: For the electroless deposition, the crystalline morphology was led by nucleation and growth conditions. The ZnO film growing in zinc nitrate and DMAB solution followed heterogeneous nucleation [12]. However, on the $SnCl_2/PdCl_2$ pretreatment surface, the primary crystallite will prior to attack and continue to grow.

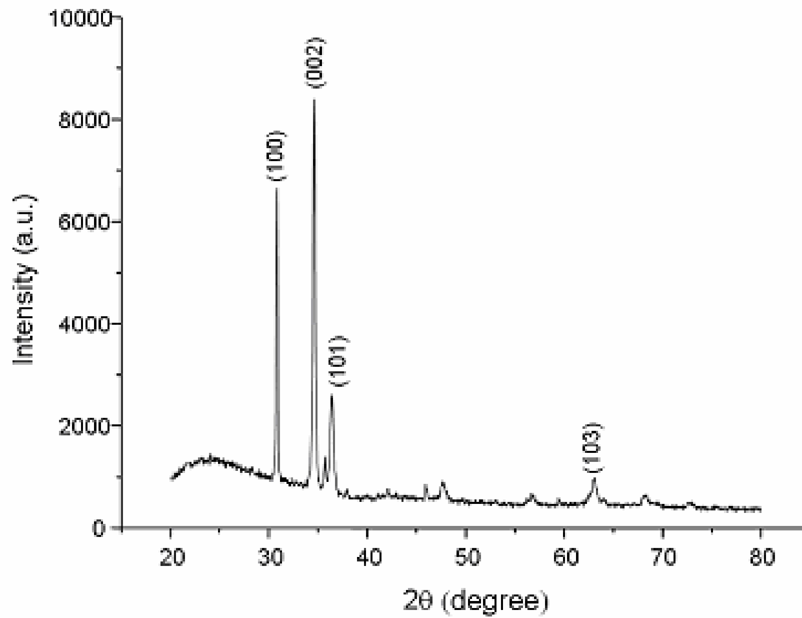

Fig. 4.2 X-ray diffraction spectrum of the ZnO thin film on SiO_2 surface prepared by the CBD.

Fig. 4.3(a) and 3(b) show the image of local ZnO film on TFT device by SEM, where are respectively cross-sectional and plane-view morphology. Hexagonal rods are observed which correspond to the basal plane of the hexagons (Fig. 4.3(a)). The ZnO film is formed of regular arrangement and compact amassment rods vertical to the substrate and the mean thickness is 400nm. As Fig. 4.3(b) shows, the grains are closely packed, that the size is largely from several ten to 200nm. For TFT application the active channel layer with larger grains size and less grain boundary can conduce to the electron mobility.

Fig. 4.4(a) and 4.4(b) show the electrical characteristics of the ZnO-TFT which the active channel layer ZnO was fabricated by CBD method without any annealed.

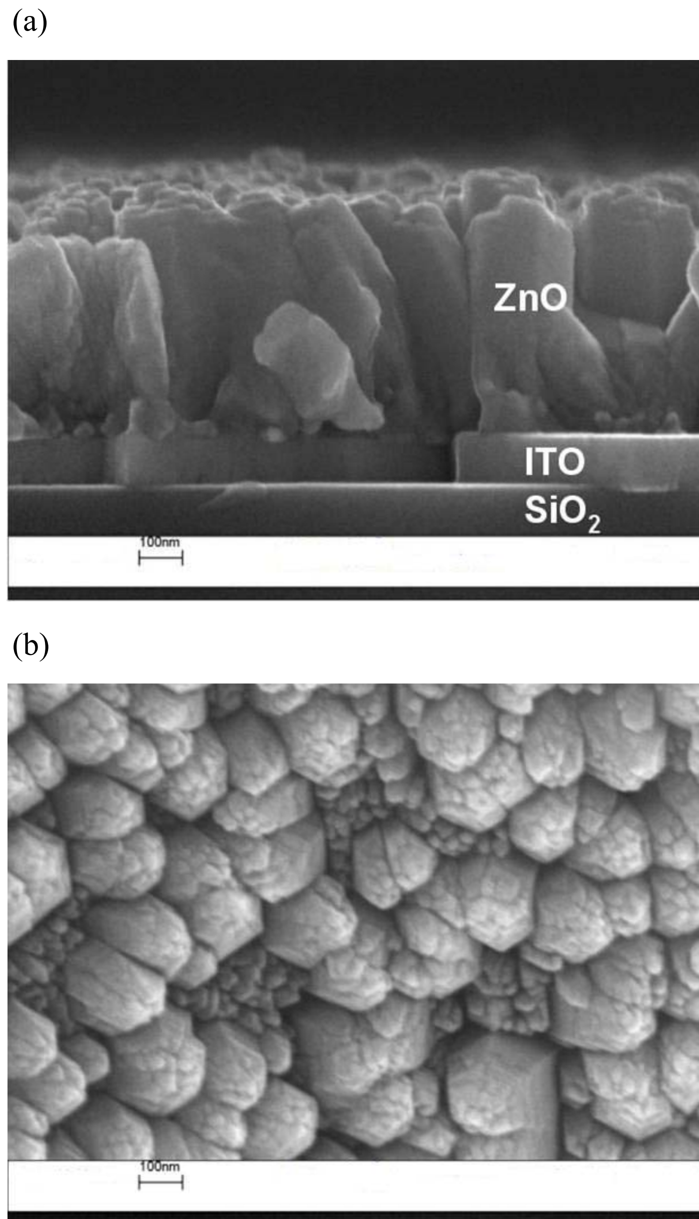

Fig. 4.3 SEM images of ZnO film deposited at 60℃ from 0.1 mol/L zinc nitrate and 0.03 mol/L

Capacitance-voltage (I-V) properties measured through the gate infer that the ZnO channel is n-type. Because some drain current can still be measured at 0 volt of gate voltage (refer to Fig. 4.4(a)), the device is a depletion-mode TFT. By refer to Fig. 4.4(b), the I_{on}/I_{off} ratio was measured more than 10^5. The field effect mobility (μ_{FE})

and threshold voltage (V_{th}) could be calculated by fitting the constant slop line to the plots of the square root of drain current vs gate voltage.

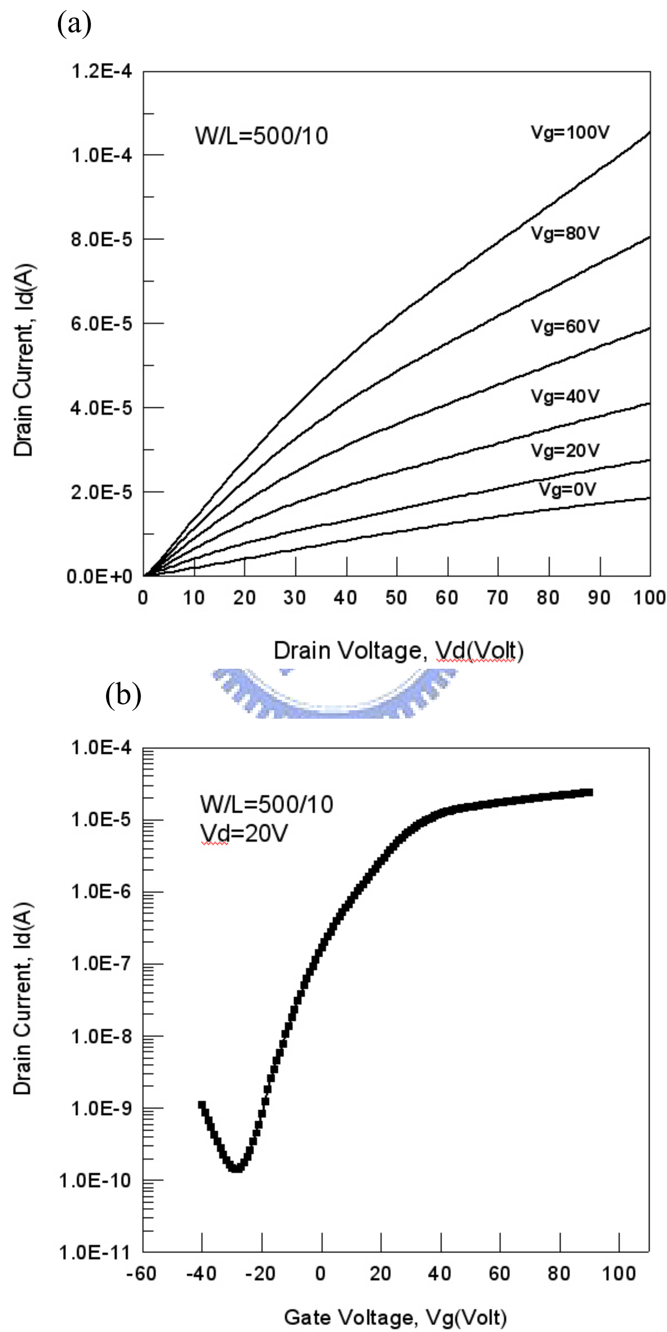

Fig. 4.4 Electrical characteristics of the ZnO-TFT which the active channel layer ZnO was fabricated by CBD method (a) I_d-V_d curve, (b) I_d-V_g curve.

The drain current in the saturated regions is calculated by the following equation.

$$Id_{sat} = \mu_{FEsat}(W/2L)C_I(V_{gs}-V_{th})^2$$

Where W and L are the channel width and length respectively, C_I is the capacitance per unit area of gate insulator. The saturated regions mobility (μ_{FEsat}) was calculated of 0.248 $cm^2\ V^{-1}\ s^{-1}$.

4.1.5 Summary

A ZnO film using for active channel layer of ZnO-TFT was fabricated by CBD in a aqueous solution containing zinc nitrate ($Zn(NO_3)_2.6H_2O$) and dimethylamineborane (DMAB) aqueous solution at 60℃. The grains of the ZnO films are mainly grown with c-axis vertical to the substrate due to high participate of (002), also the ZnO crystals are hexagons (wurtzite structure). According to the present study the TFT device was successful made, it was depletion-mode and achieved that I_{on}/I_{off} ratio was more than 10^5, the channel mobility on the order of 0.248 $cm^2\ V^{-1}\ s^{-1}$ had been determined.

4.2 Cation-Mediated Effects on Zinc Oxide Films Formed by Chemical Bath Deposition

4.2.1 Descriptions

Crystalline ZnO films with a densely packed morphology were grown on a silicon oxide (SiOx) glass substrate by chemical bath deposition (CBD) in an aqueous-solution bath containing magnesium nitrate [$Mg(NO_3)_2.2H_2O$] used as a cation-mediation compound, zinc nitrate [$Zn(NO_3)_2.6H_2O$], and dimethylamineborane (DMAB) at 65℃. Grains of ZnO films grown in nonmediated solution preferentially grew on the (002) plane. In the cation-mediated-solution bath, the films were compressed into a compact morphology by the increased tendency for films to grow in the (002) prefer orientation. The crystalline ZnO film exhibits good optical transmittance of over 90%. Additionally, the direct band-gap value was 3.22 eV, which is less than 3.38 eV, which was obtained using a nonmediated-solution bath. This was due to the lattice constant variation caused by cation mediation.

4.2.2 Conceptions

Crystalline zinc oxide (ZnO) thin films have attracted considerable interest as a transparent conductive oxide, and exhibit n-type semiconductive characteristics with a wide band gap of 3.3 eV. Their electro-optical properties, high electro-chemical stability, large band gap, abundance in nature and absence of toxicity make them very popular for use in solar cells [123], photo detectors [11], light-emitting devices [12], gas sensor elements[143] and surface acoustic wave guides.[14]

Many methods for preparing ZnO films, which include both physical and

chemical depositions, such as sputtering [15], pulsed laser deposition [131], chemical vapor deposition (CVD) [49], molecular beam epitaxy [19] and sol-gel process [27]. Chemical bath deposition (CBD) [143], a solution process is of particular interest because of its simplicity, low cost and the large area of its coatings. However, it is based on the controlled precipitation of the material to form a film upon the substrate surface. We explore the influence of cation-mediation on CBD. In this work, the orientation and band gap of ZnO crystals can be modified, the morphological structural and optical properties obtained using this procedure are demonstrated.

4.2.3 Specifics methods

4.2.3.1 Deposition of films

The ZnO films by using CBD method, made on SiOx which had already been deposited on Corning 1737 glass substrates, were soaked in mixing solutions containing DMAB at a concentration of 0.05M and two recipes of zinc source solution (a) and (b) (in Table 4.1) at 65 ℃ for 30 min. Before deposition, the substrates were activated by an industrial two-step Pd/Sn process using a sensitizer ($SnCl_2$, 1 g/L; 32% HCl, 1 ml/L) and an activator ($PdCl_2$, 0.1 g/L; 32% HCl, 0.1 mol/L) [136, 137]. After activating and CBD process, the substrate must be rinsed in DI (de-ionized) water for 1 min then dried with nitrogen gas, and baked on a hot-plate at 100℃ for 5 min.

Table 4.1 Chemical composition of the solutions used for ZnO film deposition.

Composition	Solution a (M)	Solution b (M)
$Zn(NO_3)_2 \cdot 6H_2O$	0.1	0.1
$Mg(NO_3)_2 \cdot 2H_2O$	------	0.1
DMAB	0.05	0.05
	PH ~ 6.2	PH ~ 6.2

4.2.3.2 Characterization

The crystallographic structure of ZnO films was identified by X-ray diffractometry (XRD) (Philips PW3710) using conventional 2θ scans at 50kV and 60mA. Scanning electron microscopy (SEM; Hitachi 4700) was employed to characterize the morphology and energy dispersive spectroscopy (EDS) verified the composition of the prepared film. Optical transmittance was measured using a UV-VIS-NIR scanning spectrophotometer (SHIMADZU UV-3101PC) at wavelengths from 350 to 800 nm. The band gap of the films was estimated from the absorption coefficient, which was determined from the transmittance and reflectance.

4.2.4 Achievements and explanations

The crystallographic structures of ZnO films were observed by XRD (Fig. 4.5 insert). All the diffraction peaks correspond to ZnO, and no other compound was observed, regardless of the presence of magnesium ions (Mg^{2+}). The diffraction peaks, (100), (002), and (101), of the generated ZnO crystals indicate that the wurtzite

structure and the morphology comprises hexagons. Additionally, the main peak (002) shows the preferential c-orientation of the crystals [137], whose grains are grown mainly with their c-axis perpendicular to the substrate. However, comparing the XRD patterns (Fig. 4.5) with the SEM images [Figs. 4.6(a)-4.6(d)] reveals that the crystalline structure and morphology of the films are strongly affected by the cation-mediated solution that contains Mg^{2+}. According to Saito et al., $SnCl_2/PdCl_2$ treatment can anchor to ZnO nucleus sites using a Pd catalyst [12]; the attack points of Zn^{2+} species and their environment are key parameters that determine the growth of crystals [27].

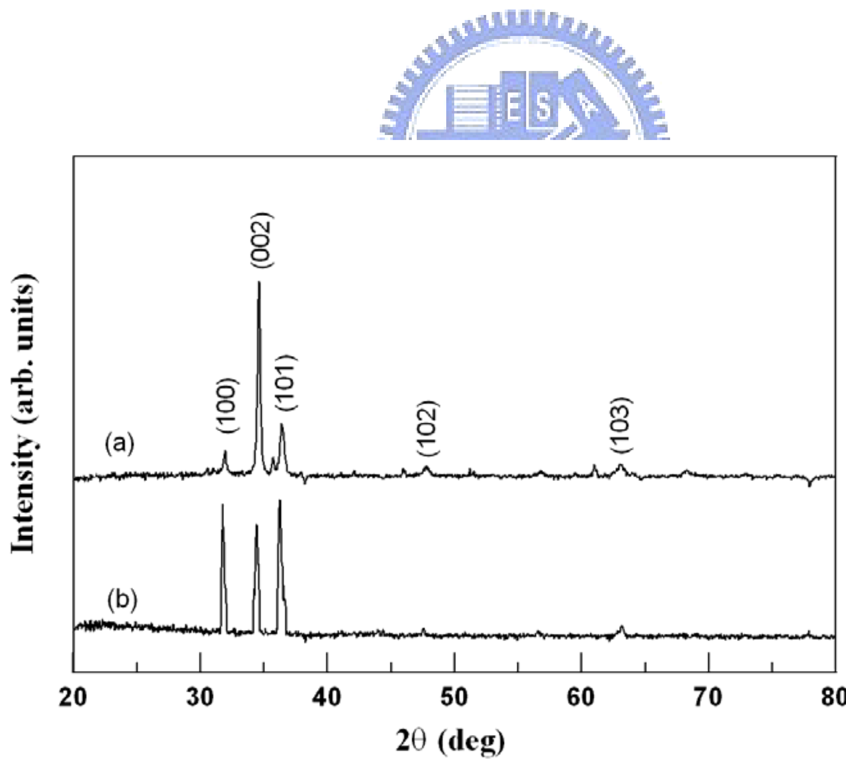

Fig. 4.5 XRD pattern of ZnO films: (a) growth without cation mediation in the solution bath and (b) growth with cation mediation in the solution bath.

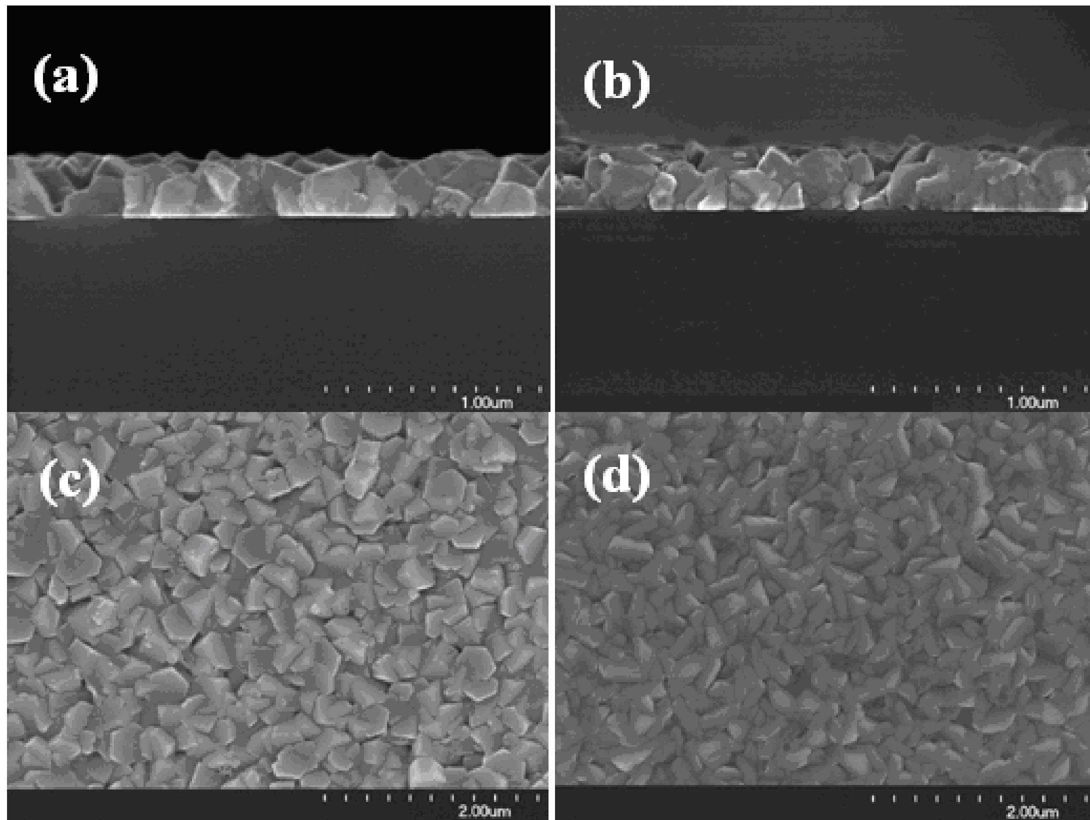

Fig. 4.6 SEM images of ZnO film: (a) cross-sectional morphology and (c) plane-view morphology of film deposited in bath without cation mediation solution; (b) cross-sectional morphology, and (d) plane-view morphology of film deposited in cation-mediated-solution bath.

The ZnO films grown in the cation-mediation bath revealed a strong preferential c-axis (002) orientation as well as (100) and (101) orientations, as shown in the spectrum in Fig. 4.5(b). The film exhibited a compact grain structure, which appeared to be different from that grown without cation mediation. According to Charbonnier and Romand [145] study, Sn^{2+} adsorb on oxygenated groups on the substrate through the formation of Sn–O covalent bonds using $SnCl_2$ solution, i.e., through the sharing of their valence electrons. Then, Pd^{2+} attach on the Sn species via chemical adsorption and are reduced to Pd. The primary ZnO crystallite was concluded to grow

beforehand on the Pd catalyst sites by means of heterogeneous nucleation [12]. Also, the ZnO film formed is typically controlled by the nucleation anchor and the propagation environment; in a cation-mediated soaking solution, the primary ZnO crystal sites are electrolessly deposited selectively on the Pd. The role of Mg^{2+} in enter mining the morphology is suggested to involve the adsorption/desorption of Mg^{2+} during ZnO deposition; the Mg^{2+} are dissociated freely in the weakly acidic soaking solution, and once the ions adsorb on the surface of growing ZnO, they will interfere with the growth, and the atomic packing and growth direction of the film will be affected; thus, the lattice constant and morphology of the film will vary.

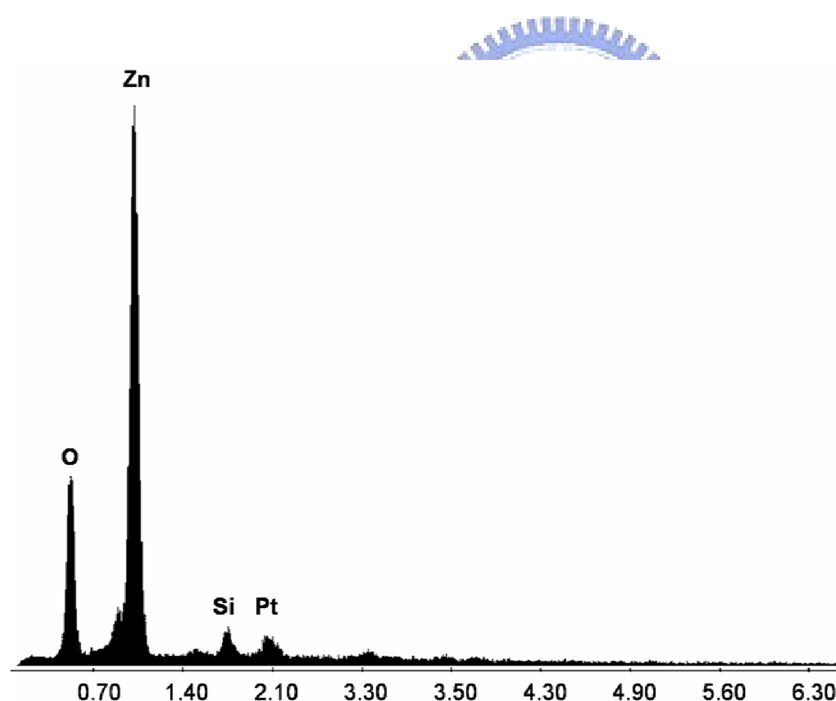

Fig. 4.7 EDS of ZnO film deposited in cation-mediated solution bath.

Since the preferred orientation during grain growth is the (002) direction, the film becomes denser due to the closer packing of grains. On the other hand, the

adsorption/desorption rate of Mg^{2+} is small and only a trace amount of Mg^{2+} is left in the ZnO lattice; therefore, the ZnO film showed no magnesium by EDS analysis (Fig. 4.7 insert). Moreover, Mg^{2+} and Zn^{2+} have similar ionic radii of 0.057 and 0.06 nm[146], respectively. By incorporating Mg^{2+} into the ZnO lattice, a small change in the lattice constants is expected because of the smaller size of Mg^{2+}. As shown in Fig. 4.8, the lattice constants of the cation-mediated ZnO lattice are shrunk in both the a and c axes compared with the nonmediated and bulk ZnO[147].

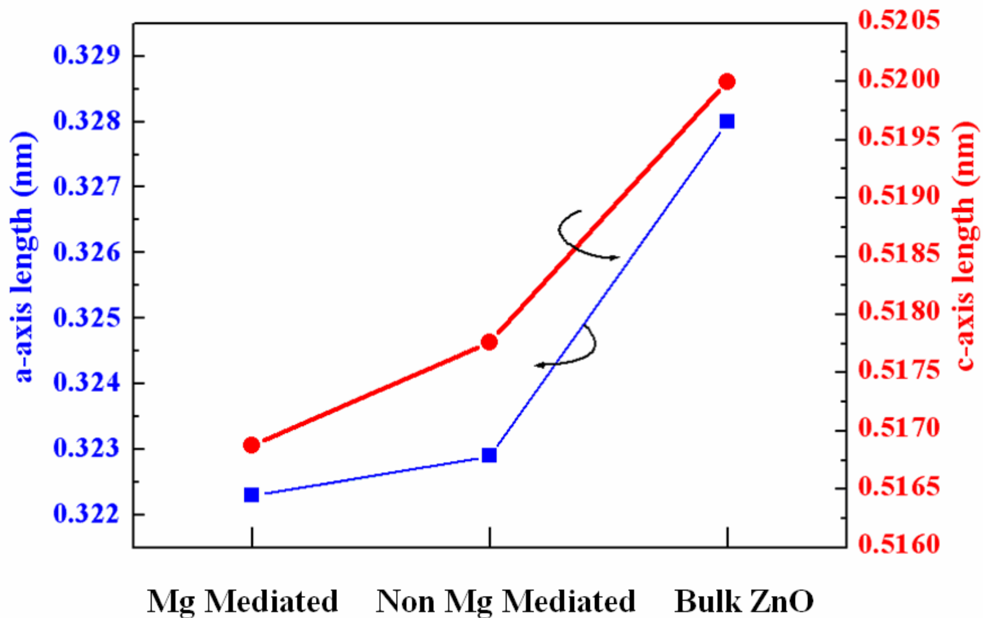

Fig. 4.8 Lattice constants of ZnO in both a and c-axes.

Figure 4.9 shows the optical transmittance of ZnO films in the wavelength range of 380~800 nm, which depended on the solution use for growth. The films were highly transparent in the visible range, with transmittance increasing from 70 to approximately 90% as the wavelength increased from 500 to 700 nm. The optical transmittance exceeded 94% at a wavelength of 800 nm. The average optical

transmittance of the films grown in solution (a) differed from that of those grown in solution (b). The morphology of the films determines their optical characteristics. Films with smoother surfaces and denser grains exhibit higher transmittance. A film deposited in solution (b), in which the grains formed are compact and the surface is smooth, will have high transmittance. In other words, more compact grains correspond to a lower scattering loss of light and increased transmittance. This explanation of the increased transmittance is the most reasonable.

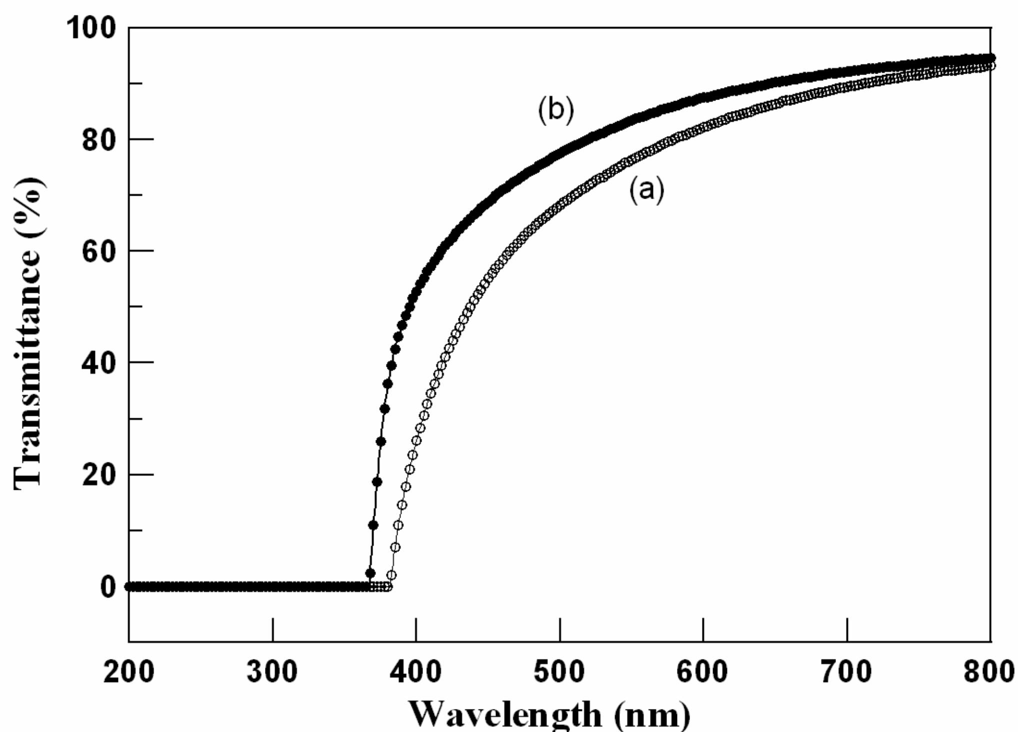

Fig. 4.9 Optical transmittance spectra of ZnO films deposited in (a) bath without cation-mediated solution and (b) cation-mediated-solution bath.

The transmission spectra in the UV region are used to calculate the absorption coefficient, α, from $I=I_0e^{-\alpha t}$ [147], where I is the intensity of the transmitted light, I_0 is

the intensity of the incident light, and t is the thickness of the ZnO film. The transmittance is defined as I/I_0; thus, this equation yields α. The relationship between α and the incident photon energy $h\nu$ is

$$\alpha h\nu = A(h\nu - E_g)^{1/2}/h\nu, \quad (1)$$

where A is a constant and E_g is the band gap energy. At photon energies, $h\nu$, that exceed the E_g of the semiconductor, the corresponding equation is $\alpha \approx (h\nu - E_g)^{1/2}$, or $\alpha^2 \approx (h\nu - E_g)$, where h is Planck's constant and ν is the frequency of the incident photon. Plotting α^2 versus $h\nu$ yields the optical band-gap values by extrapolation of the linear portion to $\alpha = 0$.

Figure 4.10 shows α^2 versus photon energy; the direct energy band gap of the films deposited in solution (a) exceeded that in solution (b). The respective values were ~3.38 and ~3.23 eV. As mentioned above, the lattice constant of ZnO grown in a cation-mediated bath is smaller than that grown in the non-cation-mediated bath. The crystalline structure with the smaller lattice constant means more vacant sites or the lattice being under strain within the grains, which leads to the band-gap shift. It is therefore concluded that the cations in the bath alter the crystal growth mechanism. At the atomic scale, the adsorption/desorption of cations may lead to a number of vacancies in the lattice and result in cell volume shrinkage. At the grain scale, the lattice grows in a specific orientation and causes the grains to pack in a more compact manner. The former leads to band gap shift and the latter increases to the film transmittance.

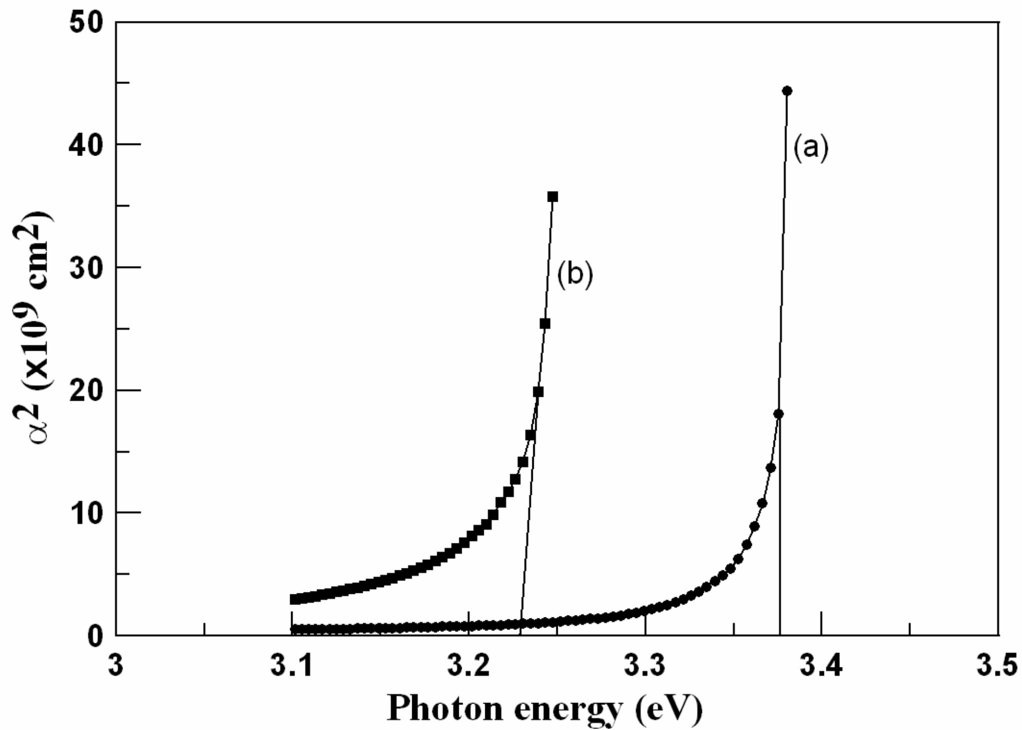

Fig. 4.10 Square of the absorption coefficient as a function of photon energy for ZnO growth in (a) bath without cation-mediated solution and (b) cation-mediated-solution bath.

1896

4.2.5 Summary

A method for improving the deposition of ZnO films by CBD was proposed. The cation-mediated solution, which contains magnesium ions, strongly influences the crystallinity, morphology, and band gap of the films. ZnO crystalline films with a densely packed regular morphology are successfully obtained, and the crystal clearly exhibited a preferential (002) orientation. Furthermore, highly transparent films are obtained at wavelengths of 500 to 800 nm with a transmittance of above 94% (at a wavelength of 800 nm), and the optical band gap of the ZnO changes from ~3.38 to ~3.23 eV, which depends on the extent of lattice distortion.

4.3 Performance of sol-gel deposited $Zn_{1-x}Mg_xO$ films used as active channel layer for thin-film transistors

4.3.1 Descriptions

ZnO thin-film transistors (TFTs) have attracted considerable R&D interest due to their high transparency and low photosensitivity compared with typical a-Si:H TFTs. The electrical characteristics of ZnO thin films may be controlled by doping with ternary element, for instance Al, Ga, In, Mg, etc. In this study, $Zn_{1-x}Mg_xO$ (x = 0 to 0.36) thin films were deposited on glass substrates by spin coating. The as-deposited films were baked at 300 ^{o}C for 10 minutes and then annealed at 500 ^{o}C for 1 hr. The results show that, addition of Mg-species in ZnO films markedly enhanced the uniformity of film thickness and improved optical properties. The $Zn_{0.8}Mg_{0.2}O$ film exhibited the best transparency of 92%, an increase of ~15% over a pure ZnO film, and the rms roughness value decreased to 1.63. The $Zn_{1-x}Mg_xO$ TFTs were demonstrated to have n-type enhancement behavior. The optimum device with $Zn_{0.8}Mg_{0.2}O$ channel layer had a mobility of 0.1 cm^2/Vs, a threshold voltage of 6.0 V, and an on/off ratio more than 10^7.

4.3.2 Conceptions

Zinc oxide (ZnO) is an n-type II-VI group compound semiconductor material with direct wide bandgap of 3.35 eV. Due to its unique electrical and optical properties it has been widely and popularly used in varistor, gas sensor, UV light emitters and surface acoustic wave devices [145]. Recently, ZnO films also attracted attention for energy and optical-electrical applications, such as window layers of solar

cells [156], transparent conductive layers of flat panel displays or touch panels [151] and the active channel layer of thin-film transistors [152]. The TFTs array fabrication process for large-area TFT-LCD has been continuously developed for simple processing steps, improving performance and reducing cost in the process of mass production. The sol-gel method offers a simple and low cost thin film deposition process as an alternative to the vacuum deposition technique, but it needs soluble types of materials. The carrier mobility of the intrinsic ZnO materials exceed the field effect mobility of a-Si:H which is the active channel layer in a typical TFT array. ZnO base TFTs possess low photosensitivity and high transparency, and have been studied by many groups [71, 152-154], but only a few reported using chemical solution processes for ZnO film deposition. Norrs et al. [51] reported fabrication of an un-doped ZnO TFT using spin coating. Lee et al. [155] prepared $Zn_{1-x}Mg_xO$ thin films as active channel using dip coating.

It has been demonstrated that the electrical characteristic of ZnO thin films could be controlled by doping with ternary element, for instance Al, Ga, In, Mg, etc. The ionic radii of Mg^{+2} (0.65 Å) and Zn^{+2} (0.74 Å) are similar, and thus the limit of solid solubility of MgO in ZnO can approach 40 at. % [156, 157]. Many reports show that the solubility limit of Mg content in $Zn_{1-x}Mg_xO$ films strongly depend on deposition or growth technique, e.g. MOVPE [163], PLD [156, 158], sputter [159] and sol-gel method [160, 161].

In the present study, dense ZnO thin films with or without doping with Mg^{+2} were prepared using the sol-gel method and microstructure, optical properties affected by Mg content were be investigated. Moreover, $Zn_{1-x}Mg_xO$ channel TFTs were fabricated and electrical characteristics of optimum devices evaluated.

4.3.3 Specifics methods

Zinc acetate dehydrate ($Zn(CH_3COO)_2 \cdot 2H_2O$) and magnesium acetate tetra-hydrate ($Mg(CH_3COO)_2 \cdot 4H_2O$) were dissolved in 2-methoxyethanol, and then monoethanolamine (MEA) was added to the solution. The concentration of metal ions in $Zn_{1-x}Mg_xO$ sols were controlled at 0.75M and Mg^{+2} was varied from 0 to 0.36 (for x values). The solution was stirred for 2 hr at 60 °C until a clear and homogenous sol was obtained. The $Zn_{1-x}Mg_xO$ thin film was deposited on alkali-free glass (Corning 1737) using the spin coating method, using 3000 rpm for 20 s. These as-coated films were dried at 300 °C for 10 minutes, and then annealed at 500 °C for 1 hr in air.

Thermal analysis of the $Zn_{1-x}Mg_xO$ sols used TG-DSC (TA Instrument, SDT 2960) to identify the evaporation, decomposition and crystallization points of the $Zn_{1-x}Mg_xO$ solution material. The crystal structure and microstructure of these thin films were examined using X-ray diffractometry (XRD, MAC Science MAXP3) and scanning electron microscopy (SEM, HITACHI S-4800), respectively. Surface morphology of the $Zn_{1-x}Mg_xO$ thin films was observed by scanning probe microscope (SPM, Digital Instrument NS4/D3100CL). Optical transmittance spectra in the visible range of these films were examined by a spectrophotometer (Mini-D2T, Ocean Optics, Inc., USA).

The typical bottom-gate structure device of $Zn_{1-x}Mg_xO$ TFTs was fabricated by a hybrid method that combined the standard micro-electrical fabricated process and sol-gel method. The MoW film (100nm thick) was deposited and patterned on a glass substrate as a bottom gate electrode. Silicon dioxide, prepared by plasma enhanced chemical vapor deposition (PECVD), served as the gate insulator with thickness 300nm. The source and drain select ITO thin film patterns were defined by standard

photolithography process. The channel length and width of the test device were 500 and 60 um, respectively. Finally, the active layer, $Zn_{1-x}Mg_xO$ thin film, was deposited by the sol-gel method to finish the $Zn_{1-x}Mg_xO$ TFTs. The current-voltage (I-V) characteristics of the transistors with $Zn_{1-x}Mg_xO$ channel layer were performed by semiconductor parameter analyzer (HP 4155B).

4.3.4 Achievements and explanations

Thermogravimetric analysis (TGA) and differential scanning calorimetry (DSC) of pure ZnO, $Zn_{0.8}Mg_{0.2}O$ and $Zn_{0.7}Mg_{0.3}O$ sols are shown in Fig. 4.11. In TGA curves of dried un-doped ZnO and $Zn_{1-x}Mg_xO$ precursors, weight losses were observed with three temperature regions at 40~90, 100~200 and 210~260 ^{o}C. The first weight loss region is caused by low temperature solvent evaporation. The second and third weight loss regions are due to evaporation of water and decomposition of organic compounds. The raw source material for the Mg ions, magnesium acetate tetrahydrate, possesses double the water of crystalization than zinc acetate. For this reason, there are lower solid content in the Mg doped ZnO sols. Moreover, one large and two small endothermic peaks, and an exothermic peak were found in DSC curves of dried undoped and Mg doped ZnO sols. The last peak of the DSC curve, the exothermic peak, results from the crystallization of $Zn_{1-x}Mg_xO$ materials. It may be noted that, the effect of Mg doped ZnO can raise and broad this exothermic peak. It reveals the prepared of $Zn_{1-x}Mg_xO$ thin films can tolerate a wider process window.

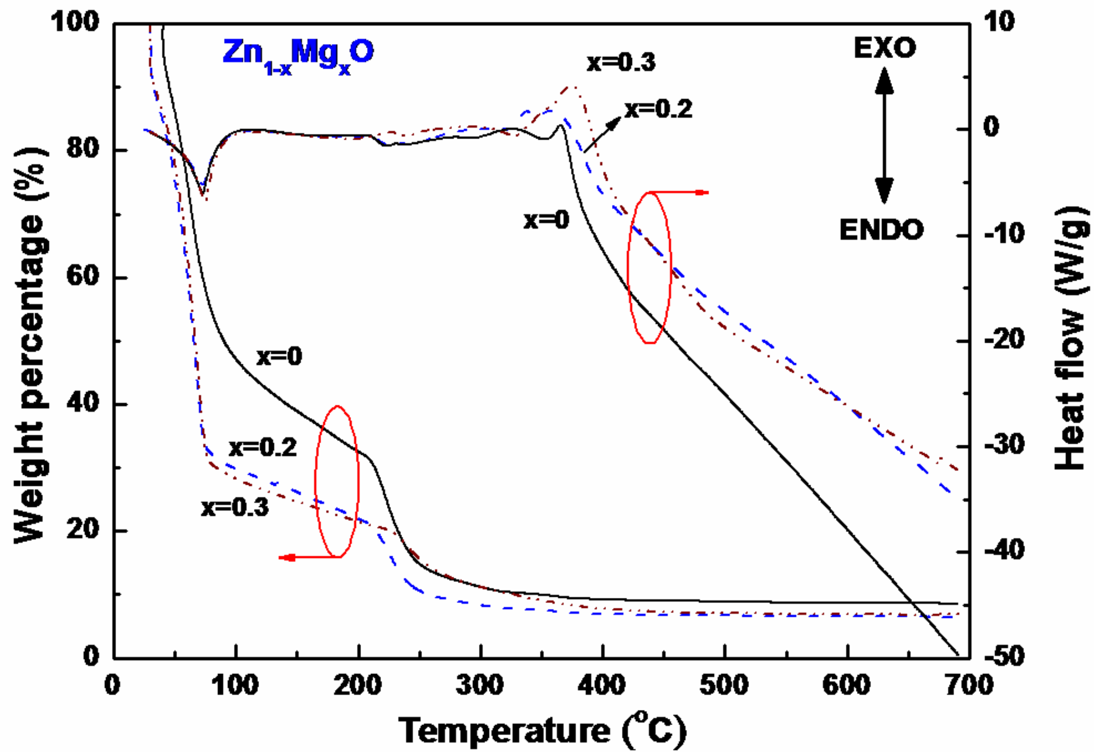

Fig. 4.11 TGA-DSC curves of the dried of $Zn_{1-x}Mg_xO$ sols with x=0, 0.2 or 0.3.

All the $Zn_{1-x}Mg_xO$ (x= 0~0.36) thin films were baked at 300 °C for 10 minutes and then annealed at 500 °C for 1 hr in air. The crystallographic structure of thin films was studied by X-ray diffraction. Fig. 4.12 shows the XRD patterns of these $Zn_{1-x}Mg_xO$ thin films, which observed that they had wurzite structure. Crystallized ZnO has a hexagonal crystal structure which was confirmed by the three main diffracted peaks for the (100), (002) and (101) planes. The diffractograph also shows that the intensity of these main peaks reduce with increasing Mg content and the $Zn_{0.8}Mg_{0.2}O$ film shows a highly c-axis oriented (002) peak. Besides, a significant shift in the (002) and (001) peaks is observed after Mg doping. Dhananjay et al. [159] have reported, Mg^{+2} replaced Zn^{+2} can increase the a-axis length and decrease c-axis, and this transformation may have caused the two main peaks to shift. In the XRD

pattern of $Zn_{0.7}Mg_{0.3}O$ and $Zn_{0.64}Mg_{0.36}O$ films, the diffracted peak of the MgO cubic phase was found at 42.9 degrees theta which is its (200) plane. The results show that at Mg content more than 30 at. % the MgO phase became segregated. An MgO phase separate from the $Zn_{1-x}Mg_xO$ film can cause degeneration of electrical and optical properties. In previously mentioned research, many reports show that the solubility limit of Mg in $Zn_{1-x}Mg_xO$ films strongly depends on deposition or growth technique. Thus, in order to retain the $Zn_{1-x}Mg_xO$ film's pure hexagonal crystal structure, the content of Mg^{+2} should not be more than x=0.3 according to our research.

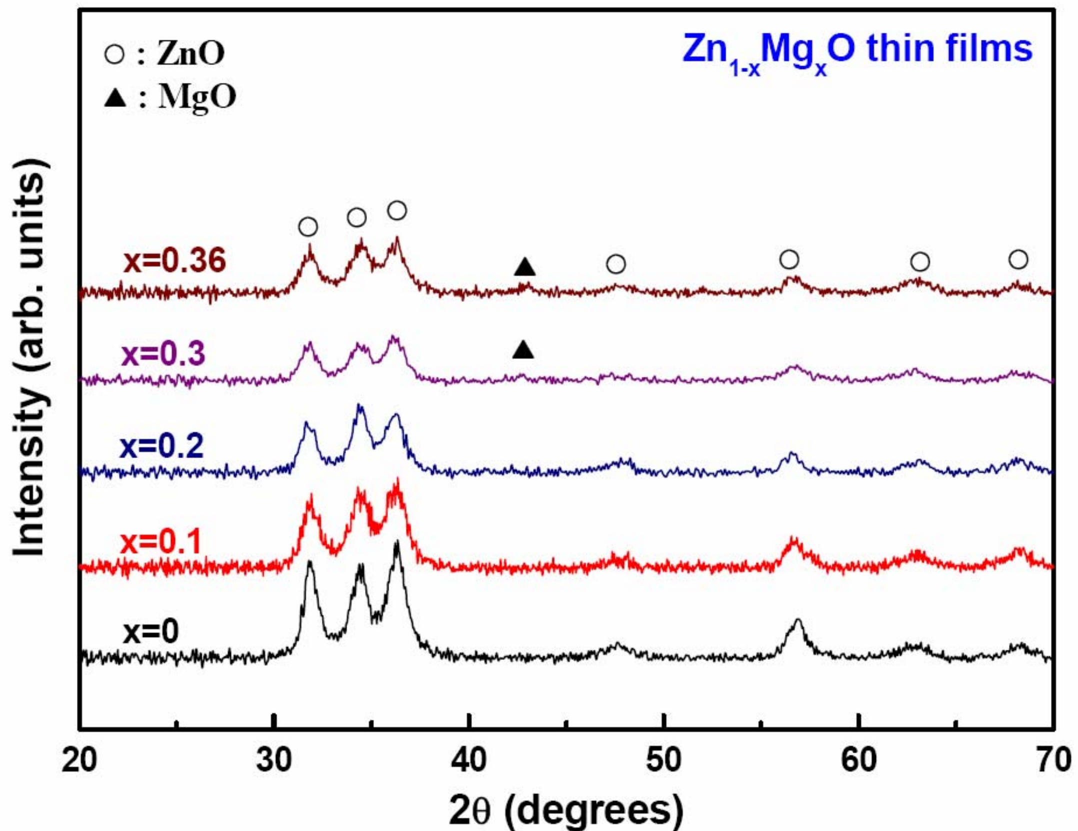

Fig. 4.12 X-ray diffraction patterns of $Zn_{1-x}Mg_xO$ thin films ($0 \leqq x \leqq 0.36$) , which were annealed at 500 ^oC for 1 hr.

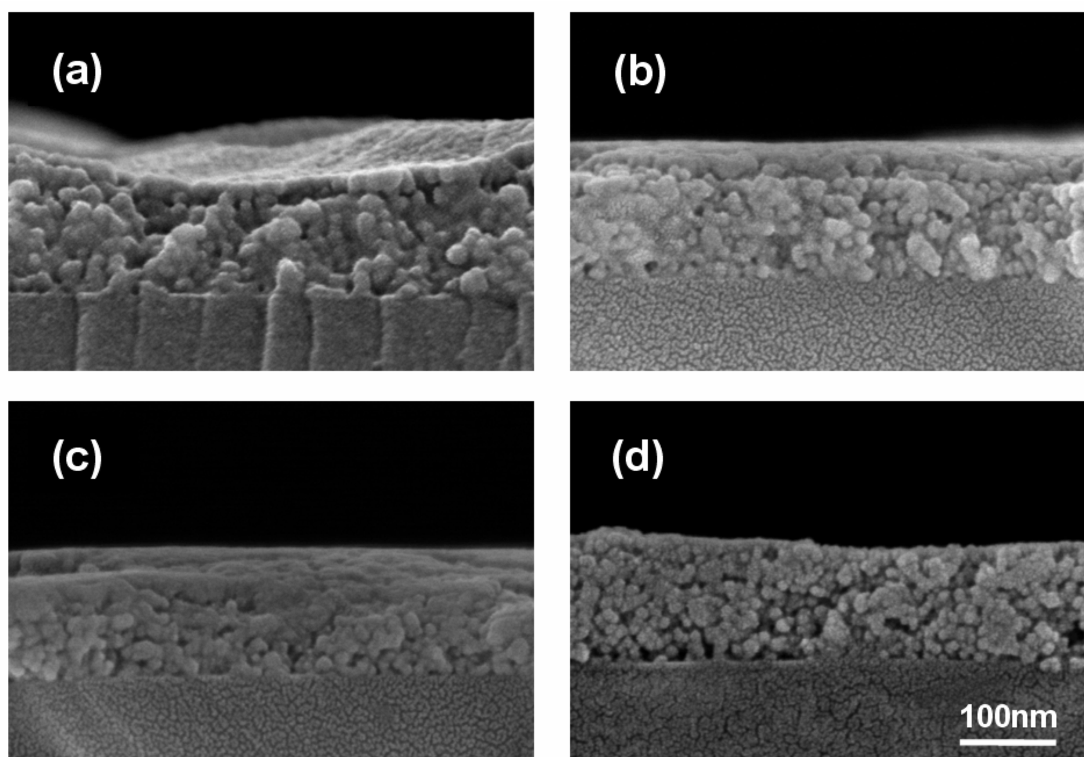

Fig. 4.13 SEM micrographs of cross-sections of $Zn_{1-x}Mg_xO$ thin films: (a) x=0; (b) x =0.2; (c) x=0.3 and (d) x=0.36.

The sol-gel method is a simple oxide thin film deposition technique. It is possible to control the film thickness by merely adjusting the solution viscosity or coating time. On the top view SEM imagine of annealed pure ZnO film can observe which surface overspread abnormally erumpent streak (no shown). However, these doped samples cannot observe that appearance. Cross-sectional SEM images of the $Zn_{1-x}Mg_xO$ thin films are shown in Fig. 4.13. Fig. 4.13(a) is an SEM micrograph of the ZnO film that shows its average thickness is about 140 nm. SEM micrographs of the nanocrystalline $Zn_{1-x}Mg_xO$ films (x=0.2, 0.3 and 0.36) are shown in Figs 4.13(b) ~4.13(d). They show that the thickness of doped film is about 150 nm. They also show that addition of

Mg-species to the ZnO films markedly enhanced the uniformity of film thickness. The average grain sizes of the pure ZnO and Mg doped films were about 20 nm and 10~15 nm, respective. These SEM images (Fig. 4.13) reveal that Mg doping of ZnO films can reduce the average grain size and improve the flatness of the $Zn_{1-x}Mg_x$ films. In addition, micrograph of the $Zn_{0.64}Mg_{0.36}O$ film, show in Fig. 4.13(d) revealed a porous and non-compact microstructure. It exhibit poorer film quality with x value than over 0.3. SPM images of the $Zn_{1-x}Mg_xO$ thin films are shown in Fig. 4.14. The surface morphology observed shows the influence of the Mg doping on the ZnO thin film. It is apparent that reduction of surface roughness results from the decrease in average grain size in ZnO film after Mg doping. The rms roughness of the $Zn_{0.8}Mg_{0.2}O$ thin films, which is approximately 1.63 nm is smaller among all the annealed $Zn_{1-x}Mg_xO$ thin films. The phase segregated impurities of x=0.3 and x=0.36 samples degenerated the surface texture of the thin films, and their rms values were 1.97 and 3.61, respectively.

Fig. 4.15 shows the optical properties of the $Zn_{1-x}Mg_xO$ thin films when examined at room temperature. From this figure, all samples showed sharp absorption edges in the UV region and this absorption edge shifted to shorter wavelengths when ZnO thin film was doped with Mg. The optical transmittance in the visible range for the pure ZnO film was about 80 % and exhibited absorption edge at about 362 nm (curve b in Fig. 4.15). The Mg doped samples show higher transparency compared with the un-doped sample. However, the transmittance spectra of higher Mg content samples, when $x \geqq 0.3$, showed a slight decrease in the 500 to 800 nm region. This result is in good agreement with the results of XRD, SEM and SPM and relates to Mg phase segregation. In this study, the $Zn_{0.8}Mg_{0.2}O$ sample exhibited the best

transparency among doped samples of 92%, which represents an increase of about 15% over the un-doped ZnO sample.

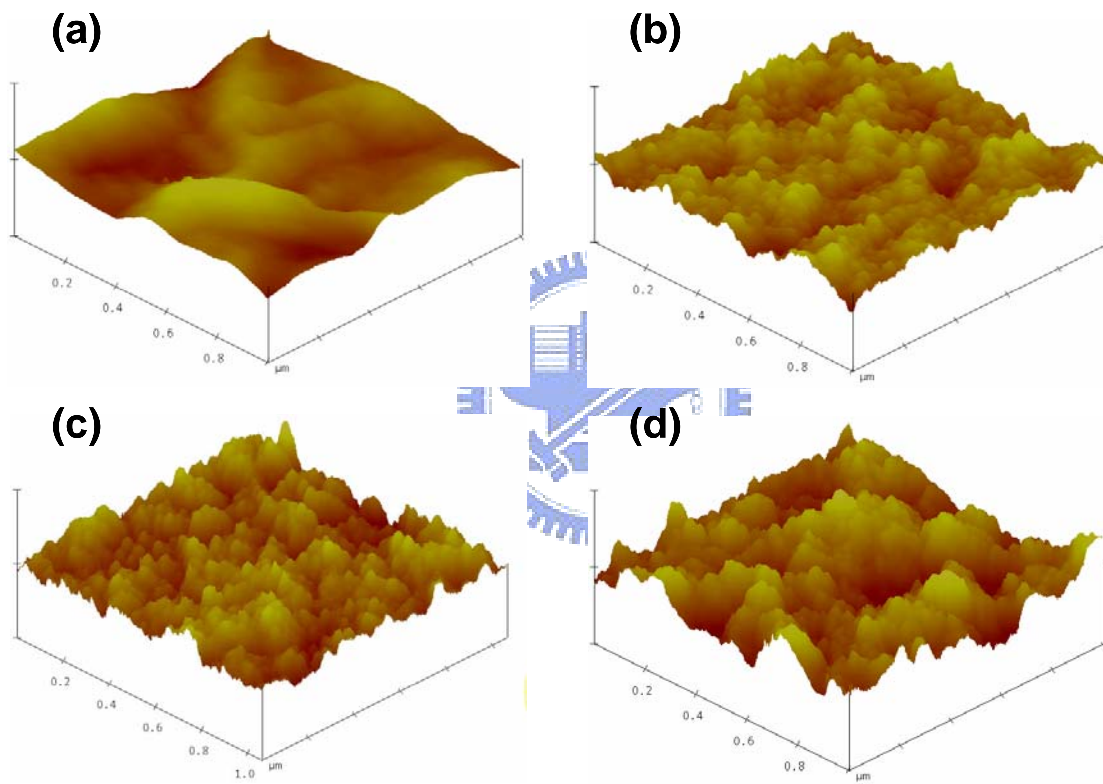

Fig. 4.14 SPM images of the surface of $Zn_{1-x}Mg_xO$ thin films: (a) x =0; (b) x= .2; (c) x=0.3 and (d) x=0.3

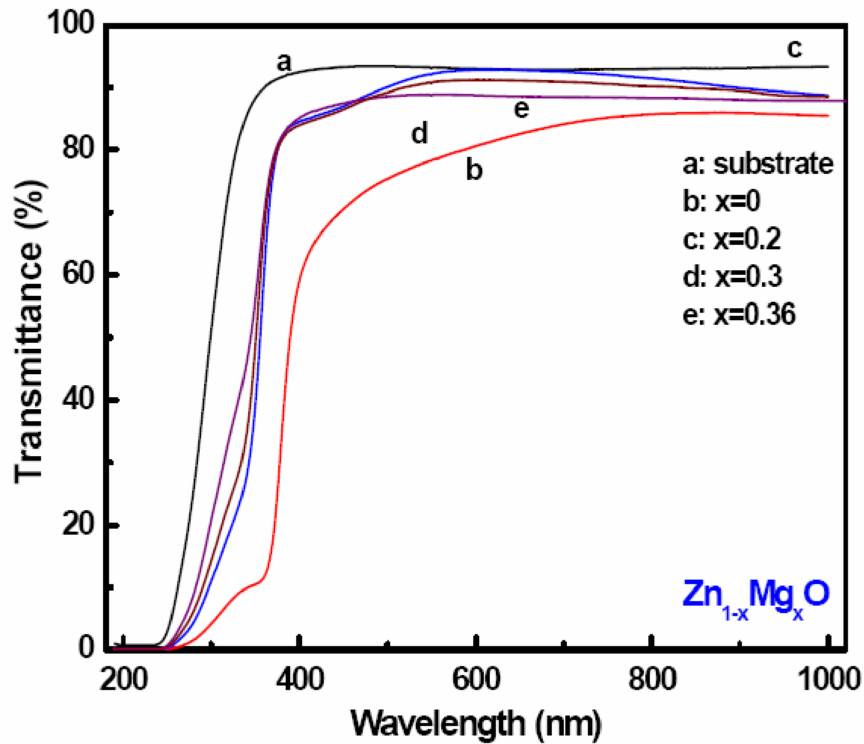

Fig. 4.15 The transmittance spectra of $Zn_{1-x}Mg_xO$ thin films with x=0, 0.2, 0.3 or 0.36.

The electrical characteristics of the devices show that all $Zn_{1-x}Mg_xO$ TFTs operated in n-type enhancement mode due to require a positive gate voltage to turn it on. The $Zn_{0.8}Mg_{0.2}O$ TFTs were optimum devices that displayed the best performance in the study. Fig. 4.16(a) shows the representative output characteristics (drain current-drain voltage, I_D-V_D) of the $Zn_{0.8}Mg_{0.2}O$ TFT measured at room temperature. The slope of each I_D curve is flat for large V_D, and hard saturation was observed, which is desirable for most circuit applications [51]. Fig. 4.16(b) shows the corresponding transfer characteristics (I_D-V_G) of the same device, measured at a fixed V_D of 30 V. This I_D-V_G curve reveals a drain current on to off ratio of more than 10^7.

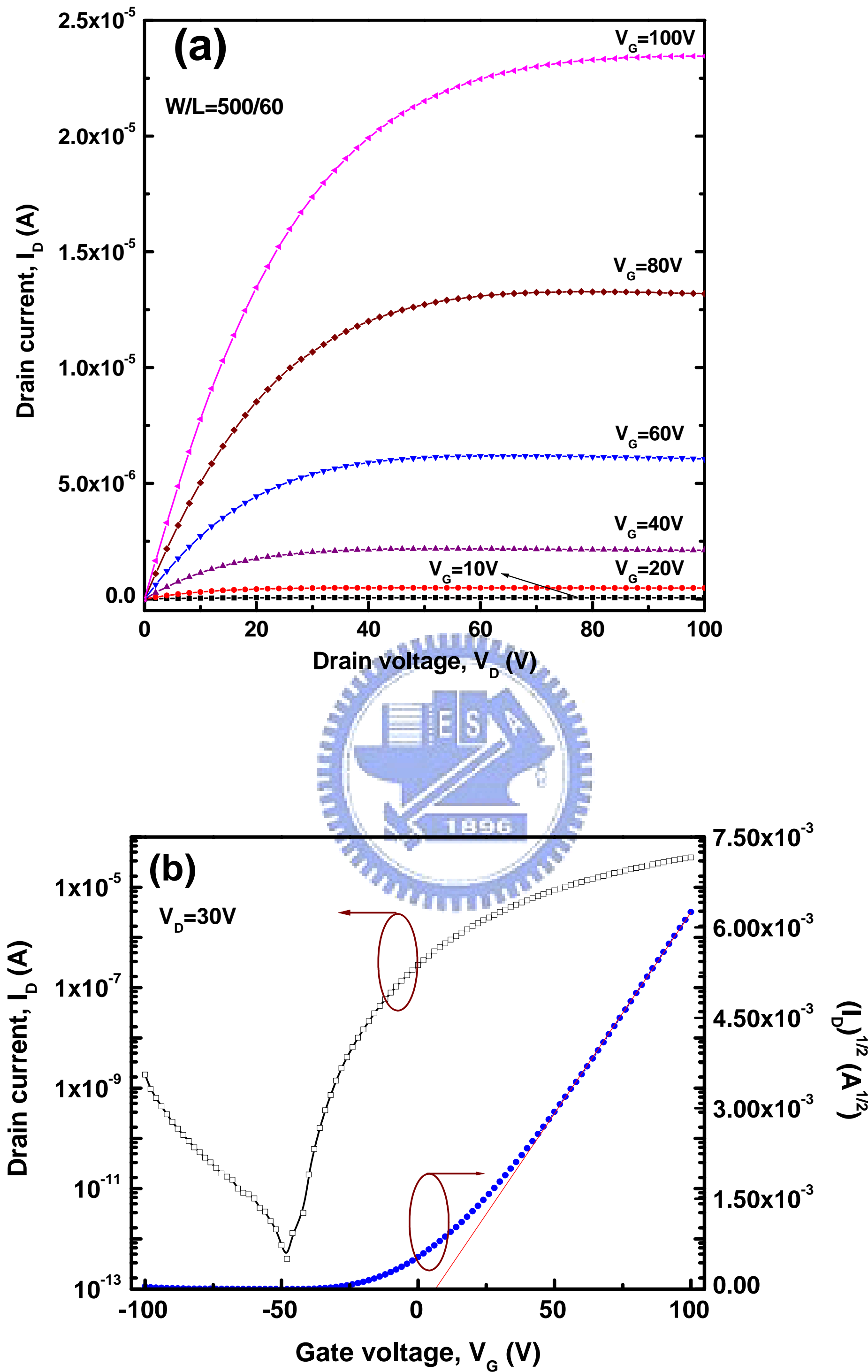

Fig. 4.16 (a) Output characteristics (I_D-V_D curve) and (b) transfer characteristics (I_D-V_G curve) of TFT using $Zn_{0.8}Mg_{0.2}O$ thin film as the active channel layer.

The threshold voltage (V_{th}) was defined by fitting a straight line and then intercepting the x-axis of the $(I_D)^{1/2}$ -V_G plot. At the same time, the saturated mobility (μ_{sat}) was determined by the following square equation [162]:

$$I_{D(sat)} = \mu_{sat} C_{OX} \left(\frac{W}{2L} \right) (V_G - V_{th})^2, \qquad for\, V_D << (V_G - V_{th})$$

Where W is the channel width, L is the channel length, C_{OX} is the unit capacitance of gate insulator, V_{th} is the threshold voltage and μ_{sat} is the saturated mobility. The V_{th} and μ_{sat} of the $Zn_{0.8}Mg_{0.2}O$ TFT were calculated to be 6.0 V and 0.1 $cm^2V^{-1}s^{-1}$, respectively.

4.3.5 Summary

Preparation and characterization of thin film transistors with Mg-doped ZnO films for the active channel layer were investigated. The results show that Mg^{+2} doped ZnO films of the form $Zn_{1-x}Mg_xO$ had markedly improved surface texture (reduced roughness), optical properties and finer microstructure than ZnO films. The $Zn_{0.8}Mg_{0.2}O$ film exhibited the best transparency at 92%, increasing by 15% value for the un-doped ZnO film (80%), and its rms roughness value decreased to 1.63. When the Mg content exceeded 0.3 (x value) MgO phase segregation would occur. This impurity phase caused the film quality to degenerate. In this study, the $Zn_{1-x}Mg_xO$ TFTs were fabricated using the sol-gel method and exhibited n-type enhancement mode. The optimum device with $Zn_{0.8}Mg_{0.2}O$ channel layer has a mobility of 0.1 cm^2/Vs, a threshold voltage of 6.0 V, and an on/off ratio more than 10^7.

4.4 High oriented ZnO films by sol-gel and chemical bath deposition combination method

4.4.1 Descriptions

Crystalline ZnO films with high-quality orientation were grown on ZnO-coated seed layers by a chemical bath deposition (CBD) in an aqueous-solution bath containing zinc nitrate [$Zn(NO_3)_2.6H_2O$], and dimethylamineborane (DMAB) at 60℃ without any pre-activation especially. The seed layers of ZnO on silicon oxide (SiO_x) glass substrates by sol-gel process at 150 to 550℃ were poly crystalline. It is proved that the mean crystals size in seed layer increased from several to 80nm when the processing temperature increases, the mean grains of ZnO films grown on the ZnO-coated seed surfaces are exhibit increased from several 10 to 150nm and preferentially grew on the (002) plane.

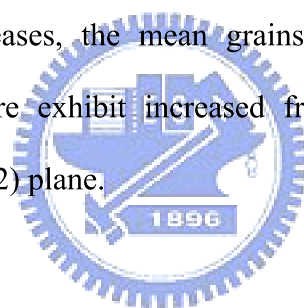
1896

4.4.2 Conceptions

ZnO is an important material for the application in next generation of optoelectronics due to its unique physical and stable chemical properties, abundance in nature and absence of toxicity make them very popular for use in solar cells [129], photo detectors [11], light-emitting devices [12], gas sensor elements [13] and surface acoustic wave guides [14]. Presently, most of the practical devices of ZnO materials are based on the polycrystalline ZnO [163]. However, for the applications of optoelectronic devices, high-quality c-axis oriented ZnO films are very favorable due to less intrinsic defects and dislocations in the crystalline domain. It is essential to grow high-quality c-axis oriented ZnO films for significant applications in future.

Many different methods are used to deposit ZnO films, such as metal-organic chemical vapor deposition (MOCVD) [164], magnetron sputtering [165], and pulse laser deposition (PLD) [154]. Among them, the deposited ZnO films usually exhibit the good crystallinity and the c-axis orientation due to high diffusivity of absorbed particles on the growth surface, and the defects in the ZnO films are less. However, these methods require expensive and complicated apparatus to attain high vacuum ambiance. Generally, by a solution method, ZnO films are prepared at the atmosphere, the orientation of the films strongly depends on the substrate materials, growth conditions, and especially difficult to obtain high orientation crystallinity at low temperature [167, 168]. Moreover, in order to form the continuity ZnO films, metal ions pre-activation is needed to assist normal chemical bath deposition [131]. However, the influences of metal ion pre-activation on intrinsic properties of ZnO films are undetermined, therefore, the applications are limit.

Followed these backdrops, the purpose of this letter is to demonstrate a high-quality oriented ZnO films which are grown without complicated apparatus or other metal ions pre-activation at lower temperature and all the procedures are at the atmosphere The prefer orientation of the ZnO films is highly in the c-axis.

4.4.3 Specifics methods

In the process of fabricating the seed layer of ZnO films, the first layer was coated with sol-gel solution [160], which has molar ratio of monoethanolamine (MEA) and zinc acetate $Zn(CH3COO)_2 \cdot 2H_2O$ equal to 1.0, and the concentration of zinc acetate equal to 0.375 mol/L. The spin-on method was used for the film coating. The pre-baking temperature was 100℃, and the post-baking temperature varying from 150

to 550℃ on hotplate. In order to obtain high orientated and crystalline film surface thus improve the second layer uniformity, the columnar grains size must be increased. This approach was accomplished by optimizing the chemical bath deposition (CBD) for the second layer of ZnO film. The CBD solution contained 0.1 mol/L zinc nitrate and 0.03 mol/L dimethylamineborane, and the substrate was immersed in the soak solution for the film growth at 60℃ [136].

4.4.4 Achievements and explanations

Thermo gravimetric analysis and differential scanning calorimeter (TGA-DSC, TA Instrunent, STD 2960) are used to identify the evaporation, decomposition and crystallization points of the ZnO sol precursor. Three weight variation zones were showed in TGA curve (dash line) of Fig. 4.17, in which low boiling point solvent evaporated at 40~90℃, water evaporated and organic compounds decomposed at 90~230℃. One large and two small endothermic peaks, and two exothermic peaks were found in DSC curves of ZnO sols. The last peak of the DSC curve, the exothermic peak, results from the crystallization of ZnO materials. However, in fact, ZnO nanocrystalline seeds were preformed under 150℃ gradually, which were verified in XRD spectra of Fig. 4.18.. As shown in Fig. 4.18, curves (a), (b), and (c) are the XRD spectra of ZnO seed layers which post-baked at 150, 250, and 550℃, respectively. Crystallized ZnO seed layers have a hexagonal crystal structure which were confirmed by the main diffracted peaks for the (100), (102), (200) and (202) planes.

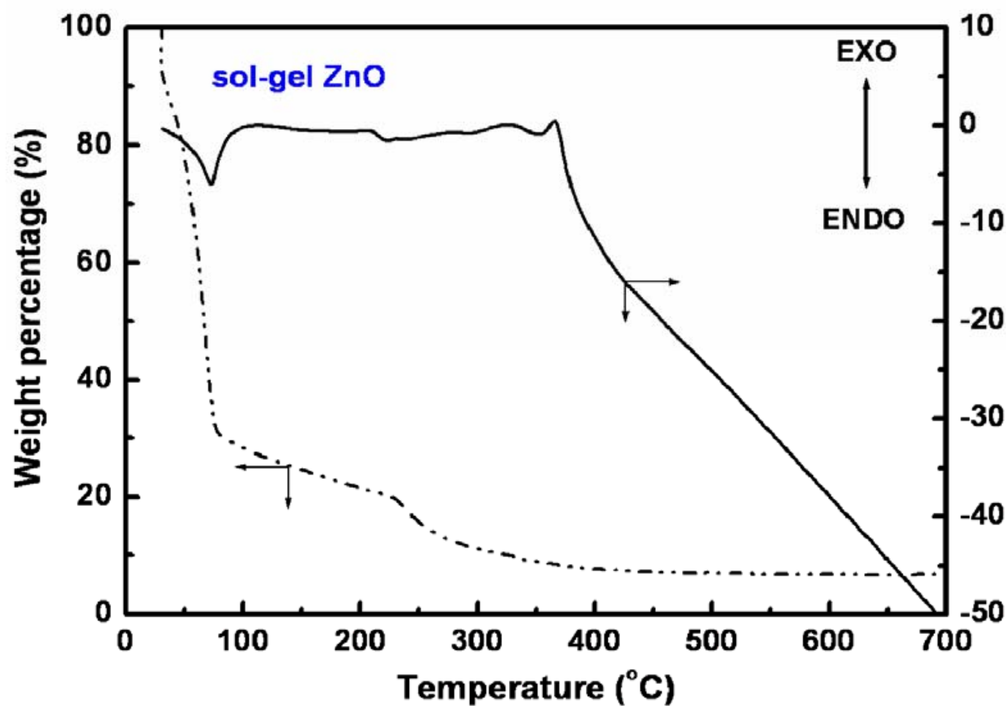

Fig. 4.17 Typical TGA/DSC curves measured in air at a heating rate of 5℃/min for ZnO sol-gel.

The XRD spectra of ZnO films grown by CBD method on the sol-gel seed layers are shown in Fig. 4.18 (curves (d), (e), and (f)) also; from the recorded spectra, the main diffraction peak of (002) shown in curves (d), (e), and (f), revealed that the most grains in ZnO film are c-axis preferred orientation. Further structural characterization of the CBD ZnO crystals was performed by high resolution transmission electron microscopy (HRTEM; FEI/ Philip Tecnai F20) and selected area electron diffraction (SAED). Figure 4.19 shows a TEM image (Fig. 4.19(a) insert) and the SEAD patterns (Fig. 4.19(b) insert) of the ZnO film. It is seen that the grains in CBD ZnO film exhibits a single crystalline structure, and from HRTEM images (Fig. 4.19(b)) that the spacing between adjacent lattice planes is about 0.26nm, which corresponds to the

space between two (002) planes of ZnO crystal. The regular direction growth can be explained as Bauer [169] proposed a two-stage orientation mode, an initial nucleation orientation and a final growth orientation of the film, both of which result from the nucleation at the film–substrate or film-film interface. In our case, the ZnO nucleation in CBD prefer to occur on the grain sites of seed layer and grow gradually. In the other words, the grains in the seed layer can induce the initial (0 0 2) orientation of ZnO nuclei and mainly grow in c-axis plane.

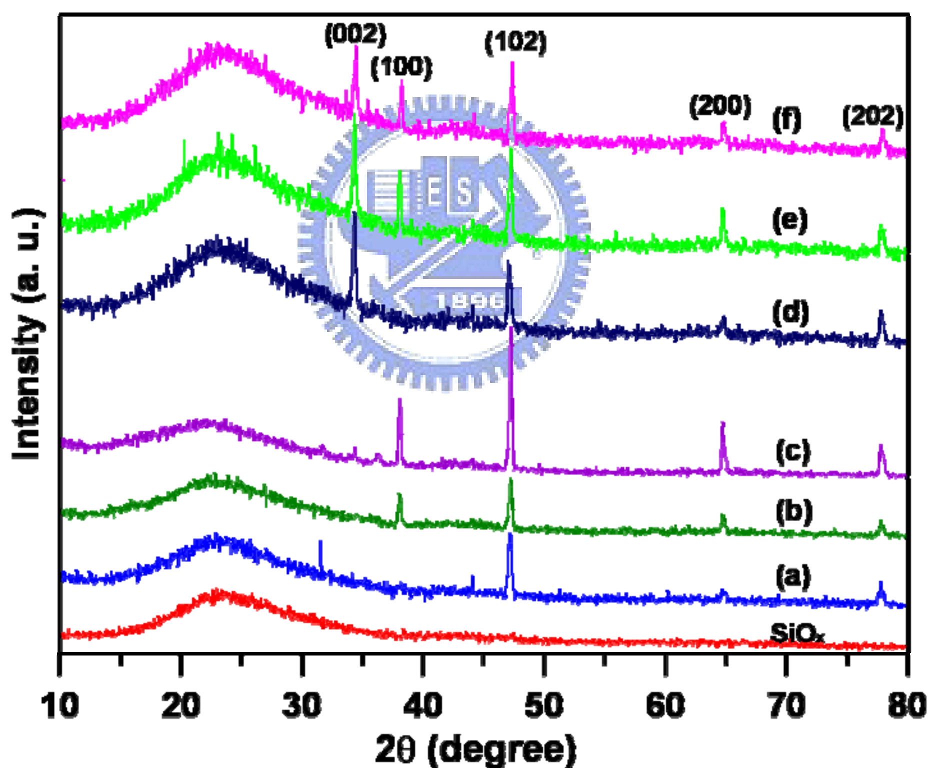

Fig. 4.18 X-ray diffraction pattern of ZnO films, seed layers post-baked at (a) 150℃, (b) 250℃, and (c) 550℃; combination ZnO films of CBD ZnO films grown on post-baked seed layers at (d) 150℃, (e) 250℃, and (f) 550℃.

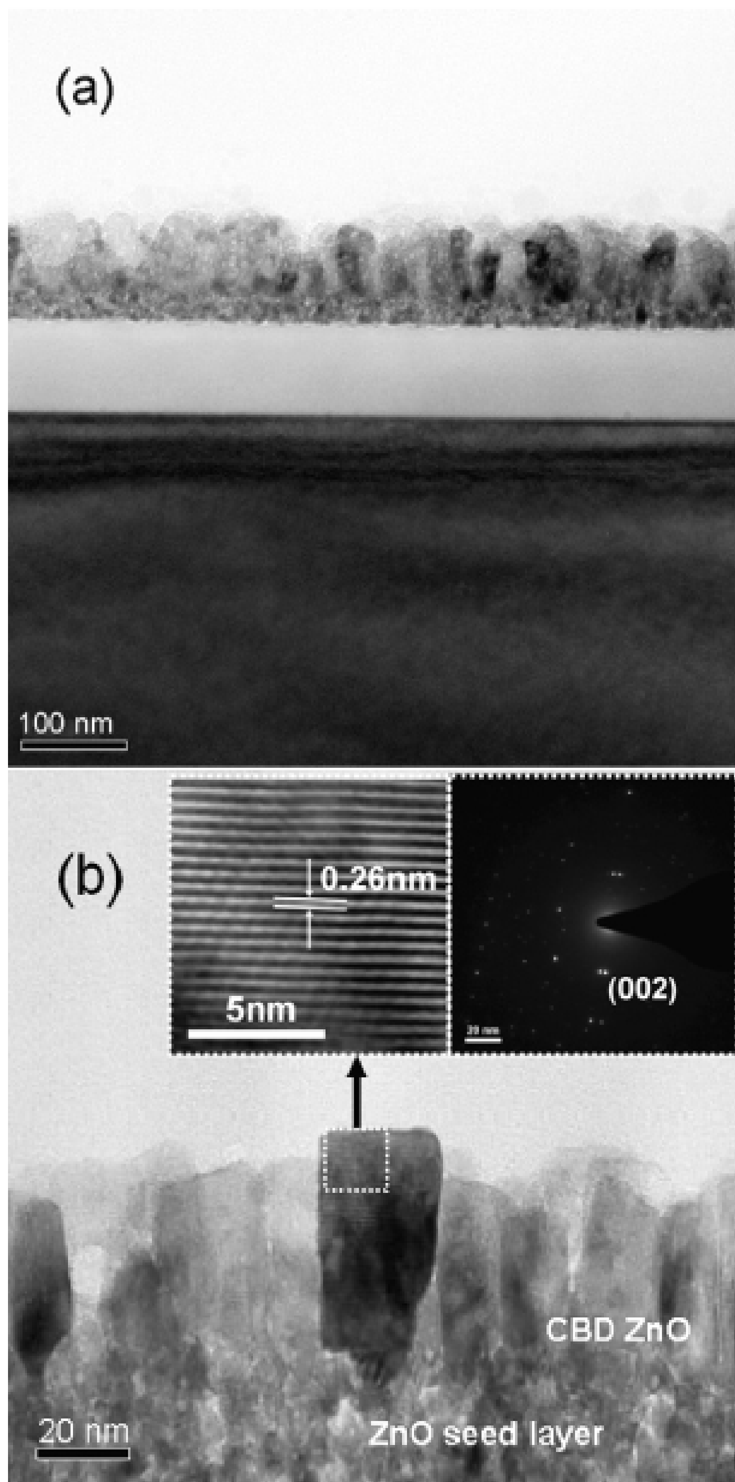

Fig. 4.19 (a) TEM image and the (b) SEAD patterns of the ZnO film on glass substrate.

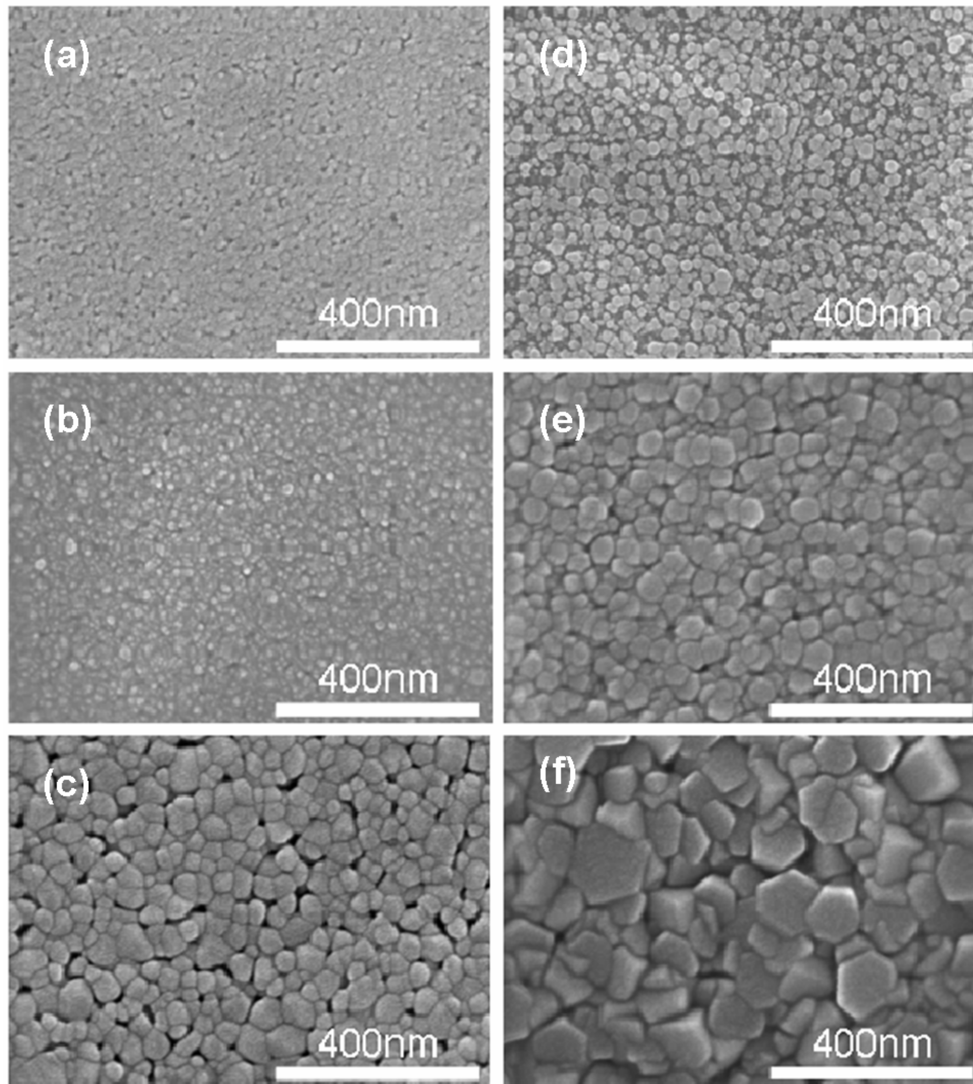

Fig. 4.20 SEM images of ZnO film; seed layers post-baked at (a) 150℃, (b) 250℃, and (c) 550℃; combination ZnO films of CBD ZnO films grown on post-baked seed layers at (d) 150℃, (e) 250℃, and (f) 550℃.

Figure 4.20 shows the SEM surface images of ZnO seeds layers and ZnO thin films grown on seed layers by CBD. Fig. 4.20(a)-4.20(c) are the images of seeds

layers post-baked at 150, 250, and 550℃ respectively; we define the crystal seeds which are possessed clear interface with each other, It is clear that the seeds size increased with baking temperature increased and revealed that the size is from several to 80 nm. As showed in Fig. 4.20(d)-4.20(f), hexagonal crystals are observed which correspond to the basal plane of the seeds layers, the size increased with the seeds size increased and is from several 10 to 150 nm. According to the above results, we can recommend that the initial (0 0 2) orientation of ZnO nuclei are induced by the grains in the seed layer and provide the sites for CBD ZnO film mainly grow in c-axis plane.

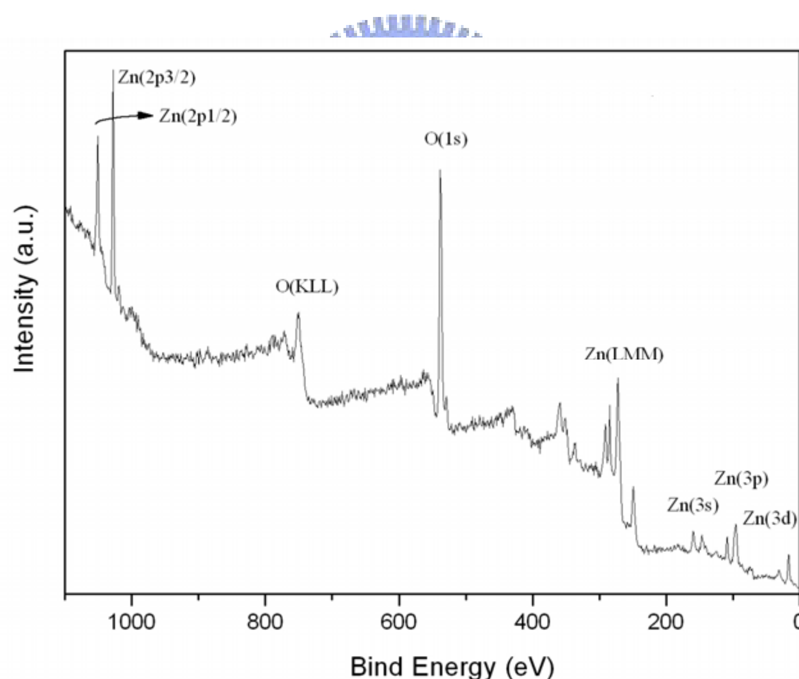

Fig. 4.21 XPS pattern of ZnO films which the CBD ZnO film grown on post-baked seed layers at 250℃

As shown in Fig. 4.21, the XPS spectrum (measured by ESCLAB MKII), there are Zn, and O elements in the ZnO film only. The two strong peaks located around

531 and 1002 eV, respectively, were agreed with the O 1s and Zn $2p_{3/2}$ binding energy for ZnO.

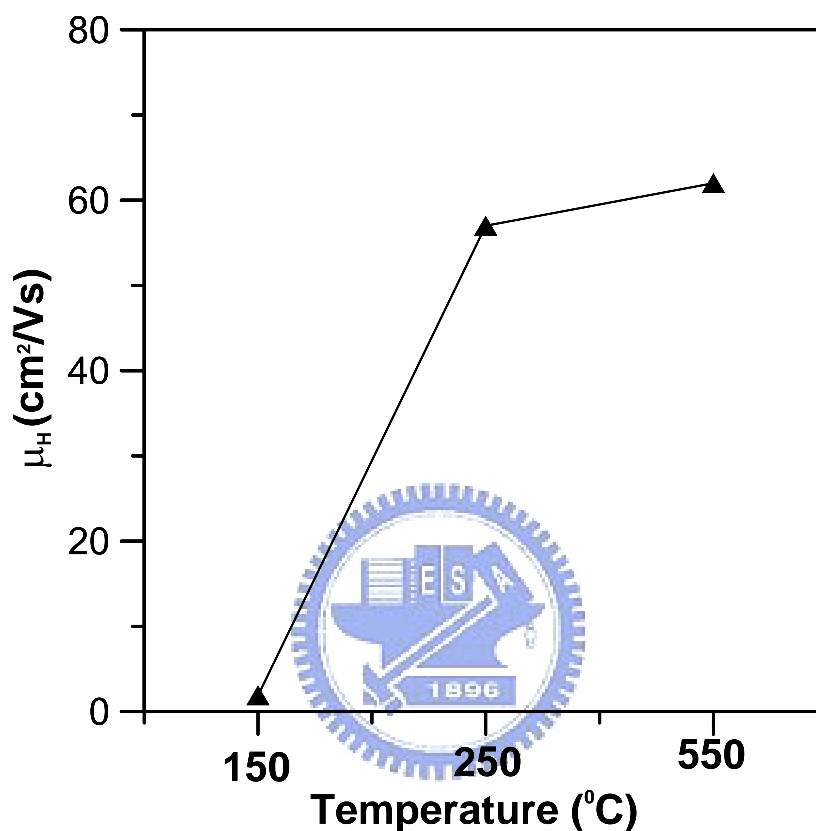

Fig. 4.22 the Hall-effect mobility of the ZnO films grow by sol-gel and CBD combination method

As shown in Fig. 4.22, the Hall-effect mobility (measured by Bio-Rad Micromeasurements, HL5500) of the combination ZnO films are increased with seed layer baking temperature; increased seed size will improve the crystals size of CBD ZnO films. In the other words, the crystals size increase can reduce the defects of the film, Hall-effect mobility increase with the crystal size increase.

4.4.5 Summary

A method for improving the high-quality orientation ZnO films by sol-gel and chemical bath deposition combination method was proposed. The so-gel ZnO seeds layers, which are influenced strongly the crystallinity, morphology and crystals size by post-baking. CBD ZnO crystalline films with densely packed regular morphologies are successfully obtained, and the crystal clearly exhibited (002) preferred orientation. Furthermore, the ZnO seed size increased with baking temperature increased and revealed that the size is from several to 80 nm. Also, the CBD ZnO films, that the hexagonal crystals are observed which correspond to the basal plane of the seeds layers; the size increased with the seeds size increased and is from several 10 to 150 nm.

4.5 Transparent ZnO thin-film transistor fabricated by sol-gel and chemical bath deposition combination method

4.5.1 Descriptions

Top-gate thin film transistors (TFTs) with n-type ZnO active channel were performed under 230℃. Especially, ZnO film was deposited by a combined method of sol-gel and chemical bath deposition without any pre-activation for film growth. Silicon nitride (SiN_x) and Indium tin oxide (ITO) were used as the gate insulator and the conducting electrodes (source, drain, and gate). These transistors were highly transparent in the visible spectrum, with transmittance as high as 75% to approximately 85% at wavelength from 500nm to 700nm. The optimum device has field-effect mobility of 0.67 cm^2/V s and an on-off ratio more than 10^7.

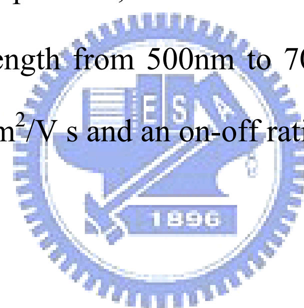

4.5.2 Conceptions

Transparent electronics are nowadays a crucial technology for the next generation of optoelectronic devices. Oxide-based transistors have recently been proposed as active channel [53, 75-80]. Among them, wurtzite structured ZnO thin films has been studied as the active layer in the thin film transistors (TFTs) because of its low cost, low photo sensitivity, no environmental concerns, and especially high mobility.

Other wide band-gap semiconductors, including GaN [9] and SiC [170] have been explored as transparent field-effect transistors (FETs). In fact, among these semi-conductive oxides, ZnO has the greatest potential to grow high quality crystalline zinc oxide at low temperature. This is particularly advantageous for

electronic drivers, which need to be processed at temperature that is low enough to be compatible with plastic substrates. Besides, because of their high transparency, high mobility, simple processing method and low cost, ZnO-based semiconductors also have been applied to be active layers of TFTs. Nowadays, thin film transistors based on a-Si:H have presented some limitations, such as light sensitivity, light degradation, and low mobility. On the contrary, thin film transistors based on ZnO are transparent in the visible region of the spectra and less light sensitive. ZnO is presently attracting much attention due to its possibilities for replacing amorphous Si that has been widely used as the channel layer in conventional TFTs [71-73]. Therefore, the future of ZnO holds great promise for applications in flexible displays and other opto-electronic devices.

A recent attempt to fabricate a ZnO-TFT utilizes chemical solution method which requires annealing steps above 600℃ [9]. Bottom gate configuration is widely used for ZnO-TFTs in order to maintain processing compatibility of a-Si:H TFTs [71-73, 170, 171]. In the crystal structure of ZnO, the defects of columnar grains may be reduced by increasing the film thickness. Therefore, high mobility is more likely to be achieved in the top gate configuration rather than in the bottom gate configuration.

Followed these backdrops, the purpose of this letter is to demonstrate a n-type field effect thin film transistor which is highly transparent in the visible region and to synthesize the ZnO thin films by a combination of sol-gel method at lower temperature and chemical bath deposition without other metal ions pre-activation.

4.5.3 Specifics methods

In the process of fabricating the active channel layer of ZnO films, the first layer

was coated with sol-gel solution [172], which has molar ratio of 2-methoxyethanol (MEA) and zinc acetate $Zn(CH3COO)_2 \bullet 2H_2O$ equal to 1.0, and the concentration of zinc acetate equal to 0.5 mol/L. The spin-on method was used for the film coating. The preheating and the post-heating temperature were respectively 100℃ and 230℃ on hotplate. In order to reduce grain boundary thus improve electrons mobility, the columnar grains size must be increased. This approach was accomplished by optimizing the chemical bath deposition (CBD) for the second layer of ZnO film. The CBD solution contained 0.1 mol/L zinc nitrate and 0.03 mol/L dimethylamineborane, and the substrate was immersed in the soak solution for the film growth at 60℃ [173]. Then the ZnO film was patterned using standard lithography and wet etching process.

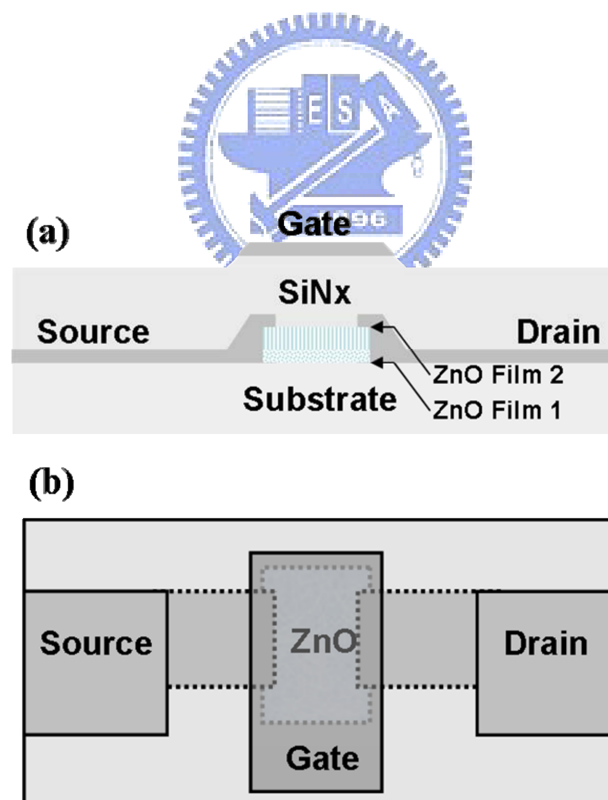

Fig. 4.23 Top-gate structure of ZnO- TFT in which (a) is cross-sectional schematic and (b) is top view schematic.

The ZnO-TFT, a simple top-gate configuration was fabricated onto a Corning 1737 glass substrate as shown in Fig. 4.23 (a) and (b). The optimized ZnO semiconductor films were fabricated, which the source and drain were coated with 100 nm-thick layer of ITO by sputtering (patterned by lift-off technique). Each source-drain pair was defined of a channel width W=500 μm and channel length L=10 μm. A silicon nitride (SiNx) film is used for the gate dielectric which thickness was 300nm and patterned by shadow mask. The ITO film of 100-nm was used as the gate electrodes.

4.5.4 Achievements and explanations

Scanning electron microscopy (SEM; Hitachi 4700) is employed to characterize the device structure and morphology of the prepared films. Figure 4.24 shows the morphology of ZnO film and local image of ZnO-TFT device, which indicate that through chemical bath deposition grains can be grown on the sol-gel film compactly without any surface treatment and the mean thickness is 200nm (as shown insert (a) of Fig. 4.24). The grains of upper layer are larger than those of the lower layer obviously, even though there exists an unclear interface between upper and lower layer.

We predicted that the ZnO film by CBD can anchor and self align on the preformed particles of sol-gel layer. The films of the Figure 4.24(a), with regular and compact amassment grains vertical to the substrate prove that the inference to be true. Moreover, we emphasize that films defects of columnar grains may be reduced with larger size of grains. Therefore, mobility improvement is achieved in the top gate configuration for the current growth method of ZnO films. The ZnO-TFT devices are demonstrated successfully (refer to insert (b) of Fig. 4.24).

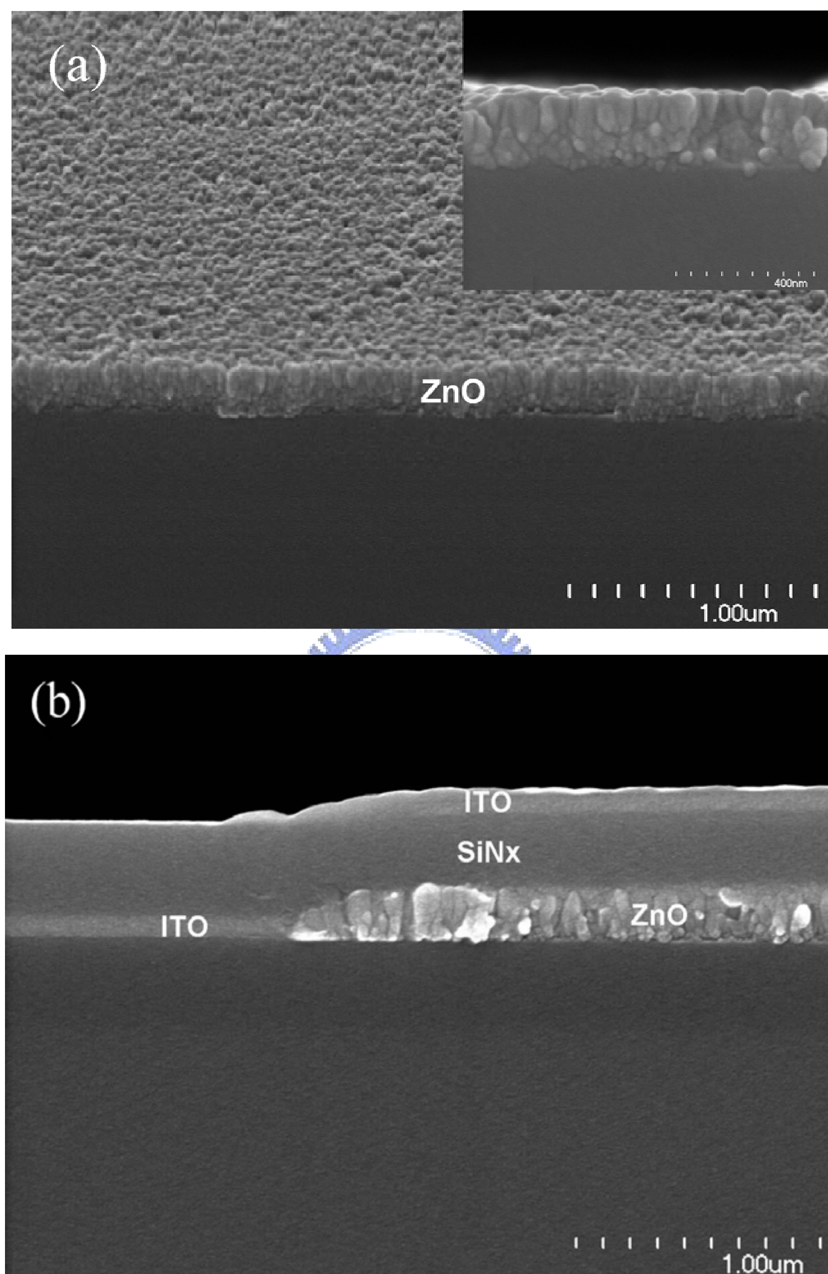

Fig. 4.24 SEM images of (a) ZnO films on Corning 1737 glass substrate by 45° tilt angle, the insert is a cross section view of scale up from the local of ZnO film with a 400 nm scale. (b) local cross section view of ZnO-TFT on Corning 1737 glass substrate.

All the optical transmittance of the deposited films was measured using a UV-VIS-NIR scanning spectrophotometer (SHIMADZU UV-3101PC) at wavelengths from 250 to 1200 nm. Figure 4.25 shows optical transmission spectra through the ZnO-TFT (except substrate), which includes the ITO film (gate), SiNx (gate insulator), and (ZnO film) channel region, of thicknesses 100nm, 300nm, and 200nm respectively. The transistors were highly transparent in the visible range, with transmittance as high as 75% to approximately 85% at wavelengths from 500nm to 700nm. The photo of the Figure 4.25 inserted shows a clearly visible 5 × 5 cm^2 glass substrate with 75 devices of ZnO-TFT.

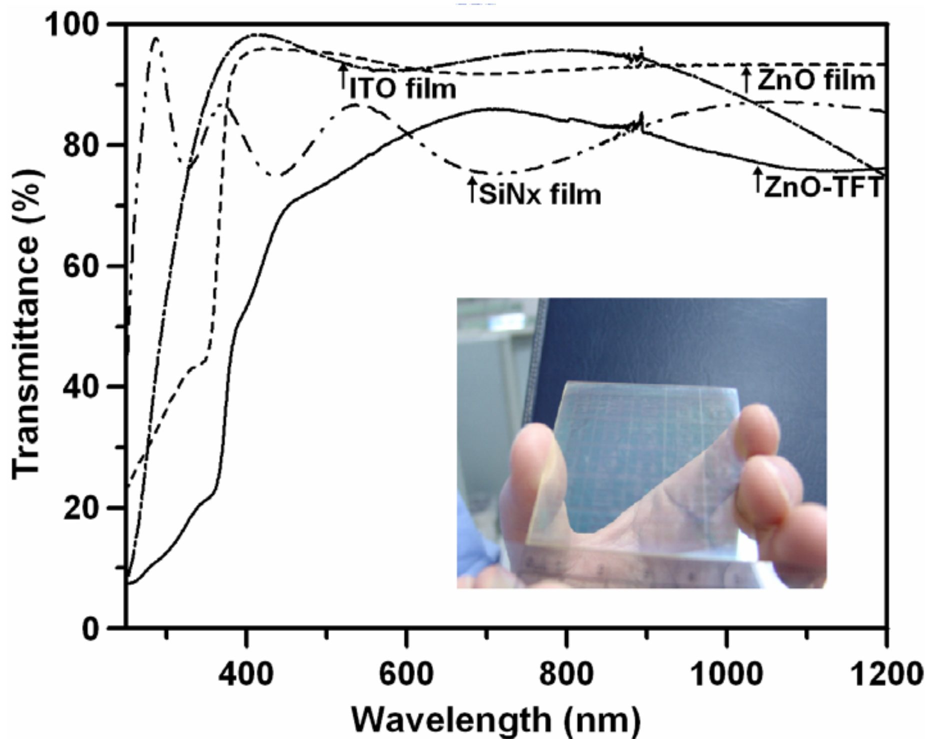

Fig. 4.25 Optical transmission spectra for the Top-gate structure of ZnO-TFT (except substrate) through the ITO film (gate), SiNx (gate insulator), and (ZnO film) channel region, and the thicknesses are 100nm, 300nm, and 200nm respectively. The insert shows a 5 × 5 cm^2 substrate with 75 devices of ZnO-TFT on Corning 1737 glass substrate.

The transistor devices were analyzed with an Agilent 4155B semiconductor parameter analyzer at room temperature and were measured in the dark room. Typical I_D-V_D curve and I_D-V_G curve of a ZnO-TFT are shown in the Figure 4.25 Current-voltage properties measured through the gate infer that the ZnO channel is n-type enhancement mode device due to a positive gate voltage is required to induce a conducting channel, and the current increases with increasing positive gate bias. Figure 4.26 (a) shows the drain current (I_D) as a function of source-drain voltage (V_D) for gate voltage (V_G) between 0 to 40 V for the device. The slope of each I_D curve is flat for large V_D, indicating hard saturation, which possesses large output impedance that is desirable for most circuit application. Figure 4.26 (b) shows the corresponding transfer characteristic of I_D versus V_G at a fixed V_{DS} of 20 V for the same TFT device. The I_D-V_G curve reveals a drain current with on to off ratio of more than 10^7. The threshold voltage (V_{th}) and saturation mobility were defined by fitting a straight line to the plot of the square root of I_D versus V_G, calculated by the formula of saturated regions:

$$I_{DS}= \mu_{FEsat}(W/2L)C_I(V_{GS}-V_{th})^2$$

Where W and L are the channel width and length respectively, C_I is the capacitance per unit area of gate insulator. The V_{th} is 6V and saturated regions mobility (μ_{FEsat}) was calculated of $0.67 cm^2 V^{-1} s^{-1}$.

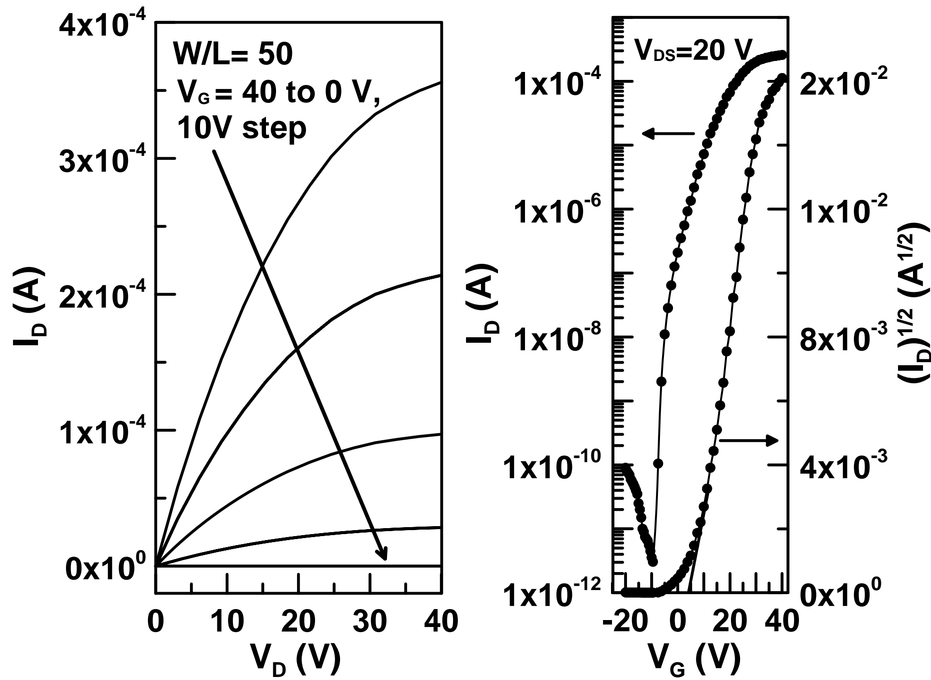

Fig. 4.26 (a) Drain current-drain voltage (I_D-V_D) curves at gate voltage (V_G) between 0 and 40V for a ZnO-TFT with channel width to length ratio (W/L) of 50. (b) Transfer characteristics, I_D versus V_G at V_{DS}=20V for the same ZnO-TFT. It is also indicated the square root of drain current versus the gate voltage from which is determined the threshold voltage.

4.5.5 Summary

We have demonstrated a method of fabricating highly transparent ZnO-TFT by sol-gel and CBD combined method at a relatively low temperature without any other metal ions pre-activation or surface treatment. Especially, for the growth of for the ZnO films, we do not require a vacuum atmosphere. ZnO is one of a few oxides that can be grown as a crystalline film by solution method, on a variety of surfaces [40, 50, 76], such as amorphous glasses, plastics and crystalline films. It can also be grown on its preformed nanocrystalline films. This result particularity extends the application of ZnO in electronics field.

Chapter 5

Conclusions and Suggestions

5.1 Conclusions

In this thesis, preparation and characterization of ZnO and Mg-doped ZnO thin films by using solution method were investigated. The high-quality orientation ZnO films by sol-gel and chemical bath deposition combination method was proposed. The so-gel ZnO seeds layers, which are influenced strongly the crystallinity, morphology and crystals size by post-baking. CBD ZnO crystalline films with densely packed regular morphologies are successfully obtained, and the crystal clearly exhibited (002) preferred orientation. Furthermore, a method, using cation-mediated for improving the ZnO films deposition by CBD was disclosed. The cation-mediated solution, which contains magnesium ions, strongly influences the crystallinity, morphology, and band gap of the films. ZnO crystalline films with a densely packed regular morphology are obtained, and the crystal clearly exhibited a preferential (002) orientation. Furthermore, highly transparent films are obtained at wavelengths of 500 to 800 nm with a transmittance of above 94% (at a wavelength of 800 nm), and the optical band gap of the ZnO changes from ~3.38 to ~3.23 eV, which depends on the extent of lattice distortion.

In thin film transistor application, with ZnO or Mg-doped ZnO films for the active channel layer are comprehensively demonstrated. The goal of this thesis has been, in large part, to provide an initial demonstration of the feasibility of metal oxides active electronic devices based upon ZnO material systems by solution bath deposition or sol-gel method at low temperature. Especially, for the growth of for the

ZnO films, those do not require a vacuum atmosphere. ZnO is one of a few oxides that can be grown as a crystalline film by solution method, on a variety of surfaces, such as amorphous glasses, plastics and crystalline films. It can also be grown on its preformed nanocrystalline films. These results particularity extend the application of ZnO in electronics field. These transistors exhibit prototypical n-channel, deplation mode or enhancement mode TFT operation, confirming that conventional electronic device behavior can, indeed, be realized using ZnO material systems Fabricated TFTs exhibit depletion- and enhancement-mode behavior. The electrical characteristics of depletion-mode exhibit a drain current on-to-off ratio > 10^5, enhancement-mode ZnO TFTs typically exhibit a drain current on-to-off ratio > 10^7 (although, typical drain drain current on-to-off ratio for all devices, including depletion-mode, is > 10^6). These transistors were highly transparent in the visible spectrum, with transmittance as high as 75% to approximately 85% at wavelength from 500nm to 700nm. The optimum device has field-effect mobility of 0.67 cm^2/V s.

5.2 Suggestions

Although ZnO TFTs have been fabricated, many questions remain resolved. This section presents recommendations for future work in the field of TFT development. The process used to fabricate TFTs exist conceivable variation in device performance. Several likely sources of process variability can be identified, including, the ITO substrates; the ITO depositions, the large device dimensions, and shadow mask misalignment. Moreover, in order to reproduce the TFT devices the solution for ZnO deposition must control to be stable. To build up a robust chemical solution system is necessary for improving reliability of TFT performance.

For the purpose of process controllability, an insulator process should be developed further. In addition, development of an insulator process will facilitate device optimization. Particularly, the gate insulator capacitance should be increased by decreasing the insulator thickness or by choosing materials with a high relative dielectric constant (> 10). This will reduce the voltage required for device operation. New high dielectric constant gate insulators will suggest being further candidates.

To increase the marketability of these devices from a commercial perspective though, a low-temperature process (< 350℃) should be developed. This will expand the application scope of TFTs and allow their fabrication onto cheaper glass substrates. If the maximum processing temperature is further reduced (below 150℃), fabrication on flexible plastic substrates, which are light-weight and cost-effective, may be accomplished. ZnO is the recommended channel layer for initial development of a low-temperature process.

References

[1] M. A. Kastner, ”Artifical atoms”, Phys. Today **46** (1993) 24.

[2] R. F. Davis, ”III-V nitrides for electronic and optoelectronic applications”, Proc. IEEE **79** (1991) 702.

[3] L. N. Lewis, “Chemical catalysis by colloids and clusters“, Chem. Rev. **93** (1993) 2693.

[4] Y. Cui, Q. Q. Wei, H. K. Park, and C. M. Lieber, “Nanowire Nanosensors for Highly Sensitive and Selective Detection of Biological and Chemical Species”, Science **293** (2001) 1289.

[5] W.-L. Lee, and R.-L. Yong, “Defects and degradation in ZnO varistor”, Appl. Phys. Lett. **69** (1996) 526.

[6] K. G. Hendrikse, W. J. Mcgill, J. Reedijk, and P. J. Nieuwenhuizen, ”Vulcanization of chlorobutyl rubber. I. The identification of crosslink precursors in compounds containing $ZnO/ZnCl_2$”, J. Appl. Polym. Sci. **78** (2000) 2290.

[7] K. G. Hendrikse, and W. J. Mcgill, “Vulcanization of chlorobutyl rubber. II. A revised cationic mechanism of $ZnO/ZnCl_2$ initiated crosslinking”, J. Appl. Polym. Sci. **78** (2000) 2302.

[8] D. E. McCormack, P. O’Brien, and R. Ramesh, “The effect of processing conditions on varistors prepared from nanocrystalline ZnO“, J. Mater. Chem. **13** (2003) 2586.

[9] J. Zhang, L. D. Sun, J. L. Yin, H. L. Su, C. S. Liao, and C. H. Yan, “Control of ZnO Morphology via a Simple Solution Route“, Chem. Mater. **14** (2002) 4172.

[10] K. Keis, E. Magnusson, H. Lindstorm, S. E. Lindquist, and A. Hagfeldt, ”

1896

Photocatalytic oxidation of nitrite by sunlight using TiO_2 supported on hollow glass microbeads", Sol. Energy, **73** (2002) 15.

[11] S. Liang, H. Sheng, Y. Liu, Z. Hio, Y. Lu and H. Shen, "ZnO Schottky ultraviolet photodetectors", J. Cryst. Growth **225** (2001) 110.

[12] N. Saito, H. Haneda, T. Sekiguchi, N. Ohashi, I. Sakaguchi, and K. Koumoto, "Low-Temperature Fabrication of Light-Emitting Zinc Oxide Micropatterns Using Self-Assembled Monolayers", Adv. Mater. **14** (2002) 418.

[13] P. Mitra, A. P. Chatterjee, and H. S. Maiti, "ZnO thin film sensor", Materials **35** (1998) 33.

[14] F. C. M. Van de Pol, "Thin-Film ZnO — Properties and Applications", Ceram, Bull. **69** (1990) 1959.

[15] Y. E. Yee, J. B. Lee, Y. J. Kim, H. K. Yang, J. C. Park, and H. J. Kim, " Microstructural evolution and preferred orientation change of radio-frequency-magnetron sputtered ZnO thin films", J. Vac. Sci. Technol., A **14** (1996) 1943.

[16] V. Craciun, J. Elders, J. G. E. Gardenievs, and I. W. Boyd, " Characteristics of high quality ZnO thin films deposited by pulsed laser deposition", Appl. Phys. Lett. **65** (1994) 2963.

[17] Y. Natsume and H. Sakata, and T. Hirayama, "Low-temperature electrical conductivity and optical absorption edge of ZnO films prepared by chemical vapour deposition", Phys. Status Solidi (a) **148** (1995) 485.

[18] K. Ogata, K. Sakurai, Sz. Fujita, Sg. Fujita, and K. Matsushige, "Effects of thermal annealing of ZnO layers grown by MBE", J. Crystal Growth **214/215** (2000) 312.

[19] Y. Natsume, and H. Sakata, "Zinc oxide films prepared by sol-gel spin-coating", Thin Solid Films **372** (2000) 30.

[20] T. Saeed, and P. O'Brien, "Deposition and characterisation of ZnO thin films grown by chemical bath deposition", Thin Solid Films **271** (1995) 35.

[21] P. O'Brien, T. Saeed, and J. Knowles, "Speciation and the nature of ZnO thin films from chemical bath deposition", J. Mater. Chem. **6** (1996) 1135.

[22] M. Izaki, and T. Omi, "Transparent Zinc Oxide Films Chemically Prepared from Aqueous Solution", J. Electrochem. Soc. **144** (1997) L3.

[23] M. Izaki, and J. Katayama, "Characterization of Boron-Incorporated Zinc Oxide Film Chemically Prepared from an Aqueous Solution", J. Electrochem. Soc. **147** (2000) 210.

[24] L. Vayssieres, K. Keis, S. E. Lindquist, and A. Hagfeldt, "Microrod Array of ZnO", J. Phys. Chem. B **105** (2001) 3350.

[25] L. Vayssieres, "Growth of Arrayed Nanorods and Nanowires of ZnO from Aqueous Solutions", Adv. Mater. **15** (2003) 464.

[26] M. Ortega-Lo´pez, A. Avila-Garcı´a, M. L. Albor-Aguilera, and V. M. Sa´nchez Resendiz, "Immproved efficiency of the chemical. bath deposition method during growth of. ZnO thin films", Materials Research Bulletin 38 (2003) 1241.

[27] P. Li, Y. Wei, H. Liu, and X. K. Wang, "Growth of well-defined ZnO microparticles with additives from aqueous solution", J. Solid State Chemistry 178 (2005) 855.

[28] A.M. Peiro´, C. Domingo, J. Peral, X. Dome`nech, E. Vigil, M.A. Herna´ndez-Fenollosa, M. Mollar, B. Marı´, and J.A. Ayllo´n, "Nanostructured zinc oxide films grown from microwave activated aqueous solutions", Thin solid films, 483 (2005) 79.

[29] H. S. Bea, C. M. Choi, Jae Hoon Kim, and S. Im, "Dynamic and static photoresponse of ultraviolet-detecting thin-film transistors based on transparent NiOx electrodes and an n-ZnO channel ", J. Appl. Phys. **97** (2005) 6104

[30] R. Navamathavan, E. J. Yang, J. H. Lim, D. K. Hwang, J. Y. Oh, J. H. Yang, J. H. Jang, and S. J. Parka, "Effects of Electrical Bias Stress on the Performance of ZnO-Based TFTs Fabricated by RF Magnetron Sputtering", J. Electrochem. Soc. **153** (2006) G385.

[31] Q. J. Yao, and D. J. Li, "Fabrication and property study of thin filmtransistor using rf sputtered ZnO as channel layer", J. Non-Cryst. Solids **351** (2005)3191.

[32] T. I. Suzuki, A. Ohtomo, A. Tsukazaki, F. Sato, J. Nishii, H. Ohno, and M. Kawasaki, "Fully Transparent ZnO Thin-Film Transistor Produced at Room Temperature", Adv. Mater. **17** (2005) 590.

[33] P. F. Carcia, R. S. McLean, and M. H. Reilly, "Switching a spin valve back and forth by current-induced domain wall motion", Appl. Phys. Lett. **83** (2003) 509.

[34] P. Barquinha, E. Fortunato, A. Goncalves, A. Pimentel, A. Marques, L. Pereira, and R. Martins, "Influence of time, light and temperature on the electrical properties of zinc oxide TFTs ", Superlattices & Microstruct., **39** (2006) 319.

[35] H. S. Bae, M. H. Yoon, J. H. Kim, and S. Im, " Photodetecting properties of ZnO-based thin-film transistors", Appl. Phys. Lett. **83** (2003) 5313.

[36] K. Lee, J. H. Kim, and S. Im, "Thermal stability of magnetic tunneling junctions with MgO barriers for high temperature spintronics", Appl. Phys. Lett. **89** (2006) 023504

[37] H. H. Hsieh, and C. C. Wu, "Scaling behavior of ZnO transparent thin-film

transistors", Appl. Phys. Lett. **89** (2006) 041109

[38] I. D. Kim M. H. Lim, K. Kang, H. G. Kim, and S. Y. Choi, "Room temperature fabricated ZnO thin film transistor using high-K $Bi_{1.5}Zn_{1.0}Nb_{1.5}O_7$ gate insulator prepared by sputtering", Appl. Phys. Lett. **89** (2006) 022905.

[39] H. S. Bae, and S. Im, "Ultraviolet detecting properties of ZnO-based thin film transistors", Thin Solid Films **75** (2004) 469.

[40] E. M. C. Fortunato, P. M. C. Barquinha, A. C. M. B. G. Pimentel, A. M. F. Goncalves, A. J. S. Martins, and L. M. N. Pereira, "Wide-bandgap high-mobility ZnO thinfilm transistors produced at room temperature", Appl. Phys. Lett. **85** (2004) 2541.

[41] R. L. Hoffman, "ZnO-channel thin-film transistors: Channel mobility", Appl. Phys. Lett. **95** (2003) 5813.

[42] Y. Kwon, Y. Li, Y. W. Heo, M. Jones, P. H. Holloway, D. P. Norton, Z. V. Park, and S. Li, "Enhancement-mode thin-film field-effect transistor using phosphorus-doped (Zn,Mg)O channel", Appl. Phys. Lett. **84** (2004) 2685

[43] I. D. Kim S. Y. Choi, and H. L. Tuller, "Low-voltage ZnO thin-film transistors with high-*K* $Bi_{1.5}Zn_{1.0}Nb_{1.5}O_7$ gate insulator for transparent and flexible electronics", Appl. Phys. Lett. **87** (2005) 043509.

[44] J. Siddiqui, E. Cagin, D. Chen, and J. D. Phillips," ZnO thin-film transistors with polycrystalline (Ba,Sr)TiO_3 gate insulators", Appl. Lett. **88** (2006) 212903.

[45] Y. J. Li, Y. W. Kwon, M. Jones, Y. W. Heo, J. Zhou, S. C. Luo, P. H. Hoilloway, E. Douglas, D. P. Norton, Z. Park and S. Li, " High-mobility

field-effect transistors based on single-crystalline ZnO channels", Semicond. Sci. Technol. **20** (2005) L1193.

[46] J. Nishii, A. Ohtomo, K. Ohtani, H. Ohno, and M. Kawasaki, "High-mobility field-effect transistors based on single-crystalline ZnO channels", Jpn. J. Appl. Phys. **44** (2005) L1193.

[47] T. I. Suzuki, A. Ohtomo, A. Tsukazaki, F. Sato, J. Nishii, H. Ohno, and M. Kawasaki, "Hall and Field-Effect Mobilities of Electrons Accumulated at a Lattice-Matched $ZnO/ScAlMgO_4$ Heterointerface", Adv. Mater. **16** (2004) 1887.

[48] Y. Ohya, T. Kume, and T. Ban, "Fabrication of Zinc Oxide Transparent Thin-Film Transistor with ZrO_2 Insulating Layer by Sol–Gel Method", Jpn. J. Appl. Phys. **44** (2005) 1919.

[49] M. Leufgen, A. Lebib, T. Muck, U. Bass, V. Bass, V. Wagner, T. Borzenko, G. Schmidt, J. Geurts, and L. W. Molenkamp, "Organic thin-film transistors fabricated by microcontact printing", Appl. Phys. Lett. **84** (2004)1582.

[50] Y. Ohya, T. Niwa, T. Ban, and Y. Takahashi, "Thin Film Transistor of ZnO Fabricated by Chemical Solution Deposition," Jpn. J. Appl. Phys., Part 1 **40** (2001) 297.

[51] B. J. Norris, J. Anderson, J. F. Wager, and D. A. Keszler, "Spin-coated zinc oxide transparent transistors", J. Phys. D: Appl. Phys. **36** (2003) L105.

[52] Y. Kuo, "Thin Film Transistors: Materials and Processes. Poly crystalline Thin Film Transistors".

[53] Y. Kuo, "Thin Film Transistors: Materials and Processes. Amorphous Thin Film Transistors".

[54] C. R. Kagan, and P. Andry, “Thin Film Transistors”.

[55] J. E. Lilienfeld, U.S. Patent 1,745,175 (1930).

[56] J. E. Lilienfeld, U.S. Patent 1,900,018 (1933).

[57] W. E. Spear, and P.G. LeComber, Philos. Mag. **33** (1976) 935.

[58] P. K. Weimer, IRE-AICE Device Research Conference, Stanford, CA, June, (1961).

[59] T. P. Brody, J. A. Asars, and G. D. Dixon, “A 6 X6 Inch 20 Lines-per-Inch Liquid-Crystal Display Panel”, IEEE Trans. Electron Devices **ED-20** (1973) 995.

[60] W. E. Spear, and P. G. LeComber, “Substitutional doping of amorphous silicon“, Solid State Commun. **17** (1975) 1193.

[61] P. G. Lecomber, W. E. Spear, and A. Ghaith, “Amorphous-silicon field-effect device and possible application”, Electron. Lett. **15** (1979) 179.

[62] W. E. Spear, P. G. LeComber, S. Kinmond, and M. H. Brodsky, “Amorphous silicon *p-n* junction”, Appl. Phys. Lett. **28** (1976) 105

[63] S. W. Depp, A. Juliana, and B. G. Huth, Proc. 1980 Int. Electron Device Mtg. (IEEE, New Tork, 1980) 703.

[64] A. Juliana, S. W. Depp, B. G. Huth, and T. Sedgwick, Digest 1982 SID Int. Symp. (Soc. For Inf. Display, San Jose, 1982) 38.

[65] T. Nishimura, Y. Akasaka, and H. Nakata, “Characteristics of TFT Fabricated in Laser-Recrystallized Polysilicon for Active LC Display”, op. cit., p36.

[66] A. R. Brown, C. P. Jarrett, D. M. de Leeuw, and M. Matters, “Field-effect transistors made from solution-processed organic semiconductors“, Synth. Met. **88** (1997) 37.

[67] H. E. Katz, ”Organic molecular solids as thin film transistor semiconductors”, J. Mater. Chem. **7** (1997) 369.

[68] C. R. Kagan, D. B. Mitzi, and C. D. Dimitrakopoulos, “Organic-Inorganic Hybrid Materials as Semiconducting Channels in Thin-Film Field-Effect Transistors“, Science **286** (1999) 945.

[69] G. N. Parsons, C. S. Yang, T. M. Klein, and L. Smith, “Device modelling of a-Si:H alloy solar cells: Calibration procedure for determination of model input parameters”, Mater. Res. Soc. Symp. Proc. **507** (1998) 19.

[70] P. M. Smith, P. G. Carey, and T. W. Sigmon, “Excimer laser crystallization and doping of silicon films on plastic substrates”, Appl. Phys. Lett. **70** (1997) 342.

[71] S. Masuda, K. Kitamura, Y. Okumura, and S. Miyatake, ”Transparent thin film transistors using ZnO as an active channel layer and their electrical properties”, J. Appl. Phys. **93** (2003) 1624.

[72] R. L. Hoffman, B. J. Norris, and J. F. Wager, “ZnO-based transparent thin-film transistors”, Appl. Phys. Lett. **82** (2003) 733.

[73] P.F. Carcia, R.S. McLean, M.H. Reilly, and G. Nunes Jr., “Transparent ZnO thin-film transistor fabricated by rf magnetron sputtering”, Appl. Phys. Lett. **82** (2003) 1117.

[74] P. F. Carcia, R. S. McLean, M. H. Reilly, I. Malajovich, K. G. Sharp, S. Agrawal, and G. Nunes Jr., “ZnO Thin Film Transistors for Flexible Electronics“, Mater. Res. Soc. Symp. Proc. **769** (2003) H7.2.1.

[75] J. Nishii, F.M. Hossain, S. Takagi, T. Aita, K. Saikusa, Y. Ohmaki, I. Ohkubo, S. Kishimoto, A. Ohtomo, T. Fukumura, F. Matsukura, Y. Ohno, H. Koinuma, H. Ohno, and M. Kawasaki, "High Mobility Thin Film Transistors with

Transparent ZnO Channels", Jpn. J. Appl. Phys., Part 2 **42** (2003) L347.

[76] E. Fortunato, A. Pimentel, L. Pereira, A. Gonc¸alves, G. Lavareda, H. A´ guas, I. Ferreira, C.N. Caravalho, and R. Martins, “High field effect mobility zinc oxide thin film transistors produced at room temperature”, J. Non-Cryst. Solids **338** (2004) 806.

[77] E. Fortunato, P. Barquinha, A. Pimentel, A. Gonc¸alves, L. Pereira, A. Marques, and R. Martins, “Next generation of thin film transistors based on zinc oxide”, Mater. Res. Soc. Symp. Proc. **811** (2004) E1.9.

[78] S. Y. Chou, C. Keimel, and J. Gu, “Ultrafast and direct imprint of nanostructures in silicon”, Nature **417** (2002) 835.

[79] A. C. Arias, S. E. Ready, R. Lujan, W. S. Wong, K. E. Paul, and A. Street, “All jet-printed polymer thin-film transistor active-matrix backplanes”, Appl. Phys. Lett. **85** (2004) 3304.

[80] H. Kawazoe and K. Ueda, “Transparent Conducting Oxides Based on the Spinel Structure”, J. Am. Ceram. Soc., vol. **82** (1999) 3330.

[81] H. Kawazoe, M. Yasukawa, H. Hyodo, M. Kurita, H. Yanagi, and H. Hosono, “P-type electrical conduction in transparent thin films of $CuAlO_2$”, Nature, **389** (1997) 939.

[82] H. Yanagi, S. Inoue, K. Ueda, H. Kawazoe, H. Hosono, and N. Hamada, “Electronic structure and optoelectronic properties of transparent *p*-type conducting $CuAlO_2$”, J. Appl. Phys. **88** (2000) 4159.

[83] J. Tate, M. K. Jayaraj, A. D. Draeseke, T. Ulbrich, A. W. Sleight, K. A. Vanaja, R. Nagarajan, J. F. Wager, and R. L. Hoffman, ” p-Type oxides for use in transparent diodes “, Thin Solid Films **411** (2002) 119.

1896

[84] K. Ueda, T. Hase, H. Yanagi, H. Kawazoe, H. Hosono, H. Ohta, M. Orita, and M. Hirano, " Epitaxial growth of transparent *p*-type conducting $CuGaO_2$ thin films on sapphire (001) substrates by pulsed laser deposition", J. Appl. Phys. **89** (2000) 1790.

[85] H. Yanagi, T. Hase, S. Ibuki, K. Ueda, and H. Hosono, "Bipolarity in electrical conduction of transparent oxide semiconductor $CuInO_2$ with delafossite structure", Appl. Phys. Lett., vol. **78** (2001) 1583.

[86] T. Coutts, D. Young, and X. Li, "Search for improved transparent conducting oxides: A fundamental investigation of CdO, Cd_2SnO_4, and Zn_2SnO_4", J. Vac. Sci. Technol. A, vol. 18, no. 6 (2000) 2646.

[87] F. Koffyberg, and F. Benko, " Cd_2SnO_4, $CdIn_2O_4$, and Cd_2GeO_4 as anodes for the photoelectrolysis of water", Appl. Phys. Lett. **37** (1980) 320.

[88] X. Wu, T. Coutts, and W. Mulligan, " Properties of transparent conducting oxides formed from CdO and ZnO alloyed with SnO_2 and In_2O_3 ", J. Vac. Sci. Technol. A, **15** (1997) 1057.

[89] K. L. Chopra, S. Major, and D. K. Pandya, "Transparent conductors-A. status review", Thin Solid Films **102** (1983) 146.

[90] K. Ellmer, "Resistivity of polycrystalline zinc oxide films: current status and physical limit", J. Phys. D.: Appl. Phys. **34** (2001) 3097.

[91] O. Lang, C. Pettenkofer, J. Sanchez-Royo, A. Segura, A. Klein, and W. Jaegermann, " Thin film growth and band lineup of In_2O_3 on the layered semiconductor InSe", J. Appl. Phys. **86** (1999) 5687.

[92] J. M. Phillips, J. Kwo, A. Thomas, A. Carter, R. Cava, and S. Hou, "Transparent conducting thin films of $GaInO_3$ ", Appl. Phys. Lett. **65** (1994)

115.

[93] T. Minami, T. Miyata, and T. Yamamoto, "Work function of transparent conducting multicomponent oxide thin films prepared by magnetron sputtering", Surf. and Coat. Tech. **108-109** (1998) 583.

[94] T. Minami, H. Sonohara, T. Kakumu, and S. Takata,"Highly Transparent and Conductive $Zn_2In_2O_5$ Thin Films Prepared by RF Magnetron Sputtering", Jpn. J. Appl. Phys. **34** (1995) 971.

[95] T. Minami, S. Takata, H. Sato, and H. Sonhana, "Properties of transparent zinc-stannate conducting films prepared by radio frequency magnetron sputtering", J. Vac. Sci. Technol. A **13** (1995) 1095.

[96] T. Minami, H. Sonohara, S. Takata, and H. Sato, "Highly Transparent and Conductive Zinc-Stannate Thin Films Prepared by RF Magnetron Sputtering", Jpn. J. Appl. Phys. **33** (1994) 1693.

[97] D. L. Young, H. Moutinho, Y. Yan, and T. J. Coutts, "Growth and characterization of radio frequency magnetron sputter-deposited zinc stannate, Zn_2SnO_4, thin films", J. Appl. Phys. **92** (2002) 310.

[98] D. Look, D. Reynolds, C. Litton, R. Jones, D. Eason, and G. Cantwell, "Characterization of homoepitaxial *p*-type ZnO grown by molecular beam epitaxy", Appl. Phys. Lett., **81** (2002) 1830.

[99] X. Li, Y. Yan, T. Gessert, C. DeHart, C. Perkins, D. Young, and T. Coutts, "p-Type ZnO Thin Films Formed by CVD Reaction of Diethylzinc and NO Gas", Electrochemical and Sol. St. Lett. **6** (2003) C56.

[100] R. D. Vispute, V. Talyansky, S. Choopun, R. P. Sharma, T. Venkatesan, M. He, X. Tang, J. B. Halpern, M. G. Spencer, Y. X. Li, L. G. Salamanca-Riba, A. A.

Iliadis, and K. A. Jones, “Heteroepitaxy of ZnO on GaN and its implications for fabrication of hybrid optoelectronic devices”, Appl. Phys. Lett. **73** (1998) 348.

[101] Michael H. Huang, Samuel Mao, Henning Feick, Haoquan Yan, Yiying Wu, Hannes Kind, Eicke Weber, Richard Russo, and Peidong Yang, “Room-Temperature Ultraviolet Nanowire Nanolasers “, Science **292** (2001) 1897.

[102] D. S. Ginley, and C. Bright, “Transparent Conducting Oxides”, MRS Bulletin, **Aug.** (2000) 15.

[103] E. G. Bylander, “Surface effects on the low-energy cathodoluminescence of zinc oxide”, J. Appl. Phys. **49** (1978) 1188.

[104] H. Nanto, T. Minami, and S. Takata, “Photoluminescence in Sputtered ZnO Thin Films”, Phys. Stat. Sol. (a), **65** (1981) K131.

[105] S. A. Studenikin, N. Golego, and M. Cocivera, ”Fabrication of green and orange photoluminescent, undoped ZnO films using spray pyrolysis”, J. Appl. Phys. **84** (1998) 2287.

[106] S. Takata, T. Minami, and H. Nanto, “DC EL in Annealed Thin Film of Sputtered ZnO”, Jpn. J. Appl. Phys., vol. 20, no. 9 (1981) 1759.

[107] J. Muller, S. Weibenrieder, and Fresenius, J. Anal. Chem. **349** (1994) 380.

[108] B. T. Khuri-Yakub, and G. S. Kino, “A monolithic zinc-oxide-on-silicon convolver”, Appl. Phys. Lett. **25** (1974) 188.

[109] D. P. Norton, Y. W. Heo, M. P. Lvill, K. Ip, S. j. Pearton, M. F. Chisholm, and T. Steiner, “ZnO: growth, doping & processing “, Materials Today, June (2004) 34.

[110] D. C. Look, D. C. Reynolds, J. W. Hemski, R. L. Jones, and J. R. Sizelove, " Production and annealing of electron irradiation damage in ZnO", Appl. Phys. Lett., **75** (1999) 811.

[111] A. Y. Polyakov, "Proton implantation effects on electrical and recombination properties of undoped ZnO", J. Appl., Phys. **94** (2003) 2895.

[112] S. O. Kucheyev, J. S. Williams, C. Jagadish, J. Zou, C. Evans, A. J. Nelson, and A. V. Hamza," Ion-beam-produced structural defects in ZnO", Phys. Rev. B **67** (2003) 094115.

[113] A. Mitra, R. K. Thareja, V. Ganesan, A. Gupta, P. K. Sahoo, and V. N. Kulkarni, "Synthesis and characterization of ZnO thin films for UV laser ", Appl. Surf. Sci. **174** (2001) 232.

[114] J. Vuillod," Properties of ZnO fiims prepared by dc and rf diode. Sputtering", J. Vac. Sci. Technol., **9** (1972) 87.

[115] A. Valentini, F. Quaranta, M. Penza, and F. R. Rizzi," The stability of zinc oxide electrodes fabricated by dual ion beam sputtering", J. Appl. Phys., **73** (1993) 1143.

[116] W. S. Lau, and S. J. Fonash, "Highly transparent and conducting zinc oxide films deposited by activated reactive evaporation", J. Electron. Mater., vol. **16**, no. 3 (1987) 141.

[117] J. D. Merchant, and M. Cocivera," Preparation and doping of zinc oxide using spray pyrolysis", Chem. Mater. **7** (1995) 1742.

[118] A. E. Jimenez-Gonzalez, J. A. S. Urueta, and R. Suarez-Parra, "Optical and electrical characteristics of aluminum-doped ZnO thin films prepared by solgel technique ", J. Crystal Growth **192** (1998) 430.

[119] S. Komuro, T. Katsumata, T. Morikawa, X. Zhao, H. Isshiki, and Y. Aoyagi, "Highly erbium-doped zinc–oxide thin film prepared by laser ablation and its 1.54 μm emission dynamics", J. Appl. Phys. **88** (2000) 7129.

[120] A. Tiburcio-Silver, J. C. Joubert, and M. Labeau, "Optical band-gap shrinkage in highly transparent and conducting ZnO thin films deposited by the Pyrosol process", J. Appl. Phys. **76** (1994) 1992.

[121] W. W. Wenas, A. Yamada, K. Takahashi, M. Yoshino, and M. Konagai," Electrical and optical properties of boron-doped ZnO thin films for solar cells grown by metalorganic chemical vapor deposition", J. Appl. Phys. **70** (1991) 7119.

[122] M. Izaki and T. Omi, "Transparent zinc oxide films prepared by electrochemical reaction", Appl. Phys. Lett. **68** (1996) 2439.

[123] C. R. Kagan, and P. Andry," Thin-film transistors", New York: Marcel Dekker, Inc., 2003.

[124] S. Bandyopadhyay, G. K. Paul, R. Roy, S. K. Sen, and S. Sen, "Study of structural and electrical properties of grain-boundary modified ZnO films prepared by sol–gel technique", Materials Chemistry and Physics **74** (2002) 83.

[125] D. C. Tsui, H. L. Stormer, and A. C. Gossard, "Two-dimensional magnetotransport in the extreme quantum limit", Phys. Rev. Lett. **48** (1982) 1559.

[126] R. B. Laughlin, ”Anomalous quantum Hall effect – an incompressible quantum fluid with fractionally charged excitations”, Phys. Rev. Lett. **50** (1983) 1395.

[127] F. D. M. Haldane, “Fractional Quantization of the Hall Effect: A Hierarchy of Incompressible Quantum Fluid States”, Phys. Rev. Lett. **51** (1983) 605.

[128] Pizzini, N. Butta, D. Narducci, and M. Palladino, “Thick Film ZnO Resistive Gas Sensors”, J. Electrochem. Soc. **136** (1989) 1945.

[129] Y. Kwon, Y. Li, Y.W. Heo, M. Jones, P. H. Holloway, D. P. Norton, Z. V. Park, and S. Li, “Enhancement-mode thin-film field-effect transistor using phosphorus-doped (Zn,Mg)O channel”, Appl. Phys. Lett. **84** (2004) 2685.

[130] S. Arulkumaran, M. Sakai, T. Egawa, H. Ishikawa, and T. Jimbo, “ Improved dc characteristics of AlGaN/GaN high-electron-mobility transistors on AlN/sapphire templates”, Appl. Phys. Lett. **81** (2002) 1131.

[131] V. Craciun, J. Elders, J. G. E. Gardenievs, and I. W. Boyd, ”Characteristics of high quality ZnO thin films deposited by pulsed laser deposition “, Appl. Phys. Lett. **65** (1994) 2963.

[132] M. Izaki, and T. Ohmi, “Characteristics of high quality ZnO thin films deposited by pulsed laser deposition”, Appl. Phys. Lett. **68** (1996) 166.

[133] K. Ito, and K. Nakamura, “Preparation of ZnO thin films using the flowing liquid film method “, Thin Solid Films **286** (1996) 35.

[134] S. Yamabi, and H. Imai,” Growth conditions for wurtzite zinc oxide films in aqueous solutions”, J. Mater. Chem. **12** (2002) 3773.

[135] L. G. Svendsen, T. Osaka, and H. Sawai, ” Behavior of Pd/Sn and Pd

Catalysts for Electroless Plating on Different Substrates Investigated by Means of Rutherford Backscattering Spectroscopy", J. Electrochem. Soc. **130** (2000) 2252.

[136] C. H. de Minjer, and P. F. J. v. d. Boom, "The Nucleation with $SnCl_2$-$PdCl_2$ Solutions of Glass Before Electroless Plating ", J. Electrochem. Soc. **120** (1997) 1644.

[137] International Centre for Diffraction Datas, Joint Committee on Powder Diffraction Standards, Swarthmore, PA, 1986, Card 36-1451.

[138] M. Izaki, "Preparation of Transparent and Conductive Zinc Oxide Films by Optimization of the Two-Step Electrolysis Technique", J. Electrochem. Soc. **146** (1999) 4517.

[139] M. Charbonnier, and M. Romand, "Polymer pretreatments for enhanced adhesion of metals deposited by the electroless process ", Adhes. Adhes. **23** (2003) 277.

[140] J. S. Meth, S. G. Zane, K. G. Sharp, and S. Agrawal, "Transplantation of neural stem cells modified by human neurotrophin-3 promotes functional recovery after transient focal cerebral ischemia in rats", Thin Solid Films **444** (2003) 227.

[141] S. Yokoyama, A. Otomo, and S. Mashiko, " Laser emission from high-gain media of dye-doped dendrimer", Appl. Phys. Lett. **80** (2003) 7.

[142] W. S. Wong, S. E. Ready, J.-P. Lu, and R. A. Street, " Hydrogenated Amorphous Silicon Thin-Film Transistor Arrays Fabricated by Digital Lithography", IEEE Electron Device Lett. **24** (2003) 577.

[143] P. Mitra, A. P. Chatterjee, and H. S. Maiti, ”ZnO thin film sensor”, Materials Letters **35** (1998) 33.

[144] T. Saeed, and P. O’Brien, “EXAFS studies on adsorption–desorption reversibility at manganese oxide–water interfaces II. Reversible adsorption of zinc on δ-MnO_2 “, Thin Solid Films **271** (1995) 35.

[145] M. Charbonnier, and M. Romand, “Polymer pretreatments for enhanced adhesion of metals deposited by the electroless process”, Adhes. Adhes. **23** (2003) 277.

[146] R. D. Shannon, "Revised Effective Ionic Radii and Systematic Studies of Interatomic Distances in Halides and Chalcogenides" , Acta Crystallogr., Sect. A **32** (1976) 751.

[147] F. Kohan, G. Ceder, D. Morgan, and C. G. Van de Walle, “First-principles study of native point defects in ZnO”, Phys. Rev. B **61** (2000) 15019.

[148] R. D. Tarey, and T. A. Raju, ”Monosomy 1p36 uncovers a role for OX40 in survival of activated CD4+ T cells“, Thin Solid Films **128** (1985) 181.

[149] S. J. Pearton, D. P. Norton, K. Ip, and W. W. Heo, “Recent advances in processing of ZnO“, J. Vac. Sci. Technol. B **22** (2004) 932.

[150] C. S. Ferekides, R. Mamazza, U. Balasubramanian, and D. L. Morel, ”Transparent conductors and buffer layers for CdTe solar cells “, Thin Solid Films **480-481** (2005) 224.

[151] T. Minami, T. Miyata, Y. Ohtani, and Y. Mochizuki, “Characterization of COOH-Terminated Self-Assembled Monolayers and Adsorption Efficiency of DNA Molecules Studied by X-ray Photoelectron Spectroscopy and Near-Edge X-ray Absorption Fine Structure Spectroscopy“, Jpn. J. Appl. Phys. **45** (2006)

L409.

[152] R. L. Hoffman, “ZnO-channel thin-film transistors: Channel mobility”, J. Appl. Phys. **95** (2004) 5813.

[153] E. Fortunato, P Barquinha, A. Pimentel, A. Gonçalves, A. Marques, L. Pereira, and R. Martins, “Recent advances in ZnO transparent thin film transistors“, Thin Solid Films **487** (2005) 205.

[154] C. J. Kao, Y. W. Kwon, Y. W. Heo, D. P. Norton, S. J. Pearton, F. Ren, and G. C. Chi, “Comparison of ZnO metal–oxide–semiconductor field effect transistor and metal–semiconductor field effect transistor structures grown on sapphire by pulsed laser deposition”, J. Vac. Sci. Technol. B **23** (2005) 1024.

[155] J. H. Lee, P. Lin, C. C. Lee, J. C. Ho, and Y. W. Wang, “Sol–Gel-Derived $Zn_{(1-x)}Mg_xO$ Thin Films Used as Active Channel Layer of Thin-Film Transistors “, Jpn. J. Appl. Phys. **44** (2005) 4784.

[156] J. W. Kim, H. S. Kang, J. H. Kim, S. Y. Lee, J. K. Lee, and M. Nastasi,“ Variation of structural, electrical, and optical properties of $Zn_{1-x}Mg_xO$ thin films”, J. Appl. Phys. **100** (2006) 033701-1.

[157] W. I. Park, G. C. Yi, and H. M. Jang, ”Metalorganic vapor-phase epitaxial growth and photoluminescent properties of $Zn_{1-x}Mg_xO(0 \leqslant x \leqslant 0.49)$ thin films”, Appl. Phys. Lett. **79** (2001) 2022.

[158] T. Maemoto, N. Ichiba, S. Sasa, and M. Inoue, “Growth of $ZnO/Zn_{1-x}Mg_xO$ films by pulsed laser ablation”, Thin Solid Films **486** (2005) 174.

[159] Dhananjay, and S. B. Krupanidhi, “Dielectric properties of *c*-axis oriented $Zn_{1-x}Mg_xO$ thin films grown by multimagnetron sputtering”, Appl. Phys. Lett.

89 (2006) 082905.

[160] C. S. Suchand Sandeep, R. Philip, R. Satheeshkumar, and V. Kumar, "Sol-gel synthesis and nonlinear optical transmission in $Zn_{(1-x)}Mg_{(x)}O$ ($x \leqslant 0.2$) thin films", Appl. Phys. Lett. **89** (2006) 063102.

[161] D. Zhao, Y. Liu, D. Shen, Y. Lu, J. Zhang, and X. Fan, "Structural and optical properties of $Mg_xZn_{1-x}O$ thin films prepared by the sol–gel method ", J. Crystal Growth **234** (2002) 427.

[162] T. Tsukada, TFT/LCD: Liquid-Crystal Displays Addressed by Thin-Film Transistors, Gordon and Breach Publishers, Tokyo, (1996), p. 59.

[163] H. Cao, Y. G. Zhao, H. C. Ong, S. T. Ho, J. Y. Dai, J. Y. Wu, and R. P. H. Chang, "Ultraviolet lasing in resonators formed by scattering in semiconductor polycrystalline films", Appl. Phys. Lett. **73** (1998) 3656.

[164] J. Y. Park, D. J. Lee, B.T. Lee, J. H. Moon, and S. S. Kim, "Improvement in microstructure and crystal alignment of ZnO films grown by metalorganic chemical vapor deposition using a seed layer", J. Crystal Growth, **276** (2005) 165.

[165] K. B. Sundaram, and A. Khan, "Identification of laminin-binding motifs of *Yersinia pestis* plasminogen activator by phage display", Thin Solid Films, **295** (1997) 87.

[166] J. Myong, W. Yoon, D. Lee, I. Yun, S. Bae, and S. Lee, "Effects of Thickness Variation on Properties of ZnO Thin Films Grown by Pulsed Laser Deposition", Jpn J. Appl. Phys., **41** (2002) 28.

[167] R. Ghosh, D. Basak, and S. Fujihara, "Effect of substrate-induced strain on the structural, electrical, and optical properties of polycrystalline ZnO thin

films“, J. Appl. Phys. **96** (2004) 2689.

[168] S. Chakrabarti, D. Ganguli, and S. Chaudhuri, “Substrate dependence of preferred orientation in sol–gel-derived zinc oxide films“, Mater. Lett. , **58** (2004) 3952.

[169] E. Bauer, M.H. Francombe, and H. Sato (Eds.), Single Crystal Films, Pergamon, London, (1964) p. 43.

[170] S. Harada, S. Suzuki, J. Senzaki, R. Kosugi, K. Adachi, K. Fukuda, and K. Arai, “Improved Channel Mobility in Normally-Off 4H-SiC MOSFETs with Buried Channel Structure“, Mater. Sci. Forum **389** (2002) 1069.

[171] E. M. C. F. Pedro, M. C. Barquinha, A. C. M. B. G. Pimentel, A. M. F. Gonçalves, A. J. S. Marques, R. F. P. Martins, and L. M. N. Pereira, “Wide-bandgap high-mobility ZnO thin-film transistors produced at room temperature”, Appl. Phys. Lett. **85** (2004) 2541.

[172] M. Ohyama, H. Kozuka, and T. Yoko, “Effects of crystal size and Si/Al ratio on the surface properties of H-ZSM-5 zeolites”, Thin Solid Films **306** (1997) 78.

[173] H.-C. Cheng, C.-F. Chen, and C.-C. Lee, “Thin-film transistors with active layers of zinc oxide (ZnO) fabricated by low-temperature chemical bath method”, Thin Solid Films **498** (2006) 142.

Publication list

Journal paper

1. **Hua-Chi Cheng**, C. F. Chen, C. Y. Tsay, " Transparent ZnO thin film transistor fabricated by sol-gel and chemical bath deposition combination method", Appl. Phys. Lett., **90** (2007) 012113.

2. **Hua-Chi Cheng**, C. F. Chen, C. Y. Tsay, " Cation-Mediated Effects on Zinc Oxide Films Formed by Chemical Bath Deposition", Jpn. J. Appl. Phys., vol **46**, No. 7A (2007) 4265.

3. **Hua-Chi Cheng**, C. F. Chen, C. Y. Tsay, " Thin-film transistors with active layers of zinc oxide (ZnO) fabricated by low-temperature chemical bath method", Thin Solid Films **498** (2006) 142.

4. **Hua-Chi Cheng**, C. F. Chen, C. Y. Tsay, "High oriented ZnO films by sol-gel and chemical bath deposition combination method", Journal of alloys and compounds, (In press).

5. C. Y. Tsay, **Hua-Chi Cheng**, C. F. Chen, "The paper of Performance of sol-gel deposited Zn1-xMgxO films used as active channel layer for thin-film transistors", Surface & Coatings Technology **202** (2007) 1323.

6. C. Y. Tsay, C. K. Lin, **Hua-Chi Cheng**, K. S. Liu, I. N. Lin, " Low temperature sintering and magnetic properties of garnet microwave magnetic materials", Materials Chemistry and Physic **105** (2007) 408.

7. C. Y. Tsay, C. Y. Chen, **Hua-Chi Cheng**, K. S. Liu, I. N. Lin, "Magnetic and Microwave Properties of Bi-substituted Calcium Vanadium Garnets", The Chinese Journal of Process Engineering, **6** (2006) 2.

8. 范凱雄、蔡健益、林中魁、**鄭華琦**, "高透光性氧化鋅薄膜之製備", 真空科技, 第20卷, 第1期 (2007). in press

Conference paper

1. **Hua-Chi Cheng**, Y. R. Peng, C. A. Chung, W. H. Hou, and Z. W. Pei, “Organic Thin Film Transiators on Synthesis Paper” **Mater. Res. Soc. Symp. Proc. Vol. 965 (2007) 0965-S06-16**

2. C.Y. Tsay, **Hua-Chi Cheng**, M.C. Wang, P.Y. Lee and C.K. Lin, “Performance of sol-gel deposited $Zn_{1-x}Mg_xO$ films used as active channel layer for thin-film transistors”, International Conference on Metallurgical Coatings and Thin Films (ICMCTF2007), San Diego, USA, April 23~ 27 (2007).

3. C.Y. Tsay, Y.T. Tung, **Hua-Chi Cheng**, W.H. Tuan and C.K. Lin, “Effect of Sn doped on microstructural and optical properties of ZnO thin films deposited by sol-gel method, International Conference on Metallurgical Coatings and Thin Films (ICMCTF2008), San Diego, USA, April 28~ May 2 (2008).

4. 鄭華琦, 蔡健益, 陳家富, “硫化物半導體在薄膜電晶體之應用”, 中國材料科學學會94年年會論文集, 台北 (2005)

5. 蔡健益, 陳錦毅, 鄭華琦, 劉國雄, 林諭男, “鉍鈣釩柘榴石之磁性與微波特性研究”, 顆粒技術研討會, 北京, August 18~21 (2006).

6. 范凱雄、蔡健益、林中魁、鄭華琦, “高透光性氧化鋅薄膜之製備”，真空科技, 第20卷，第1期 (2007).

Patent

1. **Hua-Chi Cheng**, C. C. Lee, J. H. Liao, Y. Y. Chang, J. R. Sheu, J. C. Ho, Cathode plate of a carbon nanotube field emission display and its fabrication method, US 6811457, Nov. 2, 2004.

2. J. R. Sheu C. C. Lee, J. H. Liao, **Hua-Chi Cheng**, W. C. Wang, Field emission display panels incorporating cathodes having narrow nanotube emitters formed on dielectric layers, US 6750604, Jun. 15, 2004.

3. C. C. Lee, J. H. Liao, **Hua-Chi Cheng**, W. C. Wang, Field emission display panel equipped with a dual-layer cathode and an anode on the same substrate and method for fabrication, US 6541906, Jun. 15, 2004.

4. Y. Y. Chang, **Hua-Chi Cheng**, J. R. Sheu, C. H. Chao, K. C. Chen., Method of growing isomeric carbon emitters onto triode structure of field emission display, US 6769945, Aug. 2, 2004.

5. J. R. Sheu C. C. Lee, J. H. Liao, **Hua-Chi Cheng**, W. C. Wang, Manufacturing method for an electron-emitting source of triode structure, US6705910, Mar. 15, 2004.

6. 鄭華琦, 李正中, 蕭名男, ，薄膜電晶體的製作方法，中華民國發明專利，公告中。

7. 李正中、鄭華琦、廖貞慧、王文俊，具有雙層因電擊的長發射顯示面板及其製造方法，日本發明第 3674844 號專利 2005 年 5 月。

8. 溫俊祥、鄭淑惠、鄭華琦、吳耀庭、詹明香、謝葆如、安川淳一、桑原一， Method for manufacturing color filters，韓國發明第 10-0563638 號專利，2006 年 7 月。

9. 鄭華琦、李正中、廖貞慧、張悠揚、許志榮、何家充，奈米碳管場發射顯示器之陰極板製程，中華民國發明第 172340 號專利，2003 年 6 月。

10. 許志榮、何家充、張悠揚、鄭華琦、李正中，三極結構電子發射源之製造方法，中華民國發明第 170725 號專利，2002 年 5 月。

11. 張悠揚、鄭華琦、許志榮、趙慶勳、陳光中一種場發射顯示器之三極結構的製程，中華民國發明第 I220265 號專利，2004 年 8 月。

12. 鄭華琦、溫俊祥、吳耀庭、鄭淑惠、詹明香、安川淳一、桑原一，液晶面板及其製造方法，中華民國發明第 182317 號專利，2003 年 11 月。

學 經 歷 資 料

姓名： 鄭華琦
性別： 女
生日： 53 年 12 月 5 日 彰化人
電子郵件信箱： Hua_Chi_Cheng @itri.org.tw
電 話：0910939998

學 歷：

研究所	國立交通大學材料工程研究所	材料所	2002. 9~2007. 11	博士
研究所	逢甲大學化學工程研究所	化工所	1992. 9~1994. 6	碩士
大 學	逢甲大學	化工系	1984. 9~1987. 6	學士

經 歷：

經 歷	工研院顯示中心	研 發	專案經理	95 年 1 月	96 年 ~
	工研院電子所	研 發	工程師	88 年 10 月	95 年 1 月
	奇美電子	研 發	工程師	88 年 4 月	88 年 10 月
	工研院材料所	研 發	研究員	83 年 10 月	88 年 4 月
	東海大學	化工系	助教	78 年 8 月	80 年 8 月

專 長：

研究專長	◆ 薄膜電晶體元件設計與製程 ◆ 氧化鋅薄膜製程 ◆ 光阻材料合成 ◆ 乳化聚合